Aus dem Institut für Muskelkrankheiten
Experimental and Clinical Research Center (ECRC)
der Medizinischen Fakultät Charité Universitätsmedizin Berlin
in Kooperation mit dem
Max-Delbrück-Centrum für Molekulare Medizin (MDC)

DISSERTATION

GC/MS- and LC/MS-based metabolic and proteomic analysis of dysferlin-deficient muscle from patients and animal models

zur Erlangung des akademischen Grades
Doctor medicinae (Dr. med.)

vorgelegt der Medizinischen Fakultät
Charité – Universitätsmedizin Berlin

von
Sarah Keller
aus Düsseldorf

Datum der Promotion: 14. Februar 2014

Content

Figures

Tables

Abbreviations

AAT	Alanine amino transferase
AcAc	Acetoacetate
ACO	Aconitase
ACoA	Acetyl Coenzyme A
AD	Autosomal-dominant
ADP	Adenosine Diphosphate
aKG	Alpha Ketoglutaric acid
ALA	Alanine
ALD	Aldolase
AmBic	Ammonium Bicarbonate
AMP	Adenosine Monophosphate
AMPK	5'AMP kinase
AR	Autosomal-recessive
AR	Aldose reductase
ATP	Adenosine Triphosphate
CACT	Carnitin acylcarnitin transporter
CD	Cluster of Differentiation
CIT	Citrate
CK	Creatine kinase
CPT	Carnitin palmitoyltransferase
CS	Citrate synthase
DGC	Dystrophin Glycoprotein Complex
DHAP	Dihydroxy acetone phosphate
DMAT	Distal Myopathy with Anterior Tibial Onset
DMD	Duchenne muscular dystrophy
DNA	Deoxyribonucleic acid
DTT	Dithiotreitol
DYSF	Dysferlin
EDL	Extensor digitorum longus muscle
ENO	Enolase
$FADH_2$	Flavin adenine dinucleotide
FDR	False discovery rate
FER	Ferlin
FFA	Free fatty acids
FUM	Fumaric acid
F1,6BP	Fructose 1,6 bisphosphate

F2,6BP	Fructose 2,6 bisphosphate
F6P	Fructose-6-phosphate
GAPDH	Glyceraldehyde-3-dehydrogenase
GA3P	Glyceraldehyde-3-phosphate
GC	Gas chromatography
GDH	Glutamate dehydrogenase
GLN	Glutamine
GLS	Glutamate synthase
GLU	Glutamate
GLUC	Glucose
GluDH	Glutamate dehydrogenase
GLUT	Glucose Transporter
GMD	Golm Metabolome Database
GPx	Glutathione peroxidase
GR	Glutathione reductase
G3P	Glycerol-3-phosphate
G6P	Glucose-6-phosphate
HDL	High density lipoprotein
HK	Hexokinase
HPLC	High performance liquid chromatography
IAA	Iodoacetamide
IDH	Isocitrate dehydrogenase
IMTG	Intramuscular triacylglycerol
IRS	Insulin receptor substrate
KGDH	Ketoglutarate dehydrogenase
LAC	Lactate
LC	Liquid chromatography
LDH	Lactate dehydrogenase
LGMD	Limb girdle Muscular Dystrophy
LYS-C	Lysin-C
MAC	Membrane attack complex
MACS	Magnetic Activated Cell Sorting
MAL	Malic acid
MCT	Monocarboxylate transporter
MCW	Methanol-chloroform-water
MDH	Malate dehydrogenase
MLC	Myosin regulatory light chain

MM	Miyoshi Myopathy
mRNA	Messenger ribonucleic acid
MS	Mass spectrometry
MSTFA	N-methyl-trimethylsilyl-triflouroacetamide
MyCH	Myosin heavy chain
NAD	Nicotinamide adenine dinucleotide
NH3	Ammonium
NMR	Nuclear magnetic resonance spectroscopy
OA	Oxaloacetic acid
OMIM	Online Mendelian Inheritance in Man
OXPHOS	Oxidative phosphorylation
PBM	Peripheral blood monocytes
PC	Pyruvate carboxylase
PEP	Phosphoenolpyruvic acid
PDC	Pyruvate dehydrogenase complex
PDH	Pyruvate dehydrogenase
PFK	Phosphofructokinase
PGI	Phosphoglucoisomerase
PGK	Phosphoglycerate kinase
PGM	Phosphoglycerate mutase
PK	Pyruvate kinase
PYR	Pyruvic acid
QUAD	Quadriceps muscle
R.I.	Retention Index
R.T.	Retention Time
SCoAS	Succinyl CoA synthase
SDH	Succinate dehydrogenase
SERCA	Sarcoplasmic/Endoplasmic reticulum calcium ATPase
SILAC	Stable isotope labelling by amino acids in cell culture
SIRM	Stable Isotope resolved metabolomics
SMGM	Skeletal muscle growth medium
SOL	Soleus muscle
SUC	Succinic acid
TA	Tibialis anterior muscle
TCA	Tricarboxylic acid cycle
TFA	Trifluoroacetic acid
Tnnc	Cardiac troponin C

TPI	Triosephosphate isomerase
T2DM	Diabetes mellitus type 2
VLDL	Very low density lipoproteins
1,3BPG	1,3 Bisphosphoglyceric acid
3HB	3-β-Hydroxybutyrate
3PG	3-Phosphoglyceric acid
2PG	2-Phosphoglyceric acid

Für meine Eltern

Abstract (English)

Introduction: Limb girdle muscular dystrophy type 2B (Dysferlinopathy, Miyoshi Myopathy) is a hereditary muscular dystrophy caused by mutations in the gene encoding DYSF on chromosome 2p13. Despite the fact that dysferlin was recently predicted to be implicated in muscle membrane repair upon injury, the definitive function leading to the progressive muscular disease still remains a matter of debate. One peculiar aspect delineating dysferlinopathy from other muscular diseases is the late disease onset after puberty and the clinical finding that patients are usually good athletes before that. During adolescence, muscle metabolism undergoes marked changes, switching its fibre type characteristics from a primarily oxidative (type I) to a more glycolytic (type II) metabolism. Considering these aspects, we hypothesized that dysferlin plays a key role in muscle metabolism by influencing glucose uptake and downstream glycolytic pathway.

Methods: To elucidate the underlying pathomechanism, we applied GC/MS-based metabolic profiling analysis of dysferlin-deficient human primary myotubes (c.855-1delG;c.895G>A) and dysferlin knockout (B6.A/J-Dysf^{prmd}) mice after i.v. administration of stable isotope labelled $^{13}C_6$-glucose. Dystrophin-deficient *mdx* (C57BL/10ScSn-Dmdmdx/J) mice served as a control model for other muscular dystrophies. Alterations in protein expression levels were assessed by LC-MS/MS SILAC-based proteomic analysis.

Results: Our GC/MS-based analysis revealed decreased levels of intermediates belonging to the upper glycolytic pathway, whereas metabolites of TCA-cycle associated anaplerotic reactions and fatty acid oxidation were increased in both the cell and mouse model. Metabolic alterations were enhanced in glycolytic type-II muscles. Our LC-MS/MS proteomic analysis confirmed normal metabolic enzyme expression, but we found increased expression of antioxidant enzymes belonging to the thioredoxin/peroxiredoxin family (TRX/PRXS). Furthermore, we detected different isoform expressions of IDH with predominance of IDH2 in oxidative type I muscles and reduction of mitochondrial NAD(P)-transhydrogenase in all muscles of BLA/J mice.

Conclusion: Our analysis enabled a unique insight into the metabolic network of a monogenic disease model *in vitro* and *in vivo*, thereby revealing a strongly disturbed glucose metabolism in dysferlinopathy pointing towards a reduced glucose uptake. Fuel supply was secured by compensatory upregulation of intermediates associated with an oxidative substrate metabolism. Besides that, different isoform expression of IDH in oxidative and glycolytic muscle fibres combined with decreased NAD(P)-transhydrogenase in dysferlinopathy, could further ameliorate progressive muscle damage. Our study provides a new and so far unknown insight into the metabotype of a very rare monogenic disease model, thus predicting a novel and pivotal function of dysferlin, which opens the field for future research into possible therapeutic interventions.

Abstract (German)

Einleitung: Die seltene autosomal-rezessiv vererbbare Gliedergürtelmuskeldystrophie Typ 2B (Dysferlinopathie, Miyoshi Myopathie), beruht auf Mutationen des Dysferlin Gens auf Chromosom 2p13, welches das 230kDa große Transmembranprotein Dysferlin kodiert. Die den Pathomechanismus der Dysferlinopathie begründende Funktion von Dysferlin in der Muskelzelle ist bisher unklar, bekannt ist eine Beteiligung von Dysferlin an der Kalzium-abhängigen Vesikelfusion bei Membranreparatur-vorgängen nach Muskelzelltrauma. Ein interessanter klinischer Aspekt der Dysferlinopathie ist die Koinzidenz des physiologischen Shifts des Skelettmuskels von einem kindlichen, primär oxidativen (Typ I Faser), zu einem adulten, zunehmend glykolytischen (Typ II Faser) Substratmetabolismus und dem Eintreten von postpubertären Initialsymptomen einer progressiven Muskeldystrophie. In wie fern eine Dysregulation im zentralen Muskelmetabolismus in Dysferlin-defizienten Muskeln vorkommt und möglicherweise zum Pathomechanismus der progressiven Muskeldystrophie beiträgt, sollte Ziel dieser Studie sein.

Methodik: Der zentrale Kohlenstoffmetabolismus von Dysferlin-defizienten humanen primären Myotuben (c.855-1delG;c.895G>A) und Mäusen (B6.A/J-Dysf^{prmd}) wurde mittels Gaschromatographie/ Massenspektrometrie (GC/MS) nach Applikation von ^{13}C-markierten stabilen Isotopen im Vergleich zum Wildtyp und einer Dystrophien-defizienten Muskeldystrophiekontrolle (C57BL/10ScSn-Dmdmdx/J) gemessen. Eine SILAC-basierte Flüssigkeitschromatographie/Tandemmassenspektrometrie (LC-MS/MS) basierte Proteomanalyse erfolgte zur Detektion von veränderten Expressionsmustern Metabolismus-assoziierter Proteine.

Ergebnisse: Die GC/MS-basierte metabolische Analyse zeigte deutlich verminderte Level an phosphorylierten Hexosen des oberen glykolytischen Pathways, sowie kompensatorisch erhöhte Metabolitlevel anaplerotischer Reaktionen des Citratzyklus und der Fettsäureoxidation in humanen Myotuben und BLA/J Mäusen. Dieses metabolische Profil war am stärksten im glykolytischen Typ II Muskeln ausgeprägt. Konkludent mit den Skelettmuskelmetabolitverschiebungen fanden sich erhöhte hepatische Syntheseraten von Ketonkörpern in BLA/J Mäusen. Unsere SILAC-basierte Proteomanalyse ergab normale Expressionsmuster der Glykolyse- und Citratzyklus-assoziierten Enzymkomplexe, wobei Proteine der Thioredoxin/Peroxiredoxinfamilie (TRX/PRXs) hochreguliert waren. Darüber hinaus fand sich eine muskelfaserspezifische Isoformexpression der Isocitratdehydrogenase (IDH) und eine deutliche Reduktion der mitochondrialen NAD(P)-Transhydrogenase in Dysferlin-defizienten Skelettmuskeln.

Schlussfolgerung: Unsere Proteom- und Metabolomanalyse *in vivo* und *in vitro* ermöglichte die Aufschlüsselung eines komplexen metabolischen Netzwerkes in einem monogenetischen Krankheitsmodell und die Identifizierung von pathologischen Alterationen in der Glykolyse und dem Citratzyklus. Wir fanden Dysferlin-spezifische, verminderte Level von Intermediaten der oberen Glykolyse – vermutlich durch

einen eingeschränkten Glukoseuptake in die Muskelzelle – sowie eine kompensatorische Erhöhung der Fettsäureoxidation und anaplerotischer, Citratzyklus assoziierter, Metabolite. Darüber hinaus konnten wir zeigen dass Dysferlindefizienz erhöhten oxidativen Stress in der Zelle bedingt und die Kombination aus muskelspezifischer IDH Isoform Expression zusammen mit deutlich reduzierter mitochondrialer NAD(P)-Transhydrogenase zur weiteren Muskelzellschädigung beitragen kann. Unsere GC/MS- und LC-MS/MS-basierte Analyse erbrachte neue Ergebnisse auf dem Weg zur Entschlüsselung des Pathomechanismus einer seltenen, bislang noch nicht vollständig verstandenen Erkrankung und legt damit einen Grundstein für weitere molekularbiologische Forschung und potentielle therapeutische Ansätze zur Verlangsamung der progressiven Muskelzellschädigung.

1. Introduction

1.1 Limb girdle muscular dystrophies (LGMD)

Limb girdle muscular dystrophies were first described in the mid-20th century, subsuming a clinically and genetically heterogeneous group of non-congenital muscular dystrophies, which differ substantially from the first encountered x-linked Duchenne-Becker and autosomal dominant facioscapulohumeral muscular dystrophies (Walton and Nattrass 1954; Walton 1956; Emery 1998). Classification into autosomal-dominant (LGMD 1 or AD-LGMD) and autosomal-recessive (LGMD 2 or AR-LGMD) subtypes is based on the underlying genetic defect and proteins involved (Bushby 1996). Beyond that, there are major differences concerning the clinical phenotype, laboratory findings and disease progression. According to that, limb girdle muscular dystrophies type 2 usually exhibit a more severe phenotype with higher levels of serum creatine kinase (sCK) and an earlier onset of disease, more resembling Duchenne type muscular dystrophy (Emery 1998; Nigro, Aurino et al. 2011). To date eight limb girdle muscular dystrophies of autosomal-dominant and sixteen of autosomal- recessive inheritance have been identified (Nigro, Aurino et al. 2011). Nevertheless about one third of patients still remain without any genetic diagnosis (Nigro, Aurino et al. 2011). Table 1.1 gives a detailed classification of limb girdle muscular dystrophies that have been identified. Precise diagnosis of limb girdle muscular dystrophies can be challenging regarding the vast clinical and genetic variability especially in patients without a clear family history (Guglieri, Straub et al. 2008). Generally speaking, clinical presentation usually comprises a symmetric pattern of progressive muscle weakness and wasting - initially pronounced at the pelvic and shoulder girdle - high levels of serum creatine kinase (sCK) and specific histological and immunohistochemical changes like centralization of nuclei, fibre size variation, necrosis and fibrosis. (Spuler 2004; Urtizberea, Bassez et al. 2008). Disease onset ranges from early childhood in sarcoglycanopathies to late adulthood in dysferlinopathy and progression is usually milder relative to childhood muscular dystrophies (Laval and Bushby 2004). Most important for finding the precise diagnosis is the distinct pattern of muscle involvement. Here MRI may be a powerful tool to assess this question (Wattjes, Kley et al. 2010).

Table 1.1 Classification of autosomal dominant and recessive LGMD. Adapted from (Kaplan 2011; Nigro, Aurino et al. 2011).

		Gene			Clinical phenotype			
Disease	**Locus**	**Name**	**Exons**	**Protein**	**Onset**	**Progression**	**Cardiomypathy**	**sCK**
Autosomal dominant limb girdle muscular dystrophy								
LGMD1A	5q31	***MYOT***		Myotilin	Adulthood	Slow	Not observed	3-4x
LGMD1B	1q11-q21	***LMNA***		Lamin A/C	4-38y	Slow	Often observed	1-6x
LGMD1C	3p25	***CAV3***		Caveolin 3	Childhood	Slow-moderate	Frequent	10x
LGMD1D	7q36			?	Adulthood	Slow	Not observed	1-3x
LGMD1E	6q23			?	Adulthood	Slow	Often	2-4x
LGMD1F	7q32			?	1-58y	Rapid	Not observed	
LGMD1G	4p21			?	Adulthood	Slow	Not observed	1-9x
LGMD1H	3p23-p25			?	10-50y	Slow	Not observed	1-10x
Autosomal recessive limb girdle muscular dystrophy								
LGMD2A	15q15.1	***CAPN3***		Calpain 3	Adolescence	Moderate - rapid	Rarely observed	3-20x
LGMD2B	2p13	***DYSF***		Dysferlin	Young adulthood	Slow	Possible	5-40x
LGMD2C	13q12	***SGCG***		γ-Sarcoglycan	Early childhood	Rapid	Often severe	10-70x
LGMD2D	17q12-21.33	***SGCA***		α-Sarcoglycan	Early childhood	Rapid	Rare	10-70x
LGMD2E	4q12	***SGCB***		β-Sarcoglycan	Early childhood	Rapid	Often severe	10-70x
LGMD2F	5q33	***SGCD***		δ-Sarcoglycan	Early childhood	Rapid	Often severe	10-70x
LGMD2G	17q12	***TCAP***		Telethonin	Adolescence	Slow	Yes	10x
LGMD2H	9q31-q34	***TRIM32***		Tripartite motif containing 32	Adulthood	Slow	Not observed	5-15x
LGMD2I	19q13.3	***FKRP***		Fukutin-related protein	Late childhood	Moderate	Yes	10-20x
LGMD2J	2q31	***TTN***		Titin	Young adulthood	Severe	Not observed	10-40x
LGMD2K	9q34	***POMT1***		Protein-O-mannosyl-transferase 1	Childhood	Slow	Not observed	10-40x
LGMD2L	11p14.3	***ANO5***		Anoctamin 5	Young-late adult-hood	Slow	Not observed	10-15x
LGMD2M	9q31-q33	***FKTN***		Fukutin	Early childhood	Moderate	Sometimes	10-70x
LGMD2N	14q24	***POMT2***		Protein-O-mannosyl-transferase 2	Early childhood	Slow	Rare	5-15x
LGMD2O	1p34	***POMGnT1***		Protein-O-linked mannose beta 1, 2-N-acetyl-glucosaminyltransfer-ase	Late childhood	Moderate	Not observed	2-10x
LGMD2Q	8q24	***PLEC1***		Plectin				
Recessive form with α-dystroglycan defect **(LGMD2P)**	3p21	***DAG1***		Dystroglycan	Early childhood	Moderate	Not observed	20x

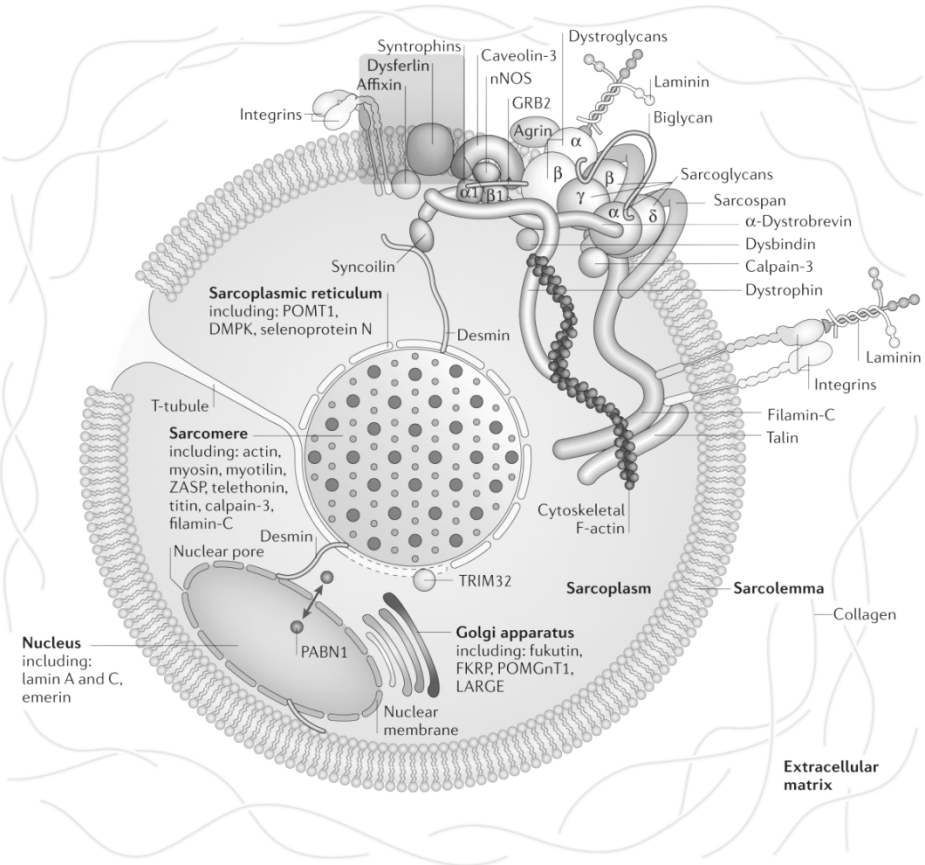

Figure 1.1 Localization of LGMD-associated proteins in the muscle cell. Adapted from (Davies and Nowak 2006).

1.2 Dysferlinopathies

1.2.1 Overview

Dysferlinopathy encompasses a wide range of muscular disease phenotypes, characterized by a complete or partial absence of dysferlin in the skeletal muscle due to mutations in the gene encoding dysferlin (*DYSF*) (Bashir, Keers et al. 1996; Liu, Aoki et al. 1998). The term dysferlinopathy was coined just fourteen years ago in 1998, when two laboratories in Newcastle and Boston, were each able to prove independently that Miyoshi myopathy and LGMD 2B were allelic disorders, caused by the same gene defect on chromosome 2p13 (Bashir, Keers et al. 1996; Liu, Aoki et al. 1998; Urtizberea, Bassez et al. 2008). To date, three clinical phenotypes of dysferlinopathy have been reported, Miyoshi myopathy (MM), limb girdle muscular dystrophy 2B (LGMD 2B) and the distal myopathy with anterior tibial onset (DMAT) (Illa, Serrano-Munuera et al. 2001). Despite that, cases of atypical presentation like pseudometabolic

forms and proximal distal phenotypes have been described in small cohorts (Nguyen, Bassez et al. 2005). As an autosomal-recessive order of inheritance, prevalence of dysferlinopathy is higher in populations with greater incidence of consanguinity. In Israel, Maghreb, India, Saudi Arabia and Iran dysferlinopathy emerges as the second common cause of recessive limb girdle muscular dystrophy in adults after calpainopathy (LGMD 2A) (Nalini and Gayathri 2008; Urtizberea, Bassez et al. 2008). In the United States dysferlinopathy is estimated to account to 15 percent of limb girdle muscular dystrophies (Moore, Shilling et al. 2006).

The clinical phenotype of DYSF mutations presents rather heterogeneous, ranging from severe functional disability with loss of ambulation to mild late-onset forms (Klinge, Dean et al. 2008; Rosales, Gastier-Foster et al. 2010). Except some outliners with very early or very late disease onset (Klinge, Dean et al. 2008; Paradas, Gonzalez-Quereda et al. 2009), all distinct phenotypes have in common the age of presentation around 17-25 years and, compared to other muscular dystrophies, the peculiar aspect that muscle strength and sporting achievements are within the normal range until onset of disease (Bushby 2009; Klinge, Aboumousa et al. 2010). Serum creatine kinase is usually massively elevated up to 20 -150 times above the normal range (Mahjneh, Passos-Bueno et al. 1996) and an acute presentation together with a frequent inflammatory infiltrate in the muscle biopsy can easily lead to the misdiagnosis of polymyositis (Rowin, Meriggioli et al. 1999; McNally, Ly et al. 2000; Gallardo, Rojas-Garcia et al. 2001; Bushby 2009). Cardiac involvement in dysferlinopathy is still a matter of debate. Stress - and exercise - induced cardiomyopathy leading to left ventricular dysfunction have been described independently by our group with mouse and patient data and by the group of Kevin Campbell (Han, Bansal et al. 2007; Wenzel, Geier et al. 2007).

1.2.2 Diagnosis

1.2.2.1 Histopathology

Muscle histopathological findings are common dystrophic changes represented by a variation of fibre size, increased content of endomysial and perimysial connective tissue, centralized nuclei and fatty infiltration at an advanced stage of disease (Mahjneh, Passos-Bueno et al. 1996; Urtizberea, Bassez et al. 2008). No correlation of muscle biopsy alterations, serum creatine kinase levels and clinical severity have been observed so far (Mahjneh, Passos-Bueno et al. 1996; Fanin and Angelini 2002).

Apart from that, muscle specimens harboring dysferlin mutations in exons corresponding to the second or third C2 domain, showed deposits of amyloid, suggesting a dysferlin-connected proteolytic cleavage product. Hence, dysferlinopathy was found to be the first muscular dystrophy featuring amyloidosis (Spuler, Carl et al. 2008). Interestingly, Fanin and Angelini first described a marked shift in fibre type distribution towards a predominance of type I fibres in an advanced stage of disease (Fanin and Angelini 2002). Whether these changes are caused by selective type II fibre atrophy or a compensatory transfor-

mation into oxidative type I fibres remains unclear. Inflammatory processes are characterized by a moderate to marked increase of MHC-I and macrophage invasion in the majority of muscle specimens. Major differences between immunopathological characteristics of dysferlinopathy and inflammatory myopathies like polymyositis, are significantly lower numbers of CD8+ T lymphocytes and inflammatory cell distribution within the muscle fibre, which enables a clear distinction in most of the cases – albeit cases of resemblance have been reported (Rowin, Meriggioli et al. 1999; Gallardo, Rojas-Garcia et al. 2001; Confalonieri, Oliva et al. 2003). Furthermore, down-regulation of the decay-accelerating factor CD55 (DAF/CD55) in skeletal muscle biopsies of dysferlin-deficient mice and patients is supposed to be decisive for the deposition of the membrane attack complex (MAC) on the surface of non-necrotic muscle fibres, sequentially leading to an increased susceptibility to complement attack (Selcen, Stilling et al. 2001; Wenzel, Zabojszcza et al. 2005; Han, Frett et al. 2010). Reduction or total absence of dysferlin at the sarcolemma is visualized by immunohistochemistry using monoclonal antibodies directed against two far-apart epitopes of dysferlin (Anderson, Davison et al. 1999). Immunoblotting and DNA analysis of muscle specimens or peripheral blood monocytes (PBM) provide additional tools to confirm the diagnosis (Ho, Gallardo et al. 2002; De Luna, Freixas et al. 2007).

1.2.2.2 Clinical phenotypes

Miyoshi myopathy (OMIM #254310)

Miyoshi myopathy was the first phenotype described in 1967 by the Japanese physician Miyoshi. Miyoshi reported four patients from two consanguineous families, presenting with a late-onset distal myopathy, high levels of serum creatine kinase and recessive inheritance scheme. Nowadays, Miyoshi myopathy is the most common form of autosomal-recessive distal myopathy. Main characteristics of Miyoshi myopathy are an initial affectation of the gastrocnemius muscle from the late teens to early adulthood accompanied by a massive elevation of creatine kinase, lactic dehydrogenase (LDH) and aldolase. Clinical correlation is the inability of tiptoe-standing and progressive difficulties in descending stairs (Urtizberea, Bassez et al. 2008). Disease progression is usually estimated as slow, with only one third of patients getting wheelchair bound within approximately ten years after disease onset (Bushby 1999). Surprisingly, contrary to the clear clinical distinction of phenotypes in dysferlinopathy, MRI analysis of twenty-nine patients with confirmed DYSF mutation showed an overall similar affection of gastrocnemius medialis and adductor magnus muscle at an early stage of muscle disease (Paradas, Llauger et al. 2010).

Limb girdle muscular dystrophy 2B (LGMD 2B, OMIM #253601)

Despite great resemblance between LGMD 2B and MM, especially in the later disease stages, initial clinical presentation shows a rather distinct pattern of muscle involvement. In the LGMD phenotype, distribution of muscle weakness is predominant in the proximal pelvic muscles, causing difficulties climbing stairs, whereas periscapular muscles are relatively spared in the early course (Urtizberea, Bassez et al.

2008). Disease progression is estimated to be slow and loss of ambulation occurs in the fourth decade of life (Kirschner and Bonnemann 2004). Similar to Miyoshi myopathy, serum creatine kinase levels tend to be very high, particularly in the early stages of the disease. Involvement of distal muscles usually occurs after years and results in a mixed phenotype (Mahjneh, Passos-Bueno et al. 1996).

Distal myopathy with anterior tibial onset (OMIM #606768)

This phenotype, also known as distal anterior compartment myopathy (DACM), represents a new entity of dysferlinopathy. Illa et al. first reported this phenotype in a Spanish consanguineous family carrying a homozygous DYSF mutation, but showing an atypical clinical presentation with different muscle involvement compared to the phenotypes described previously (Illa, Serrano-Munuera et al. 2001). During disease progression, muscle weakness also shifts to the posterior compartment of the lower leg, beginning to resemble Miyoshi myopathy (Urtizberea, Bassez et al. 2008).

1.2.3 Dysferlin

The mammalian dysferlin gene (DYSF) is located on chromosome 2p13, encompasses 55 exons and produces a 230kD transmembrane protein consisting of seven intracellular C2-domains and a short twelve amino acid C-terminal extracellular domain (Matsuda, Aoki et al. 1999).

Dysferlin expression ranges from kidney cells to monocytes, with particular abundance in skeletal and cardiac muscle (Bashir, Britton et al. 1998; Liu, Aoki et al. 1998; Ho, Gallardo et al. 2002). Recent studies identified 14 isoforms of DYSF, differently expressed in mammalian tissues. Among these, isoform 8 constitutes the major transcript in skeletal muscle, albeit not expressed in monocytes, where isoform 13 is favourably present (Pramono, Tan et al. 2009). Localization of dysferlin is predominantly at the muscle surface membrane in adult muscle and the t-tubules during embryonic development (Anderson, Davison et al. 1999; Matsuda, Aoki et al. 1999; Piccolo, Moore et al. 2000; Klinge, Laval et al. 2007). Furthermore Piccolo et al. described an accumulation of vesicles in the skeletal muscle cell cytoplasm of Miyoshi myopathy patients, leading them to the assumption that in healthy skeletal muscle, dysferlin might be associated with vesicles influencing their intracytoplasmic transport (Piccolo, Moore et al. 2000).

1.2.3.1 Ferlin family

Dysferlin is a homologue of the *Caenorhabditis elegans* fer-1 gene, which mediates fusion of intracellular vesicles to the spermatid plasma membrane during spermatogenesis (Ward, Argon et al. 1981; Achanzar and Ward 1997). The essential role of dysferlin in promoting membrane fusion and transport of vesicles is comprehensible, considering the fact that fer-1 mutants exhibit a major defect in membrane fusion, leading to shortened pseudopodia and immobile spermatozoa (Glover and Brown 2007). To date, six human and mice ferlin-like genes have been identified, forming the ferlin family: dysferlin (Fer1L1), otofer-

lin (Fer1L2), myoferlin (Fer1L3) and Fer1L4-6 (Lek, Lek et al. 2010; Posey, Demonbreun et al. 2011). Only two of them, dysferlin and otoferlin, are predicted to be associated with human disease (Glover and Brown 2007). Otoferlin is mainly expressed in the inner ear sensory hair cells, mutation was found to cause the autosomal-recessive nonsyndromic prelingual deafness (DFNB9) (Yasunaga, Grati et al. 1999). Myoferlin is a type II transmembrane protein, expressed in striated muscle, but in contrast to dysferlin, which is highly abundant in mature myofibres, myoferlin is mainly found in immature and early differentiating myoblasts, where it is primarily enriched at contraction sites (Doherty, Cave et al. 2005). Like dysferlin, expression of myoferlin levels is extremely increased upon muscle injury (Doherty, Cave et al. 2005).

1.2.3.2 Dysferlin mutations

The huge dysferlin gene located on chromosome 2p13 contains 55 coding exons and spans about 150kb of genomic DNA (Aoki, Liu et al. 2001). Produced is a cDNA around 6.9kb and a dysferlin protein of 2,088 amino acids (Liu, Aoki et al. 1998). Regarding the large size of the DYSF gene, spanning a genomic locus about 233kbp, screening and identification of disease-causing mutations is a quite challenging task. Beyond that, genetic diagnosis is further impeded by a large mutational spectrum, consisting of an ever-growing quantity of point mutations, small deletions and insertions, which are wildly spotted over the entire coding sequence and canonical splice sites, sequentially resulting in missense, frameshift and nonsense mutations, which lead to a premature truncation of the dysferlin protein (Liu, Aoki et al. 1998; Aoki, Liu et al. 2001; Nguyen, Bassez et al. 2005). According to the Leiden Muscular Dystrophy database (http://www.dmd.nl), which was established in 1998, 455 unique DNA sequence variants, either disease-causing or polymorphisms, have been reported until March 2012. A complex bioinformatics tool additionally enabling the interactive analysis of mutational data and sequence variants is provided by The Universal Mutation Database (UMD-DYSF). Among the total number of 401 index cases (557 mutations) entered, 266 disease-causing coding sequence variants were identified, 175 (65.8%) of them single base substitutions, 54 (20.3%) deletions, 26 (9.8%) duplications, 6 (2.3%) insertions and 5 (1.9%) insertions/deletions (Blandin, Beroud et al. 2012). Furthermore, seven of the disease-causing mutations have been suggested as founder mutations in patients from different geographical areas and genetic origins, 51 mutations were additionally found among three non-related index patients (Blandin, Beroud et al. 2012).Various properties of zygosity have been described in dysferlinopathy patients, among them, homozygous mutations are holding the majority, although compound heterozygous mutations composed of splice-site variants and missense variants are reported frequently (Wenzel, Carl et al. 2006; Krahn, Beroud et al. 2009).

1.2.3.3 Dysferlin function

An important step towards understanding the functional role of dysferlin is the knowledge of its location and connection to the dystrophin-glycoprotein complex (DGC) inside the muscle cell. Figure 1.2.3.3 gives an overview.

Various muscular dystrophies, like Duchenne/Becker MD are linked to mutations in components of the DGG, which plays an important role in the connection between the muscle cell's sub-sarcolemma cytoskeleton and extracellular matrix (Campbell and Kahl 1989; Cohn and Campbell 2000; Durbeej and Campbell 2002). Disruption causes instability of the sarcolemma, leading to an increased susceptibility of contraction-induced injuries (Petrof, Shrager et al. 1993). However, in dysferlinopathy no instability of the DGC has been observed, suggesting an alternative pathway of muscular dystrophy due to another mechanism of exercise-induced muscle damage. In 2003 two studies confirmed the role of dysferlin in membrane repair following injury (Bansal, Miyake et al. 2003; Lennon, Kho et al. 2003). Dysferlin was shown to interact with annexins A1 and A2 after injury in a calcium-dependent manner, thereby contributing to intracellular vesicle trafficking and fusion for membrane healing. In dysferlinopathic muscle interaction and thus membrane healing is disrupted (Lennon, Kho et al. 2003). The so called patchy repair hypothesis of dysferlin function in vesicle transport is strengthened by the functional role of the homologous fer-1 protein, described above, and an abnormal accumulation of vesicles at the plasma membrane, which is visible under the electron microscope (Selcen, Stilling et al. 2001). A study by Chiu and coworkers published in 2009 underlines the predicted role of dysferlin in membrane sealing through patch repair vesicle fusion by extending it to a participation of dysferlin in the release of vesicles containing cytokines, which sequentially causes impaired neutrophil recruitment and prolonged inflammatory intervals (Chiu, Hornsey et al. 2009).

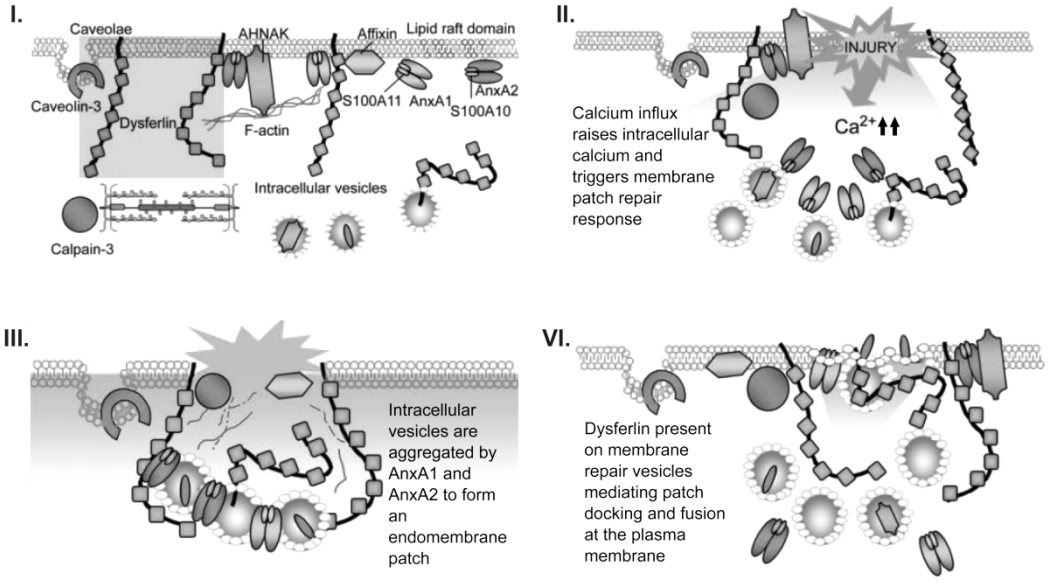

Figure 1.2.3.3 Dysferlin function and interaction in membrane repair upon injury. Adapted from (Glover and Brown 2007).

1.2.3.4 Protein interactions of dysferlin

Various interactions of dysferlin with other proteins like AHNAK, calpain-3, caveolin-3 and the previously mentioned Annexins A1 and A2 have been published so far (Matsuda, Hayashi et al. 2001; Lennon, Kho et al. 2003; Huang, Laval et al. 2007; Huang, de Morree et al. 2008).

Annexins

Annexins are calcium and phospholipid-binding proteins involved in the aggregation of intracellular vesicles and lipid rafts at the cytosolic surface the plasma membrane (Lambert, Gerke et al. 1997; Babiychuk and Draeger 2000). Dysferlin interacts with annexins A1 and A2 in a calcium-dependent manner upon injury. In dysferlinopathic muscle, distribution of Annexins and the efficiency of sarcolemmal wound-healing are significantly disrupted (Lennon, Kho et al. 2003).

Calpain-3

Calpain-3, a skeletal muscle specific protein and member of the calpain superfamily of calcium-dependent cysteine proteases, is suspected of being implicated in muscles patch fusion repair through its interaction with annexin A1 and A2 (Goll, Thompson et al. 2003; Lennon, Kho et al. 2003). Predicted function of calpain-3 is the cleavage of both proteins during membrane insertion via putative calpain recognition sequences in their amino termini (Barnes and Gomes 2002).

AHNAK

Another interaction partner of dysferlin is the 700kD protein AHNAK (Desmoyokin), which is highly expressed in muscle cells (Gentil, Delphin et al. 2003). The functional role of AHNAK in the skeletal muscle remains largely unknown, although in myotubes AHNAK was found to accumulate inside enlargeosomes - cytoplasmic vesicle determined for exocytosis after intracellular Ca^{2+} rising (Zacharias, Purfurst et al. 2011). Co-localization is found at the sarcolemma and t-tubules, where interaction occurs via binding sites of the dysferlin C2A domain and the carboxyterminal domain of AHNAK. In dysferlinopathies, reduction or absence of dysferlin was shown to correlate with a secondary reduction of AHNAK, losing its localization at the sarcolemmal site of the muscle fibre (Huang, Laval et al. 2007). Furthermore, immunohistochemical analysis of myotubes and muscle samples obtained from calpainopathy (LGMD 2A) and dysferlinopathy patients revealed a predominant localization of AHNAK1 in the extracellular matrix compared to healthy controls (Zacharias, Purfurst et al. 2011).

Caveolin-3

Caveolin-3 is a muscle-specific member of the caveolin family constituting the major structural component of caveolae membranes, which are 50-150 nm invaginations in the plasma membrane found in most cell types (Parton 1996). Caveolin-3 mutations are the underlying pathogenesis for the dominantly inherited limb girdle muscular dystrophy type 1C (LGMD 1C) (Minetti, Sotgia et al. 1998) and rippling mus-

cle disease (Betz, Schoser et al. 2001). In striated muscle, dysferlin and caveolin show a partial co-localization at the sarcolemma and they precipitate with the dihydropyridine receptor, an L-type Ca^{2+} channel localized at T-tubules (Matsuda, Hayashi et al. 2001; Ampong, Imamura et al. 2005; Hernandez-Deviez, Martin et al. 2006). In caveolin-1 and caveolin-3 mutant cell lines, dysferlin association with the plasma membrane is remarkably reduced and an accumulation in the Golgi complex occurs, suggesting a functional role of caveolin in post-Golgi transport, possibly by forming specialized caveolin carriers (Hernandez-Deviez, Martin et al. 2006).

1.2.3.5 Animal models of dysferlinopathy

Several mouse models either harbouring a naturally occurring or an induced dysferlin mutation are available for research aims. Major differences exist in disease onset, prevalent sites of muscle lesions and skeletal muscle gene-expression profiles.

A/J mice

The A/J strain harbours a naturally occurring dysferlin mutation due to an ETn retrotransposon insertion of 5-6kb into intron 4 of the dysferlin gene. First histological signs of muscular dystrophy are usually detected between 4-5 month of age, but disease progression is estimated to be slower compared to SJL/J, *Dysf* -/- (Campbell/Brown) and C57BL/10.SJL mice (Ho, Post et al. 2004; Kobayashi, Izawa et al. 2010). It is worth mentioning, that A/J as well as SJL/J mice do not exhibit any clinical signs of muscle weakness, which makes it almost impossible to conduct physiological studies. As in *Dysf* -/- (Brown) mice, abdominal muscles are most severely affected, followed by proximal and distal muscles later on. Interestingly, A/J mice are also more susceptible to malignant diseases like lung adenomas and mammary adenocarcinomas. Furthermore, A/J mice are homozygous for an age-related hearing loss allele (Cdh23 gene) and for haemolytic complement deficiency (C5, Hc gene). Control strains are A/HeJ, A/WySnJ mice.

SJL/J mice

Like A/J mice, this inbred strain contains a naturally occurring dysferlin mutation in the 3' splice junction, causing an mRNA deletion of exon 45 (171 base pairs, aa1628-1685) (Bittner, Anderson et al. 1999; Vafiadaki, Reis et al. 2001). Compared to A/J mice, first histological signs of muscle weakness are detected earlier, around 1 month of age (Weller, Magliato et al. 1997). Remarkably, mice develop a severe muscular atrophy around the 10^{th} month of age, rapidly leading to fatty infiltration and replacement of muscle tissue. Extramuscular characteristics are lymphomas, autoimmune disorders with higher incidence of viral infections and a high aggression potential in male mice. Furthermore, a higher susceptibility to many induced autoimmune diseases like experimental autoimmune encephalitis (EAE) and inflammatory myopathy have been described (Bernard and Carnegie 1975). Unfortunately, there is no control mouse model available.

BLA/J mice (B6.A-Dysfprmd/GeneJ)

This mouse model was generated by the laboratory of Isabelle Richard by crossing the progressive muscular dystrophy (prmd) allele (ETn retrotransposon insertion into dysferlins intron 4) from the A/J inbred strain onto a C57BL/6 genetic background (Lostal, Bartoli et al. 2010). Histological signs are characterized by centronucleated fibres and areas of inflammation at 2 month of age, most affected muscles are psoas, quadriceps femoris, tibialis anterior and gastrocnemius muscle. Due to the A/J genetic background, disease progression is also slightly slower compared to other dysferlinopathy mouse models. C57BL/6 mice serve as controls for homozygous BLA/J.

Dysferlin -/- mice

Two dysferlin knock out strains, both harbouring the same deletion in exons 53-55 of the dysferlin gene, are available. Mutation was generated by replacement of a 12kb region, spanning over the last three coding exons, with a targeting vector containing a neomycin resistance gene. This construct was then electroporated into (129X1/SvJ x 129S1/Sv)F1-Kit+-derived R1 embryonic stem cells (ES) and correctly targeted ES injected into blastocytes (Bansal, Miyake et al. 2003). The major genetic difference between these two Dysf -/- mice was the backcrossing strategy. Whereas B6.129-Dysf^{tm1Kcam}/J mice were backcrossed for seven generations onto a C57BL/6 background, the 129-Dysftm1Kcam/J mouse strain was maintained on a 129 background. Joint clinical and histological signs are necrotic and centrally nucleated fibres by the age of two months, leading to a full pattern of muscular dystrophy by the age of 8 months. Disease progression is comparable to SJL/J and faster than A/J mice. Controls for both strains are C57BL/6 mice.

1.3 Skeletal muscle energy metabolism

With over 40 % of body mass, skeletal muscle is essential for systemic homeostasis and regulation of the whole body energy metabolism. Various systemic and muscular disorders have been implicated with alterations in skeletal muscle energy consumption and storage, like metabolic myopathies and type-2 diabetes. To understand the underlying pathomechanisms, a detailed overview of the main pathways for energy metabolism in muscle is of great value.

1.3.1 Skeletal muscle composition and fibre types

Mammalian and human skeletal muscles are composed of two main muscle fibre types based on different enzymatic characteristics of myosin ATPase activity and molecular species of myosin heavy chain (MyHC). Slow twitching type I muscle fibres are highly abundant in mitochondria and myoglobin, supporting their oxidative metabolism during long-lasting contractions, like maintenance of body posture.

Fast twitching type II muscle fibres are further divided into three subtypes: Type IIa and IIx (also known as IId) fibres contain high levels of glycogen which serves as the main glycolytic energy resource during short contractions of high intensity, as performed in sprints. Fast twitching type IIa fibres on the other hand, are metabolically more oxidative, comparable to their type I counterpart. Muscle fibres are classified based on their different expression of myosin heavy chain isoforms (MyHC), type I muscle fibres express MyHCIβ and type II fibres MyHCIIa, MyHCIIb and MyHCIIx, respectively (Schiaffino and Reggiani 1994; Pette and Staron 2000). Beyond that, other markers have been described, including the sarcoplasmic reticulum calcium ATPase pumps (SERCA) 1 and 2, the cardiac troponin C (Tnnc1) in cardiac and slow type muscle fibres and troponin C/STNC (Tnnc2) in fast twitch muscle fibres (Dhoot and Perry 1979; MacLennan and Toyofuku 1992). Remarkably, the fibre type distribution in skeletal muscle is not an unchangeable condition, but rather a dynamic process due to the capability of muscle fibres to adapt another phenotype profile in respond to altered functional demands (Suarez 2003). Several studies focusing on oxygen consumption levels, ADP, pH and lactate levels during exercise, indicate that there are marked age-dependent differences in muscle energy metabolism, especially before and after puberty (Timmons, Bar-Or et al. 2003; Stephens, Cole et al. 2006; Timmons, Bar-Or et al. 2007). Muscle energy consumption in children follows an almost oxidative, type I fibre pathway, whereas higher levels of glycolytic, type II fibre carbohydrate utilization, corresponding to an increase in lactate levels upon exercise, have been observed in adults (Taylor, Kemp et al. 1997; Stephens, Cole et al. 2006; Armstrong and Barker 2009).

Recent advances in mass spectrometry-based shotgun proteomics have opened the field for the analysis of several proteins involved in the different metabolic phenotypes of type I and type II muscle fibres. These proteome analyses support previously published data (Gleeson 1983; Takekura and Yoshioka 1987), according to which both fibre types also exhibit a markedly different protein expression pattern with high abundance of glycolysis driving enzymes in type II fibres and oxidative (TCA-cycle) enzymes in type I fibres (Okumura, Hashida-Okumura et al. 2005; Drexler, Ruhs et al. 2011).

Table 1.3.1 Human and mouse skeletal muscle fibre type characteristics

Fiber type	Metabolism	Contraction	MHC gene	MyHC isoform	ATPase stain pH 4.3	ATPase stain pH 4.6	ATPase stain pH 10.4
MOUSE							
I	oxidative	slow	MYH7	**Iβ**	●	●	○
IIa	oxidative	fast	MYH2	**IIA**	○	◐	◑
IIb	glycolytic	fast	MYH4	**IIX**	○	◐	◐
IIx/d	glycolytic	fast	MYH1	**IIx**	○	◑	◑
HUMAN							
I	oxidative	slow	MYH7	**Iβ**	●	●	◐
IIa	oxidative	fast	MYH2	**IIA**	○	○	◑
IIb	glycolytic	fast	MYH4	**IIX**	○	◐	●
IIc	hybrid	hybrid	mixed	**Hybrid I/IIA**	◐	●	●
IId	glycolytic	fast	MYH1	**IIx**	○	◑	●

1.3.2 Glucose uptake

The physiological regulation of glucose uptake into muscle cells not only requires a proper regulation of the glucose transporter (GLUT4), but also depends on systemic conditions like blood glucose content, muscle blood flow, capillary recruitment and the activity of hexokinase, which irreversibly traps glucose once it enters the cell by phosphorylating it to glucose-6-phosphate (Wasserman, Kang et al. 2011). Under basal conditions skeletal muscle contributes up to 25 % of glucose uptake, enhancement up to 75 % occurs after insulin stimulation (DeFronzo, Bonadonna et al. 1992).

Two main pathways contribute to the muscle glucose uptake *in vivo*: In resting muscle, glucose uptake followed by either glycolysis or glycogen storage is realized by activation of the insulin receptor (IR) tyrosine kinase upon insulin stimulation. Downstream substrate activation takes places after docking of muscle specific insulin receptor substrate-1 (IRS-1) to the insulin receptor, finally leading to an insulin-stimulated GLUT4 translocation to the plasma membrane (Krook, Wallberg-Henriksson et al. 2004). The second pathway is enabled during muscle exercise/contraction or hypoxia through activation of 5'-AMP-activated kinase (AMPK) subsequently resulting in GLUT4 being transported to the plasma membrane

(Vavvas, Apazidis et al. 1997; Hayashi, Hirshman et al. 1998). No matter which pathway is activated, both rely on the translocation of the glucose transporter GLUT4, the predominant isoform in skeletal muscle.

1.3.3 Glycolysis

Skeletal muscle glycolysis occurs under aerobic and anaerobic conditions and constitutes one of the main metabolic pathways for providing cells with energy in the form of adenosine triphosphate (ATP) and nicotinamide adenine dinucleotide (NADH) (Boiteux and Hess 1981). On the enzymatic level, the activity of the four key enzymes is essential for regulating the glycolytic flux: Hexokinase (HK), phosphofructokinase (PFK), pyruvate kinase (PK) and glycogen phosphorylase (UGP). As outlined in Fig. 1.3.3, ten steps are essential for converting glucose to pyruvate. The initial and irreversible step of phosphorylating glucose to glucose-6-phosphate is catalyzed by one of the glycolytic key enzymes, hexokinase, consuming two ATP molecules (Wilson 2003). Two isoforms of hexokinase (type I and II) with different regulatory properties and subcellular localization are expressed in skeletal muscle (Ritov and Kelley 2001). Inhibition of all three isoenzymes is effected by their product, glucose-6-phosphate. Hexokinase type II and III are additionally inhibited by Pi, supporting a rather anabolic metabolism by directing glucose to glycogen synthesis, pentose phosphate way, or lipid synthesis, whereas hexokinase type I inhibition is antagonized by Pi leading to catabolic glucose consumption by anaerobic glycolysis (Wilson 2003). The rate-limiting and ATP-consuming reaction converting fructose-6-phosphate to fructose-1,6-bisphosphate by phosphofructokinase is another step of central importance. Phosphofructokinase exists in three isoforms, PFK-M (muscle), PFK-P (platelets) and PFK-L (liver) (Sola-Penna, Da Silva et al. 2010). In muscle, only PFK-M is subject to a vast range of allosteric regulators, considerably changing the glycolytic activity (Dunaway 1983; Kemp and Foe 1983). For example, ATP, lactate and citrate, indicators for a high glycolytic rate and sufficient supply of energy, inhibit PFK by stabilizing its dimeric formation, whereas ADP, AMP and F2,6BP, as signals for cellular ATP depletion, counteract this inhibition (Zancan, Marinho-Carvalho et al. 2008; Sola-Penna, Da Silva et al. 2010). Another interesting enzyme contributing to the glycolytic pathway by forming phosphoenolpyruvate from 2-phosphoglyceric acid is the muscle specific dimeric enzyme enolase β (2-phospho-D-glycerate hydrolase), which exhibits a different fibre type expression in striated muscle (Keller, Demeurie et al. 2000). Pyruvate kinase is the third glycolytic key enzyme conducting an energy gaining, irreversible transphosphorylation of phosphoenolpyruvate into pyruvate. Four pyruvate kinase isoenzymes are contributed to mammalian tissue, one of these, namely the PK-M1, is muscle specific and the only isoenzyme which displays rather hyperbolic kinetics and no allosteric control (Mattevi, Bolognesi et al. 1996; Munoz and Ponce 2003). Enhancement of catalytic activity is realized by its substrate, phosphoenolpyruvate and the glycolytic intermediate fructose-1,6-bisphosphate, whereas high levels of ATP and presumably acetyl-CoA serve as inhibitors.

Further metabolization of pyruvate, the endproduct of glycolysis, depends on the current status of muscle activity. During high intensive exercise of short to medium duration, lactate dehydrogenase effects the anaerobic metabolization of pyruvate to lactate, resulting in a net glycolytic energy gain of 2 ATP and NADH molecules (Wells, Selvadurai et al. 2009). Under aerobic conditions, pyruvate is decarboxylated to acetyl-CoA by pyruvate dehydrogenase (PDH), which opens the way for further metabolization in the tricarboxylic acid cycle (TCA-cycle) and oxidative phosphorylation (OXPHOS).

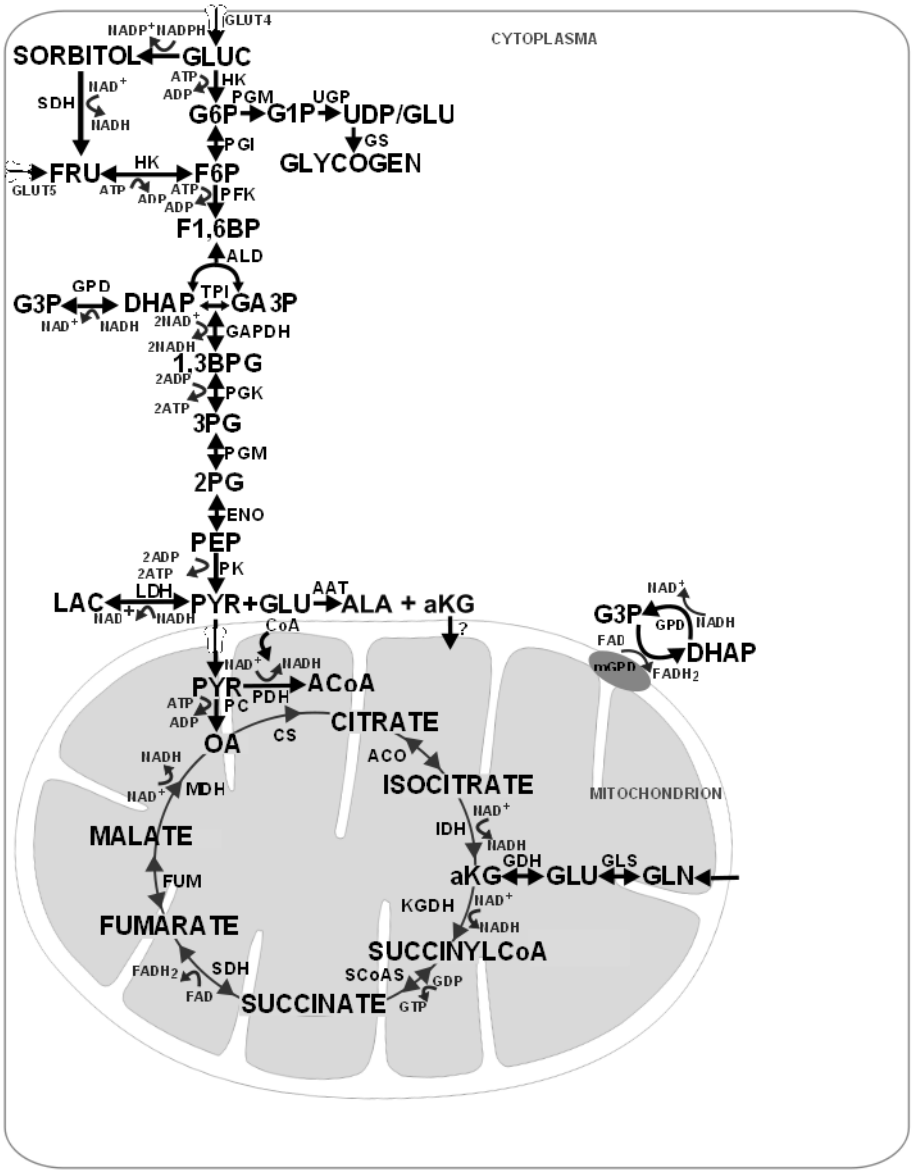

Figure 1.3.3 Central carbon metabolism including polyol way, glycogen synthesis, glutamate metabolism and glycerol-3-phosphate shuttle.

1.3.4 The tricarboxylic acid cycle (TCA-cycle)

This aerobic-oxidative system provides the main metabolic pathway during prolonged muscle activity of low to moderate intensity and permits the production of 30 to 38 molecules of ATP per glucose oxidized (Wells, Selvadurai et al. 2009; Gaster, Nehlin et al. 2012). Main function of the TCA-cycle is the catabolism of acetyl-CoA, derived from carbohydrates, lipids and amino acids, to two molecules of carbon dioxide as well as the liberation of reduction equivalents which are sequentially conducted to the respiratory chain (Gaster, Nehlin et al. 2012). Besides, the TCA-cycle has major anabolic functions, as it is a source for the synthesis of lipids, amino acids and gluconeogenesis, corresponding to the current need of the cell. Anaplerotic reactions take place at various points in the TCA-cycle and are defined as the entry of a carbon molecule into the cycle by routes other than the main reaction of acetyl-CoA with the citrate synthase (CS) (Bowtell, Marwood et al. 2007).

1.3.5 TCA-cycle anaplerosis

To secure energy supply in various daily conditions like exercise or over-night fasting, the TCA-cycle relies on anaplerotic and cataplerotic reactions, either replenishing or draining its intermediate pool size. Focusing on skeletal muscle, one anaplerotic reaction is predicted to be predominant during exercise: The formation of glutamate and pyruvate to α-ketoglutarate and alanine by reaction of alanine-amino-transferase (AAT) (Sahlin, Katz et al. 1990; Gibala, Tarnopolsky et al. 1997). Presumably, this reaction is largely driven by the formation of pyruvate from the glycolytic pathway, as the pyruvate dehydrogenase complex (PDC) activity, forming acetyl-CoA from pyruvate, lags behind the onset of exercise (Constantin-Teodosiu, Peirce et al. 2004). Another anaplerotic reaction catalyzed by glutamate-dehydrogenase (GluDH), forming α-ketoglutarate and ammonium (NH3) from glutamate, does not seem likely to be involved in the exercise-induced increase of intermediates, as studies could not measure any associated ammonium increase (Gibala, Tarnopolsky et al. 1997). Other anaplerotic reactions catalyzed by pyruvate carboxylase (PC) and phosphoenolpyruvate-carboxykinase (PEPCK) do not seem to play a significant part in the exercise-induced replenishment of the TCA-cycle in skeletal muscle (Davis, Spydevold et al. 1980; Gibala, Tarnopolsky et al. 1997). During caloric restriction, amino acids also provide a source of energy by refilling the TCA-cycle. Although most amino acids enter the TCA-cycle as 4- or 5-carbon compounds, only acetyl-CoA produced from their catabolism can be fully oxidized (Owen, Kalhan et al. 2002). The carbon skeleton of asparagine, aspartate, valine and glutamate are used for the synthesis of intermediates or glutamine. They represent alternative anaplerotic mechanisms, despite holding only a small amount in comparison to the alanin-amino-transferase (AAT) reaction (Wagenmakers 1998).

1.3.6 Beta oxidation of free fatty acids

Free fatty acids (FFA), originating from adipose tissue, plasma very low density lipoproteins (VLDL-TG) or intramuscular triacylglycerol (IMTG), are the main energy sources for skeletal muscle during light to moderate or long term exercise (Frayn 2010; Kiens, Alsted et al. 2011). Before FFA are metabolized in the mitochondrial β-oxidation, they are activated by acyl-CoA synthase following transport across the outer and inner mitochondrial membrane catalyzed by the carnitine palmitoyltransferase-1 (CPT-1), the carnitine-acylcarnitin transporter (CACT) and the carnitine-palmitoyltransferase-2 (CPT-2), respectively. Various enzymatic reactions catalyze the β-oxidation reaction chain, including acyl-CoA dehydrogenase, enoyl-CoA hydratase, $_{L}$-3-hydroxyacyl-CoA dehydrogenase, and 3-ketoacyl-CoA thiolase. All reactions lead to a shortening of the fatty acid by two carbons and the production of 1,5 dihydro-flavin adenine dinucleotide ($FADH_2$), nicotinamide adenine dinucleotide (NADH) and acetyl-CoA finally entering the TCA-cycle for further metabolization (Lopaschuk, Belke et al. 1994). β-oxidation of rare odd-numbered fatty acids follows a similar pathway, involving different enzymes but leading to the end products acetyl-CoA and propionyl-CoA, the latter entering the TCA-cycle as succinyl-CoA (Gotoh, Moroda et al. 2008).

1.3.7 Ketone bodies

Ketone bodies, mainly comprising 3-β-hydroxybutyrate (3-HB), acetoacetate (AcAc) and acetone, are life-sustaining metabolites, produced only in the liver mitochondria upon long-term starvation to secure fuel supply for brain, muscle, myocardium and kidney cells. Beyond that, low basal levels of ketone bodies are produced physiologically every day, whereas skeletal muscle accounts for the highest fraction of ketone body metabolism during rest (Balasse and Fery 1989). Besides this essential function, ketone bodies suppress muscle protein degradation and lipolysis, thereby protecting energy stores and prolonging survival during starvation (Wu and Thompson 1990; Taggart, Kero et al. 2005). Synthesis of ketone bodies in perivenous hepatocytes takes places when acetyl-CoA, derived from β-oxidation of fatty acids, accumulates due to low levels of glycolysis (Finn and Dice 2006). Oxaloacetate, condensing with acetyl-CoA in the rate-limiting step of the TCA-cycle, is decreased during low levels of glycolysis and is preferentially used for gluconeogenesis. Accumulating acetyl-CoA sequentially undergoes different conversion steps forming acetoacetate, further reduced to 3-β-hydroxybutyrate. Acetoacetate and 3-β-hydroxybutyrate are short chain (4-carbon) organic acids which can freely diffuse across cell membranes, necessary to provide the brain with energy (Pardridge 1991). Extrahepatic mitochondrial ketolysis involves two key steps and leads to a liberation of acetyl-CoA as energy source for TCA-cycle metabolization (Laffel 1999).

1.4 Mass spectrometry

1.4.1 Proteomics

The term proteomics comprises the entirety of all proteins expressed in a certain state of an organism's entire genome. A common technique since the 1970s is the two dimensional gel-electrophoresis (2-D-PAGE), allowing the separation and estimation of the abundance of many proteins. However, major disadvantages of 2-D gel-electrophoresis are the difficulties of resolving proteins with low abundance, extreme high or low molecular weight and hydrophobic proteins as in the case of membranes (Gygi, Corthals et al. 2000; Oh-Ishi, Satoh et al. 2000; Santoni, Molloy et al. 2000). Recent advances in mass spectrometry (MS)-based proteomics, especially regarding quantitative proteomic approaches like stable isotope labelling by amino acids (SILAC) in cell cultures and whole organisms, have opened the field for a robust and powerful analysis of hundreds of proteins in a complex mixture (Ong and Mann 2006). Furthermore, the SILAC approach facilitates the relative quantification of proteins, based on the ratio of signal intensities produced by light and heavy labelled peptide pairs (Schwanhausser, Gossen et al. 2009). SILAC depends on the cellular ability to incorporate heavy labelled (^{13}C) essential amino acids like arginine or lysine into their protein synthesis. As Figure 1.4.1 illustrates, the reference-linked SILAC approach is based on the mixing of the targeted light sample with the heavy reference in equal amounts. During the experimental procedure, a Lys-C digest liberates peptides bearing $^{13}C_6$-lysine. The residue-specific mass shift of 6Da enables the distinction of the light and heavy peptide pair for mass spectrometry-based quantification.

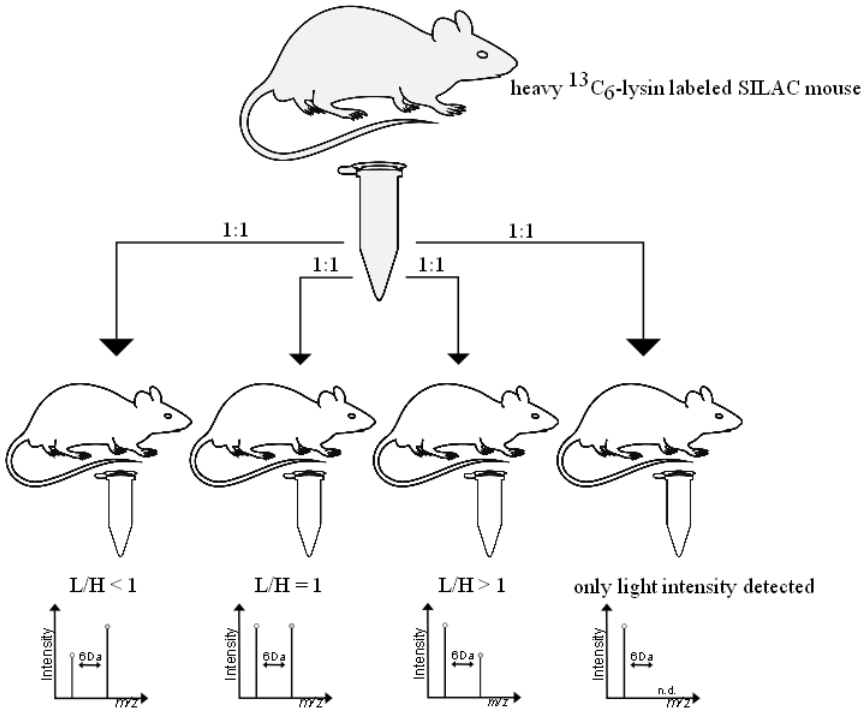

Figure 1.4.1 SILAC-based proteomic analysis and relative quantification using light to heavy ratios

1.4.2 Metabolomics

Referring to the proteome or genome synonym, the metabolome is a newly emerging field in biotechnologies and describes the entirety of metabolites within a complex biological network. Metabolites are compounds of biochemical reactions with a size smaller than 1000 Da. Depending on the organism, the metabolite content investigated ranges from 600 database entries for *Saccharomyces cerevisiae* (Forster, Famili et al. 2003) to 1170 for *Escherichia coli* (Keseler, Collado-Vides et al. 2005), setting the requirement for the establishment of complex metabolic networks. In the past decade, two complementary technologies yielding the accurate analysis of metabolic profiles have evolved. Nuclear magnetic resonance spectroscopy (NMR) provides a highly developed non-invasive technique but it also has the disadvantage of lower sensitivity compared to the counterpart of mass spectrometry-based methods (Fernie, Trethewey et al. 2004). Gas chromatography-coupled mass spectrometry-based metabolic profiling generates large and complex datasets of about 300-500 metabolites, thereby producing a file of about 20 megabytes, which requires highly advanced software and algorithms allowing their extraction and quantification (Fernie, Trethewey et al. 2004). Libraries like the Golm metabolome database, containing more than 1500 spectra of labelled, unlabelled and internal chemical defined molecules, facilitate the high throughput analysis of cellular processes on the metabolic level (Kopka, Schauer et al. 2005). A chemical modification during the experimental procedure enables the detection of a wide range of metabolites such as amino acids, phosphates and hexoses, hence allowing the determination and comparison of metabolic networks in a single run.

a

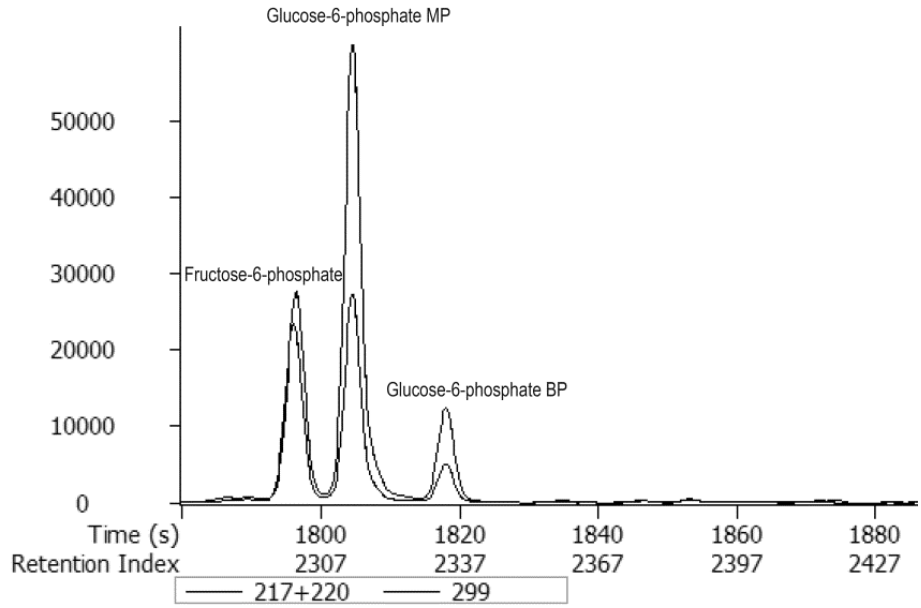

b

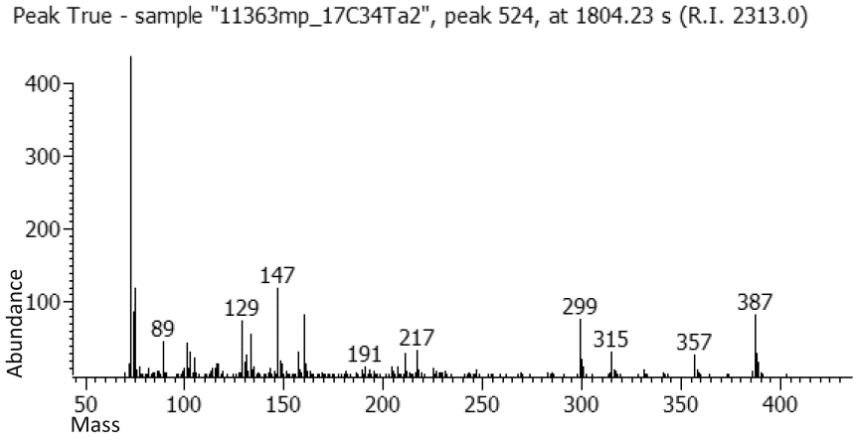

Figure 1.4.2 Combination of chromatography and mass spectrometry for metabolite identification.
a) Identification of phosphorylated hexoses upon retention time (R.T.), retention index (R.I.) and peak analysis. b) Metabolite specific mass fractionation in mass spectrometry

2. Aim of study

2.1 Building the hypothesis

To date, various studies have been conducted on the precise function of dysferlin. As chapter 1.2.3.3 summarizes, dysferlin is predicted to be mainly involved in intracellular vesicle trafficking and sarcolemmal fusion, thus contributing to membrane repair upon injury. However there are certain aspects in the disease phenotype, exceptionally found in dysferlinopathy. One peculiar aspect is the delayed onset of the clinical phenotype, which is usually set in young adulthood. Remarkably, before post-puberty disease onset, dysferlin patients do not exhibit any symptoms indicating a muscular disease, as they usually develop normal motor milestones and are generally good athletes (Chiu, Hornsey et al. 2009; Paradas, Llauger et al. 2010). As outlined in chapter 1.3.1, muscle metabolism undergoes marked changes during puberty, leading to a switch from mainly oxidative to more anaerobic/glycolytic energy consumption. Furthermore, immunohistochemical studies conducted by our group showed a higher abundance of dysferlin in glycolytic type II muscle fibres, supporting the assumption that glycolytic fibres are more affected by a lack of this protein. Figure 2.1.2 illustrates immunohistochemical detection of dysferlin in normal human cryosections.

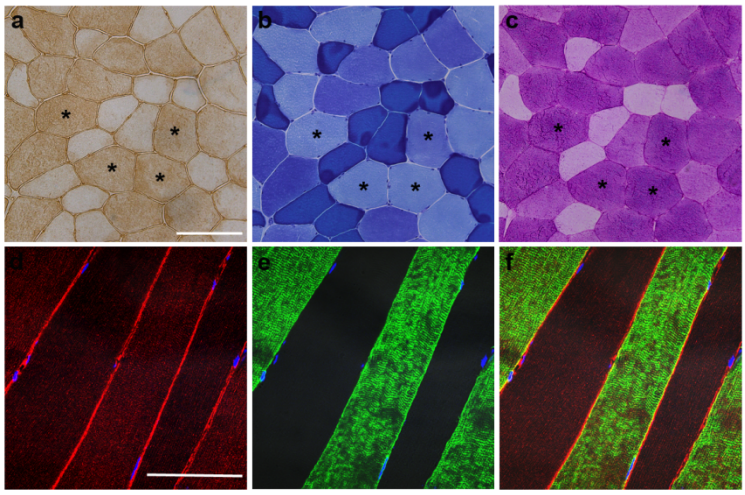

Figure 2.1.1 Higher abundance of dysferlin in human type II muscle fibers. a-c) Serial sections of human normal transverse cryosections. a) Immunohistochemical detection of dysferlin using HAMLET antibody after antigen retrieval. b) Toluidine blue ATPase treatment discloses dysferlin positive fibres as type II fibres. c) Pas staining of type II fibres detects a higher glycogen content. d-f) Predominant expression of intracellular dysferlin in type II fibers is confirmed in normal longitudinal cryosections. d) Dysferlin red. e) SERCA1, specific for type II fibers, green. f) Merge. Bar 50µm. (Experiment performed by Dr. Verena Schöwel)

We therefore hypothesized that dysferlin might also be involved in the maintenance of skeletal muscle metabolism, especially regarding the glycolytic pathway and glucose uptake cascades, which would give a reasonable explanation for the coincidence of disease onset and adjusted energy metabolism after puber-

ty. Furthermore, studies conducted in our laboratory regarding the glucose transporter GLUT4 in human muscle specimens and the energy metabolism of human primary dysferlin-deficient myotubes supported our hypothesis of a disturbed glycolytic pathway. First evidence of a somehow disturbed glucose uptake was obtained by immunostaining of GLUT4 in human transverse muscle cryosections obtained from six adult patients suffering from dysferlinopathy, five healthy controls and patients with various muscular dystrophies and metabolic disorders like type 2 diabetes. Whereas GLUT4 in normal human muscle as well as other muscular dystrophies and metabolic disorders was localized to intracellular compartments at perinuclear sites and the sarcolemma, muscles from patients with dysferlinopathy revealed an abnormal cytoplasmic distribution and subsarcolemmal accumulation of GLUT4.

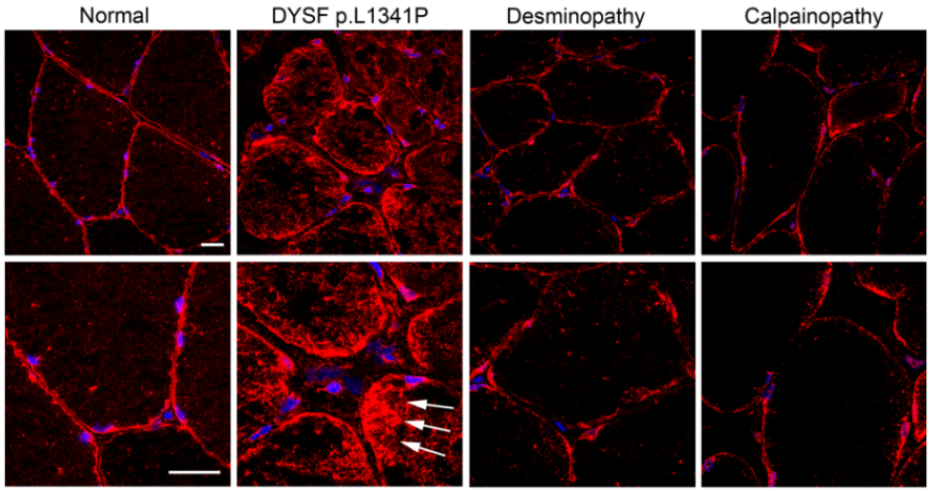

Figure 2.1.2 Immunostaining of GLUT4 in transverse human muscle cryosections obtained from patients suffering dysferlinopathy, desminopathy and calpainopathy. A custom-made anti-GLUT4 polyclonal rabbit antibody was used for GLUT4 staining (Al-Hasani, Kunamneni et al. 2002). Dysferlin-deficient muscle sections show an abnormal cytoplasmic distribution and subsarcolemmal accumulation compared to healthy control and dystrophy sections.(Experiment performed by Joanna Schneider).

To further assess this novel finding in dysferlinopathy, our group conducted a calorimetric tetrazolium-based redox assay (Bochner, Siri et al. 2011), offering media with different fuel substrates to dysferlin-deficient myotubes and controls after 12 hours of serum-free starvation. This experiment revealed a preference of dysferlin-deficient myotubes for ketone bodies like acetoacetate and 3-hydroxybutyrate, whereas control myotubes and myotubes derived from other muscular dystrophies strongly preferred glucose for energy consumption.

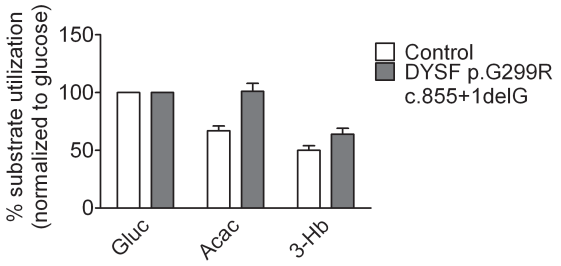

Figure 2.1.2 Calorimetric tetrazolium-based redox assay conducted with dysferlin-deficient and control myotubes. Data shown are normalized to glucose. Krebs-Ringer-Henseleit buffer containing different amounts of glucose, acetoacetate or 3-β-hydroxybutyrate was added to dysferlin-deficient and control myotubes after 12 hours of serum-free starvation. Dysferlin-deficient myotubes exhibit a preference to ketone body utilization to secure fuel supply (Experiment performed by Dr. Ute Zacharias).

The aim of this study was therefore the elucidation of central carbon metabolism alterations using the novel techniques of gas chromatography-coupled mass spectrometry (GC/MS), which enables a unique insight into the distribution and characteristic of biochemical pathways in disease phenotypes. Thanks to the exact measurement of nearly all metabolites contributing to the glycolytic as well as the oxidative pathway, a detailed analysis of disturbed single steps regarding the energy flux and above all the detection and assessment of compensatory and bypass-pathways is achievable.

2.2 Establishment of the GC/MS protocol for myotubes

First step of this study was the *in vitro* application of metabolome analysis in dysferlin-deficient human primary myotubes obtained from muscular biopsy specimens of patients suffering dysferlinopathy and the assessment of alterations in the central carbon metabolic compared to healthy control myotubes. As the technique of primary myotube incubation and harvest poses major difficulties compared to non-adjacent cells, the first step towards metabolic profiling was the adaptation of laboratory procedures to obtain a clear pattern of metabolites in general and phosphorylated aldo- and ketohexoses like glucose-6-phosphate in particular.

2.3 Metabolic profiling of a dysferlin-deficient (BLA/J) mouse model

To confirm the metabotype of dysferlin-deficient myotubes *in vivo*, especially with focus on systemically accelerated compensatory mechanisms, like ketone body synthesis, we conducted a metabolic profiling analysis of a dysferlin-deficient (BLA/J) and wildtype (C57BL/6) mouse model. Two sets of conditions regarding the length of time after i.v. injection of glucose solution were applied. Furthermore, one condition comprised a period of light to moderate exercise to enhance intramuscular glycolytic flux. We per-

formed the analysis of metabolites considering distinct fibre type distributions in mouse muscles, soleus muscle (type I), tibialis anterior (type II) and quadriceps muscle (mixed). These muscles served as metabolic models enabling the correlation of metabolic alterations and muscle fibre type preponderance. To confirm the activation of compensatory systemic pathways, liver from BLA/J and wildtype mice, was extracted and metabolite levels of 3-β-hydroxybutyrate analysed by GC/MS.

2.4 Comparison of metabolic alterations in dysferlinopathy to dystrophin-deficient muscular dystrophy (*mdx*) mice

Metabolic alterations are a common feature in systemic and progressive diseases involving skeletal muscle as a major regulator of the body's energy homeostasis. To assess whether the metabolic alterations found in dysferlin-deficient human myotubes and mice were specific for dysferlinopathy, we conducted a GC/MS metabolic profiling analysis of dystrophin-deficient *mdx* (C57BL/10ScSn-Dmdmdx/J) mice and their corresponding healthy controls (C57BL/10). Based on the metabolic profiling protocol used for the analysis of BLA/J mice, mdx and control mice received same amounts of intravenous $^{13}C_6$ glucose. TA, SOL and QUAD muscle were then sequentially extracted and metabolite extraction and measurement techniques applied.

2.5 Application of SILAC-based proteomics

For evaluation of the newly discovered dysferlin metabotype, a stable isotope-labelled amino acid (SILAC) based proteome analysis was performed using liquid-chromatography-coupled Orbitrap mass spectrometry (LC-MS/MS). This novel technique fully meets the high demands on detailed analysis and relative quantification of low abundant glycolytic, TCA-cycle and respiratory chain enzymes, allowing a localization of disturbed substrate flux in our dysferlin mouse model. We performed the proteome analysis on muscles obtained from BLA/J and wildtype mice, which underwent the injection procedure for metabolic analysis. Corresponding to the metabolic profiling protocol, SOL, TA and QUAD muscles were used to obtain a fibre type specific insight into metabolic alterations and compensatory mechanisms activated. Besides that, the SILAC-based approach generated a unique access into the protein expression patterns of oxidative and glycolytic fibre types, with focus on metabolic enzyme subunits and isoforms never published before.

3. Methods

3.1 Human cell experiments

3.1.1 Patient material

Primary myoblasts were obtained from human muscle biopsy specimens of a patient suffering from LGMD 2B and a healthy control. The dysferlinopathy patient was diagnosed with two heterozygous missense mutations in exon 8 and 9 of the DYSF gene (c.855+1delG; c.895G>A), one of them causing a total mRNA decay and resulting in a severe reduction of the dysferlin protein expression. All experiments were performed after obtaining permission from the local ethics commission (EA 1/203/08 and EA 2/051/10). All biopsies from patients were taken for diagnostic purposes in the first instance and involved into our study after informed consent was obtained. Healthy control biopsies were taken in cooperation with the Center for Orthopedics and Trauma Surgery at Helios Hospital Berlin Buch from patients undergoing hip surgery. Informed consent was obtained 24 hours prior to surgery.

3.1.2 Cell cultivation and extension

Table 3.1.2 Chemicals and devices used for cell culture

Solution	Components	Company
Cell culture media	Skeletal Muscle Growth Medium (SMGM)	Provitro, Germany
	Supplement	Provitro, Germany
	Gentamicin 50µg	Provitro, Germany
	Amphotericin B 50ng	Provitro, Germany
	Fetal calf serum (FCS) 10%	Lonza, Switzerland
	GlutaMAX™ 0.015%	Invitrogen, Germany
Cell passage solutions	Trypsin-EDTA 0.25%	Invitrogen, Germany
	Physiological Buffer Solution (PBS)	Invitrogen, Germany
	Trypan Blue 0.4%	Sigma-Aldrich, USA
Cell fusion media	Dulbecco's modified eagle medium (DMEM)	Fa. Invitrogen
	Horse serum (FCS) 2%	PAA (Pasching), Austria
	Gentamycin	Invitrogen, Germany
Material		
Falcon Tubes		BD Becton Dickinson, USA
Tissue culture dish		BD Becton Dickinson, USA

Devices	
Neubauer chamber	MARIENFELD, Germany
Microscope	Leica Microsystems, Germany
Centrifuge 3-18k	Sigma, Germany
CO_2 Incubator BBD 6220	Thermo Fisher Scientific, USA

Primary human myoblasts were obtained from human muscle biopsy specimens, extraction procedure and biopsy took place on the same day. First, muscle specimens were washed with cold PBS to remove blood and tissue remnants. Afterwards muscle specimens were minced using sterile autoclaved scissors and the homogenised solution was transferred to a sterile 15 ml falcon tube, followed by a 5 minute centrifugation step at 1000 rpm and 22°C to remove the supernatant. Washing procedure following centrifugation was performed two times. The remaining muscle pellet was then diluted in an enzyme solvent (4 ml Collagenase type III, 100µl Dispase1 and 500µl Trypsin/EDTA) and incubated by shaking 45 minutes at 37°C. After 45 minutes, the suspension was again centrifuged under the same conditions used before, the supernatant was discharged and the muscle pellet suspended in 3 ml of skeletal muscle grow medium (SMGM), supplemented with gentamycin 40µg/ml (Invitrogen, CA), 10% fetal calf serum and 3mM glutamine. Cultivation for the first three days was performed using a 6 cm petri dish in a 37°C humidified and 5% CO_2 enriched atmosphere. After three days, cell growth was assessed microscopically and the medium was changed. Myoblasts reaching a confluence of about 50% were split and transferred into new 10-cm petri dishes for further cultivation. For the splitting procedure, the medium was discharged and cells were washed with 5 ml of prewarmed PBS to remove cell debris. A 5-minute incubation step using 1 ml of trypsin under cultivation atmosphere, secured detachment of the adherent myoblasts from the petri dish bottom. After 5 minutes, trypsin activity was stopped by adding 3 ml skeletal muscle growth medium. Cell count and viability were assessed using a Neugebauer chamber in combination with trypan blue staining. For that purpose, 20µl of trypan blue and 20µl of cell solution were mixed and half transferred to the cell counter chamber. All viable cells in at least two out of the four opposite squares were counted and cell content calculated using the formula:

cells/ml = average cell number x dilution factor x chamber factor

Depending on the specific myoblast growth behaviour and age, a variable number of cells were then transferred into 10 cm Petri dishes for further cultivation and expansion. Differentiation of myoblasts into multinucleated myotubes was stimulated at 80-90% confluence, using DMEM supplemented with 2% Horse serum and gentamycin 40 µg/ml for 5-7 days. Differentiation process was evaluated daily by microscopic surveillance.

3.1.3 Anti-CD56/NCAM Antibody Immuno-Magnetic Cell Sorting

Table 3.1.3 Chemicals used for immune-magnetic cell sorting

Solution	Components	Company
MACS Buffer	PBS pH 7.2	Invitrogen, Germany
	Bovine Serum Albumin (BSA) 0.5%	Sigma-Aldrich, USA
	EDTA Disodium Salt 2mM	Calbiochem, Germany
CD56 micro beads		Miltenyi Biotec GmbH, Germany
Antibodies	Anti-Desmin M0760 monoclonal mouse IgG	DAKO, Germany
	Alexa Flour® anti-mouse IgG	Invitrogen, Germany
Bis Benzimide	(Hoechst) 33258	Sigma-Aldrich, USA
Vectashield®	Mounting Medium	Vector Laboratories, USA

Immuno-magnetic cell sorting was performed between the third to fifth cell passage to avoid contamination and overgrowth of fibroblasts, which are naturally present in every muscle biopsy specimen. The application of magnetic cell sorting procedure enables the separation of different cell types, expressing different immuno-phenotypic surface antigens (cluster of differentiation-CD). For that purpose, CD 56^+ cell lines, like myoblasts, were magnetically labelled with anti-CD56 micro beads. A MACS column, which is placed in the magnetic field of a MACS separator, enabled the positive selection of the desired cell lines by attaching them inside the column for later elution outside the magnetic field. Myoblast adhesion was cleaved with trypsin as described for the cell passage procedure, trypsin activity was stopped by adding 3 ml of SMGM and cell count was determined using the Neugebauer cell chamber. To evaluate efficiency of the cells sorting procedure, some microliters of cell suspension were transferred to a 8er glass slide for desmin staining. Cell suspensions were transferred to 15 ml falcon tubes and centrifuged at 4°C for 5 minutes at 1000 rpm. Supernatant was discharged and cell pellet dissolved with 5 ml MACS buffer, followed by a second centrifugation under similar conditions. For myoblast CD56 tagging, cell pellet was dissolved in 80 µl MACS buffer and 20 µl CD 56 micro-beads (according to $1x10^7$ cells), and incubated for 15 minutes at 4°C. After 15 minutes of incubation, another 2 ml of MACS buffer was added to each sample followed by centrifugation at 4°C for 5 minutes at 1000 rpm. During the centrifugation step, the MACS column was equilibrated with 3 ml cold buffer. Cell pellets were dissolved in 1.5 ml cold MACS buffer and transferred to the column. The flow containing predicted non-labelled fibroblasts was discharged. After three washing steps with 3 ml MACS buffer to remove remaining fibroblasts, the column was removed from the magnetic field, all magnetic CD56 labelled myoblasts tagged to its wall, and myoblast eluate was collected. Cells were then centrifuged to remove MACS buffer and cultivated in SMGM under conditions described for cell cultivation and expansion. Some microliters of SMGM containing myoblasts were collected for efficiency control via desmin staining.

3.1.4 Anti-desmin staining as purity control after anti-CD56 MACS

Purity of the myoblast preparation after immuno-magnetic cell sorting with the anti-CD56 antibody was confirmed by staining with an anti-desmin antibody before and after MACS procedure. Cells were washed one time with prewarmed PBS following fixation with formaldehyde (3.7% in PBS) for 20 minutes at room temperature. After three washing steps with PBS, permeability of adjacent cells was increased by incubation with triton 0.2% for 15 minutes and cells were blocked for another 10 minutes with BSA 1%. Both the first and second antibodies, were prediluted (anti-desmin IgG, monoclonal mouse 1:100, Alexa flour anti-mouse IgG 1:500) in a BSA (1% in PBS) and 50 µl of each administered consecutively, intermitted by three washing steps with PBS. Incubation time for the first antibody was set at 60 minutes and for the second one at 30 minutes. After a third incubation step with Hoechst (1:5000 in PBS) for 3 minutes, followed by three washing steps, slides were fixed with glycerol-based Vectashield® medium and immunofluorescense assessed microscopically.

3.2 Metabolic profiling

Table 3.2.1 Devices and chemicals used for GC/MS analysis

Solution	Components	Company
Labelling Buffer	DMEM (glucose-free)	Genaxxon Bioscience, Germany
	$^{13}C_6$-Glucose	Campro Scientific, Germany
	L-Glutamine 580 mg/l	Invitrogen, Germany
	Sodium-Pyruvate 110 mg/l	Alfa Aesar, USA
	L-Arginine 84 mg/l	Sigma-Aldrich, Germany
	Lysine 146 mg/l	Sigma-Aldrich, Germany
Extraction Buffer	Methanol LC/MS grade (5x)	Sigma-Aldrich, Germany
	Chloroform Reagent Plus® (2x)	Sigma-Aldrich, Germany
	Milli-Q-water (1x)	
	Cinnamic acid 9 µg/ml	Sigma-Aldrich, Germany
Solution A	Pyridine 1 ml	Sigma-Aldrich, Germany
	Metoxamine hydrochloride 40mg	Sigma-Aldrich, Germany
Solution B	MSTFA 1 ml	Macherey-Nagel, Germany
Material		**Company**
SiLibeads ceramic beads type ZY		Sigmund Lindner, Germany
Polypropylene Microtubes		VWR, USA
Safelock 1.5 ml tubes		Eppendorf, Germany

Device	Company
Precellys®24 Homogenizer	Bertin Technologies, France
Centrifuges Eppendorf 5430	Eppendorf, Germany
Eppendorf 5417R	
Thermomixer comfort	Eppendorf, Germany
Speed Vac	Christ RVC 2-33 CD plus
Vacuum chamber	Christ Alpha L-4 LD plus
Gas chromatograph Agilent 6890N	LECO, USA
Pegasus III mass-spectrometer	LECO, USA
Software	**Company**
Pegasus ChromaTOF	Leco, USA
MaxQuant	MPI for Biochemistry Martinsried, Germany

3.2.1 Myotube incubation and harvest for metabolomic analysis

Twelve hours prior to the experiment, myotubes were washed twice with PBS and serum-starved in DMEM medium lacking supplements and insulin under atmospheric conditions described above. After twelve hours, myotubes were washed one time with PBS, following incubation with 7 ml labelling medium for 10 and 30 minutes under similar atmospheric conditions. Incubation protocol was conducted with biological triplicates for control and dysferlin-deficient myotubes of each condition. Labelling medium was prepared from glucose-free DMEM-media by adding $^{13}C_6$-glucose, glutamine, arginine and sodium-pyruvate in concentrations based on the composition of the skeletal muscle growth medium (SMGM) used daily. After incubation, the labelling medium was discarded and metabolism was immediately stopped by adding 3 ml of prechilled (-20°C) 50% methanol. Cells were then scratched and transferred to 15 ml polypropylene tubes containing 0.6 ml chloroform and shaken for 45 minutes at 750 rpm and 4°C. Phase separation was reached by centrifugation for 10 minutes at 14000 rpm (20000 g) and the polar phase (supernatant) was transferred to 15 ml Falcon tubes for concentration in a vacuum device at 40°C for 12 hours. This step was repeated the next day by adding 300 µl of 20% cold methanol to each sample following incubation and centrifugation under conditions described above. Supernatant was then transferred in constant volume to 1.5 ml safelock Eppendorf tubes and vacuum dried in a vacuum device for another 5 hours to continue with the derivatization procedure.

3.2.2 Derivatization procedure

Dried samples were chemically modified in two steps by derivatization with N-methyl-trimethylsilyl-trifluoracetamide (MSTFA) and methoxyamination (MeOX). First, 20 µl of solution A, containing 40 mg methoxamine solved in 1 ml pyridine, was added to each sample and to twelve additional standard samples containing an metabolite identification mix (Ident A-D) and a quantification standard (Quant 1:1, 1:2, 1:5, 1:10, 1:20, 1:50, 1:100, 1:200). Samples were shaken at 30°C and 750 rpm for 1 hour until solved, meanwhile the solution B was prepared by merging 20 µl of 30°C prewarmed n-alkanmix with 1 ml of MSTFA. After incubation of solution A, 80 µl of solution B was added to each sample followed by a second incubation for another hour at 37°C at 750 rpm. Remaining insoluble parts were then removed by centrifugation at 14000 rpm (20000 g) and 30 µl of supernatant was transferred to four crimp top glass vials, yielding three replicates for each sample.

3.2.3 GC/MS analysis

Derivatized endo- and exometabolites were measured using a Pegasus III mass-spectrometer (LECO, St. Joseph, USA) equipped with an Agilent 6890N gas chromatograph and a VF-5ms column whose length was 30 m and inner diameter 250 µm (Agilent, USA). 1 µl of sample was injected into a baffled liner (Gerstel, Austria) with 1:5 split-ratio under a helium flow of 1.2 ml/min. The oven was heated from 70°C to 350°C with 5°C/min to 120°C and 7°C/min to 350°C followed by 2 minutes hold time. Scan rates of 20 Hz and mass ranges of 70-600 Da were used. Samples were measured in triplicates, separated by washing samples containing solution B to avoid carry over. Identification and quantification standards were measured twice, once at the beginning and once at the end of the experimental batches. To prevent a transfer of substances, quantification standards were arranged in the order of increasing concentration.

3.2.4 Metabolite identification and data processing

The GC/MS chromatograms were initially processed with the ChromaTOF software, enabling the automatic baseline processing, deconvolution of chromatograms and peak area calculation over the entire acquisition time. The baseline set in each chromatogram was just above the noise level. To allow a direct comparison between different GC/MS runs, which can cause deviations in the retention time (R.T.) profile, a defined mixture of alkanes of different length was introduced to each sample during the derivatization procedure, enabling a correspondent time-independent annotation of compounds using the retention index. The golm metabolome database (GMD) was used to identify substances with respect to spectra-similarity and identical retention index (Schiaffino 2010). Metabolites, not identified by the software due to a certain mass shift by label incorporation, were annotated manually. The additional application of the in-house generated identification mix (Ident A-D) secured an exact distinction between kindred metabo-

lites of similar retention behaviour. Data matrices for relative quantification in Excel were extracted from the mass spectra using MetMax software (Kempa, Hummel et al. 2009).

Table 3.2.4 Metabolite identification data (Retention Index (RI), mass, reverse (REV) match)

TAG MASS	TAG RI		REV MATCH		COMPOUND	TAG MASS	TAG RI	REV MATCH
	MICE EXPERIMENTS					**CELL EXPERIMENT**		
Cond. 1/2	**Cond. 1**	**Cond. 2**	**Cond. 1**	**Cond. 2**				
198+200	**1581.3**	1581.7	633	905	**Alpha-ketoglutaric acid**	198+200	1580.7	882
273+275	**1811.5**	1811.7	970	968	**Citric acid**	273+275	1810.8	907
217+220	**1860.8**	1860.8	958	938	**Fructose MP**	217+220	1860.8	958
217+220	**2301.5**	2301.5	934	938	**Fructose-6-phosphate**	217+220	2299.8	833
245+247	**1363.9**	1364.0	960	938	**Fumaric acid**	245+247	1364.3	910
217+220	**1885.1**	1885.4	958	921	**Glucose MP**	217+220	1891.2	870
217+220	**1903.7**	1904.0	950	919	**Glucose BP**	217+220	1907.0	968
217+220	**2313.6**	2314.2	944	944	**Glucose-6-phosphate MP**	299	2313.0	805
217+220	**2333.5**	2334.1	966	978	**Glucose-6-phosphate BP**	217+220	2333.2	808
n.d.	n.d.	n.d.	n.d.	n.d.	**Glutamic acid**	246	1623.9	830
n.d.	n.d.	n.d.	n.d.	n.d.	**Glutamine**	156	1770.7	801
247+251	**1578.6**	1579.0	928	901	**Glutaric acid, 2-hydroxy**	247+251	1577.9	790
218+219	**1278.8**	1279.0	938	795	**Glycerol**	218+219	1280.4	740
357+359	**1758.9**	1759.1	960	982	**Glycerol-3-phosphate**	357+359	1757.8	867
117+119	**1051.8**	1051.9	938	950	**Lactic acid**	117+119	1052.2	952
233+235	**1487.6**	1487.9	968	969	**Malic acid**	233+235	1487.1	971
211	**1602.5**	1602.9	913	899	**Phosphoenolpyruvic acid**	n.d.	n.d.	n.d.
174+177	**1043.9**	1043.6	962	942	**Pyruvic acid**	174+177	1047.4	988
319	**1923.8**	1923.5	927	905	**Sorbitol**	319	1923.3	857
247+249	**1325.4**	1325.6	971	969	**Succinic acid**	247+249	1326.6	891
233	**1154.6**	1154.6	943	958	**3-β-hydroxybutyrate**	n.d.	n.d.	n.d.
299	**1799.2**	1799.4	966	968	**3-phosphoglyceric acid**	299	1798.6	879

3.3 Metabolome and proteome analysis in dysferlin-deficient BLA/J mice

3.3.1 Mice origin and material

B6.A/J-Dysf^{prmd} (Dysf^{prmd}) mice (BLA/J) harbouring a transposon in DYSF were provided by Isabelle Richard, Genethon, Evry Cedex, France (Lostal, Bartoli et al. 2010). In these mice the progressive muscular dystrophy (*prmd*) allele from the A/J inbred strain is crossed onto the C57BL/6 background. Disease onset is usually observed at two month of age, displaying an increasing number of centro-nucleated fibres and signs of inflammation, whereas immobilization due to muscle weakness is observed around the fourth month. Male *mdx* (C57BL/10ScSn-Dmdmdx/J) and their corresponding control (C57BL/10) mice were used as control for metabolic alterations in muscular dystrophies other than dysferlinopathy. *Mdx* mutant mice were discovered by Bulfield and colleagues in a colony of C57BL/10ScSn inbred mice in 1984 (Bulfield, Siller et al. 1984). Male *mdx* mice are hemizygous for the Dmd^{mdx} allele leading to a complete absence of dystrophin at the sarcolemma. Skeletal muscle of *mdx* mice is usually normal during early postnatal development, clinical signs of muscle weakness associated with histological signs of necrosis start around three weeks of age. Interestingly the progressive muscle degeneration and necrosis is offset around the 5th week followed by regeneration processes due to activation of satellite cells (Cooper 1989). Breeding and housing of both BLA/J and C57BL/6 mice was performed in the animal facility of the Max Delbrück Center for Molecular Medicine. *Mdx* and C57BL/10 mice were purchased from Jackson Laboratory, USA and kept under regular housing conditions until the day of injection. All animal had free access to water and feed during any time of their housing. All mice experiments were performed fully in accordance with the local ethics commission (G 0127/06). For metabolomic and proteomic investigation, five BLA/J mice and four wildtype (C57BL/6) mice with an average age of 12 weeks and 18 weeks, respectively, were used. *Mdx* and C57BL/10 mice were 36 and 38 weeks of age, respectively. Extensor digitorum longus (EDL) muscle and tibialis anterior (TA) muscle mainly composed of glycolytic type II muscle fibres Soleus (SOL) muscle, mainly containing oxidative type I muscle fibres and the mixed fiber type muscle Quadriceps (QUAD), were extracted. Quadriceps muscle was further analyzed as an example of a proximal muscle, primary involved during disease progression of the LGMD 2B phenotype. All protocols were approved by the Berlin animal research committee, strictly according to guidelines the BGBI and Charité University medicine animal protection protocol.

3.3.2 Mice injection and euthanasia for metabolic profiling

For the metabolic profiling analysis of male BLA/J and wildtype mice, two conditions regarding time and exercise were implemented. The first condition (Condition 1) reflected resting conditions, including a post-injection time of 5 minutes. For the second condition (Condition 2), mice were placed on a treadmill for 20 minutes after a 5 minute post-injection resting period, sequentially reaching a stadium of exhaustion with total consumption of the glucose levels offered intravenously. *Mdx* and C57BL/10 mice were

examined under condition 2. A detailed overview is given in table 3.3.2. Until the day of injection, mice were kept under common housing conditions, with free access to food and water prior to the experiments. Injection was performed by administration of a prewarmed $^{13}C_6$ glucose solution (100 µl, 20% solved in NaCl 0.9% corresponding to 20 mg per animal) intravenously into the tail vein without anaesthesia. Treadmill velocity was set to 12.4 m/min. Mice were decapitated after inhalation anaesthesia with isoflurane (1.5-2.5%). TA, SOL and QUAD muscle and liver were extracted sequentially from the left to right side, placed into 2 ml conical polypropylene tubes and immediately frozen in liquid nitrogen.

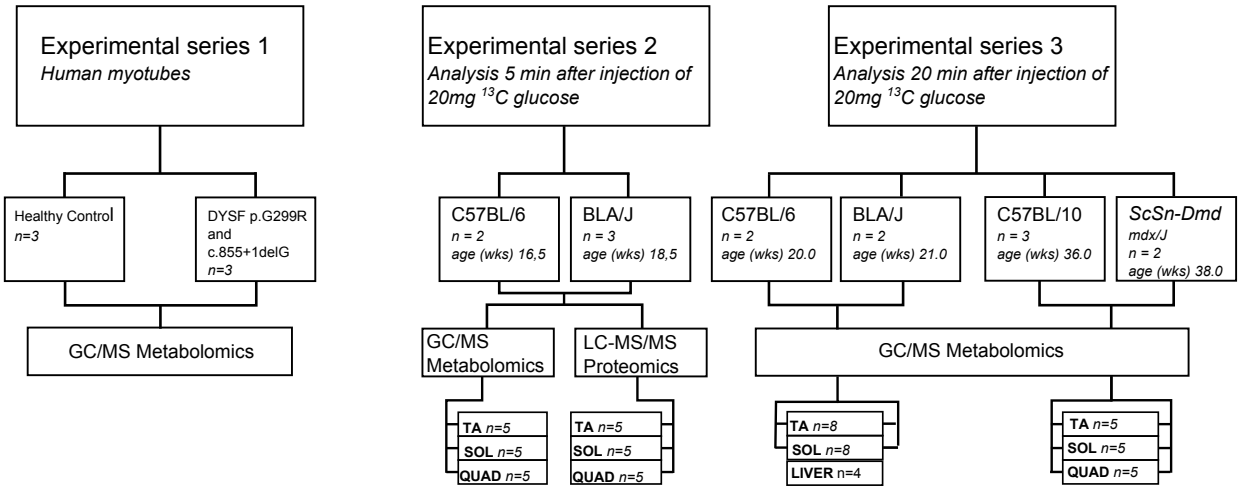

Table 3.3.2 Experimental design of myotubes and mouse metabolomics and proteomic analysis

3.3.3 Muscle metabolite extraction

Muscle weight was determined in 2 ml conical polypropylene microtubes. A mixture of methanol-chloroform-water (MCW) (5:2:1/v:v:v) containing cinnamic acid (9 µg/ml) as internal standard was added, corresponding to the muscle weight (50 mg muscle equals 1 ml of MCW). Muscles were then homogenized in a tissue lyzer using yttrium stabilized zirconoxid ceramic beads of 0.4 -0.6 mm diameter at a speed of 6200 Hz for 20 sec runtime for 2 cycles. Homogenization cycles were repeated until the mixture achieved a milky consistency. Then ceramic beads were removed by a centrifugation step at 8000 g for 10 minutes. Supernatant was collected and transferred to safelock 1.5 ml Eppendorf® tubes and MilliQ® water was added in an amount corresponding to ½ of the MCW-volume added to each muscle sample. Samples were then shaken at 750 rpm and 4°C for 60 minutes followed again by centrifugation for 10 minutes at 5000 g to separate the polar (top), lipid (bottom) and interface (tissue debris) layers. Polar and lipid phases were collected in similar amounts corresponding to the muscle type and dried under vacuum for 12 hrs and 4 hrs, respectively. Dried samples were chemically modified by derivatization as described for the cell metabolic profiling protocol in chapter 3.2.2. For GC/MS measurement, samples were measured in triplicates. GC/MS settings and data analysis was performed as described in chapter 3.2.3 and 3.2.4.

3.4 Proteomic analysis

3.4.1 Muscle material

For the proteomic analysis right TA, SOL and QUAD muscle were extracted. Quadriceps muscle obtained from 129 50- to 60- day-old female mice with incorporated heavy labelled $^{13}C_6$-lysine upon stable isotope enriched feeding was used as heavy reference. Protein labelling efficiency over 96% was determined by LC-MS/MS-based proteomics.

3.4.2 Protein extraction

For homogenization and extraction of proteins, 500 µl Urea Buffer (8 mM, TrisHCL 100 mM at pH 8.5) was added to each sample containing one frozen muscle. The muscles were homogenized by mechanical mincing using yttrium stabilized zirconoxid ceramic beads in a tissue lyzer and by high concentrated urea leading to a chemical disruption of non-covalent interactions in proteins. For reduction of disulfide bonds, dithiotreitol (DTT) was added to a final concentration of 2 mM followed by incubation at room temperature for 30 minutes. Sonification for 45 seconds (2 cycles, 60 % of power) was performed to reach denaturation of protein bonds, followed by a centrifugation step at 14000 rpm (20000g) to remove cell debris. Protein content of the supernatant was then determined by Bradford.

3.4.3 Bradford assay

The sample's protein amount was determined using a standard curve (BSA, 0-2 µg/ml) for the calculation of unknown concentrations. For this purpose, a BSA standard (2 mg/ml) stored at -21°C was diluted using MilliQ® water in eight different amounts. Sample dilutions (1:500, 1:250, 1:100) were prepared using the same procedure. Table 3.4.3 gives a detailed overview.

Table 3.4.3 Bradford assay standard curve pipette scheme

Std. dilution no.	MilliQ water (µl)	BSA stock solution (µl)	Concentration (µg/ml)	Sample conc. (µg/ml)
1	395	5	25	500
2	495	5	20	250
3	660	5	15	100
4	200	200 of 2	10	
5	200	200 of 4	5	
6	200	200 of 5	2.5	
7	200	200 of 6	1.25	
8	180	20 of 4	1	

150 µl of each sample and standard volume, including one blank sample with MilliQ® water, were transferred into a 96-well plate and 150 µl of Bradford solution was added followed by shaking for 30 seconds. After an incubation period of 10 minutes absorbance was measured at λ=595 nm (Kolwicz and Tian 2011) by a plate reader (Infinite M2000, TECAN Group Ltd., Switzerland).

3.4.4 Protein digestion

After the Bradford assay, 100 µg of sample protein and 100 µg of SILAC reference were mixed and incubated for 15 minutes with Iodoacetamide (IAA, 200 mM). IAA served as alkylation reagent and prevented reoxidation of cysteine residues. Protein digestion was achieved by addition of Lysin-C in a ratio of 1:40 (w/w) following incubation over night at 30°C. The following day, samples were diluted using ammonium bicarbonate (AmBic, 1:4 v/v) and incubated with trypsin beads in a ratio of 1:80 (w/w) for 4 hrs at 30°C. Acidification with 10 µl trifluoroacetic acid (TFA) stopped further digestion and trypsin beads were removed by centrifugation for another 4 minutes at 1400 rpm (20000 g).

3.4.5 Stage tip procedure

Sample desalting and purification for LC/MS analysis was performed using stage tip procedure (Rappsilber, Mann et al. 2007). For that purpose, Empore discs C18 (3M) were mounted three times into a 200 µl pipette tip and arranged over a vacuum system. Washing steps to activate and equilibrate membranes followed in this order: Methanol 50 µl, Buffer B 50 µl, Buffer A 50 µl. Each stage tip was then loaded with 18 µg of sample protein and desalted by adding 50 µl of Buffer A. Elution of sample peptides from the C18 material was reached by administration of 50 µl Buffer B following collection of the eluate in low-bind siliconated microfuge tubes. Eluates were evaporated for 20 minutes in a vacuum device (0.1 mbar). Immediately before measurement procedure, samples were diluted in 25 µl Buffer A and separated into duplicates.

3.4.6 Nano LC-MS/MS analysis

First step was the separation of peptides by reverse-phase chromatography on an in-house-made 30 cm column C18-Reprosil-Saphir (inner diameter: 75 µm, particle diameter: 1.8 µm) using a nanoflow high performance liquid chromatography (HPLC) system (Agilent 2000). A nano-electrospray ion source (Proxeon) with a spray voltage of 1.9 kV enabled the coupling of this system to the LTQ Orbitrap mass spectrometer. Mass spectra were acquired with a mass range of 400 m/z at a resolution of R=60 000. The 20 most intense ions of each survey MS scan were fragmented and MS/MS spectra acquired. Once selected for fragmentation, ions were excluded from further selection for 30 seconds in order to increase new

sequencing events. Identification and quantification of heavy (H) and light (L) labelled peptides was performed using the MaxQuant proteomics pipeline (v1.2.2.5) (Cox and Mann 2008; Cox, Matic et al. 2009) and the Mascot search engine. All spectra were searched against the International Protein Index (IPI) mouse database version 3.70 (Kersey, Duarte et al. 2004). Carbamidomethylation of cysteines was chosen as fixed modification, oxidation of methionine and acetylation of N-terminus were chosen as variable modifications. Two missed cleavage sites were allowed and peptide tolerance was set to 7 ppm. Identification was restricted by a false discovery rate (FDR) of one per cent.

3.4.7 Data analysis

Prior to the data analysis, reverse and contaminant as well as proteins identified in less than 80% of all samples were rejected. Two quantification methods are available to depict the abundance of a certain protein, the SILAC method, generating H/L ratios between a determined reference, and the sample protein provides a very sensitive method for the measurement of proteins expressed in both of them. Proteins uniquely expressed in the sample are quantified using the light intensity of its expression. This method facilitates the determination of proteins uniquely expressed in a certain condition or genetic background, although it lacks the high sensitivity of the SILAC method. Automatically determined H/L ratios of sample and reference peptides were reversed to L/H ratios. All ratios were normalized to the mean of all protein ratios obtained. The UniProt database was used for identification of central carbon metabolism associated proteins.

3.5 Western blot analysis

Table 3.5 Chemicals and devices used for western blot analysis

Solution	Components	Company
Lysisbuffer	Tris-buffered saline 20 mM	Carl Roth, Germany
	NaCl 150 mM	Carl Roth, Germany
	EDTA 1 mM	Carl Roth, Germany
	EGTA 1 mM	Carl Roth, Germany
	TritonX100 1%	Sigma-Aldrich, USA
Protease inhibitors	Complete Ultra Tablets	Roche Applied Science
Phosphatase inhibitors	PMSF 1 mM	Carl Roth, Germany
	Glycerol-phosphate 1 mM	" " "
	Na_3VO_4 1 mM	" " "
	NaF 1 mM	Applichem, Germany
	Sodiumpyrophosphate 2.5 mM	Applichem, Germany
Semi dry buffer system	Tris base 25 mM	Carl Roth, Germany
	Methanol 20% (v/v)	" " "
	Glycine 192 mM	" " "
TBS-T	Tris buffered saline	Carl Roth, Germany
	Tween 0.1%	Merck, Germany
Material		**Company**
Protran® Nitrocellulose membranes		Whatman®, UK
BCA Assay Kit	Reagent A, B	Thermo Scientific, USA
	Albumin Standard 2mg/ml	
Western blot Detection Kit	Amersham™ ECL Advance™	GE Healthcare, UK
ODYSSEY Infrared Imaging System		LI-COR, USA
Software		**Company**
Image Studio Software		LI-COR, USA
Adobe Photoshop 11.0.2		Adobe, USA
Devices		
PowerPac HC Power Supply		Bio Rad, USA
Trans Blot® SD Cell		Bio Rad, USA
Antibody		**Company**
T5168 mouse monoclonal anti α-tubulin antibody 1:6000		Sigma-Aldrich, USA
NovocastraTM Lyophilized Mouse Monoclonal Antibody		Leica Microsystems, UK
Dysferlin Hamlet 1:500		
IRDye 800 donkey anti-mouse IgG 1:5000		Rockland, USA

Unfixed QUAD, EDL and SOL muscles were extracted from wildtype and BLA/J mice and immediately frozen in liquid nitrogen. Lysisbuffer completed with protease and phosphatase inhibitors was used for

homogenization of muscle proteins. After incubation for 30 minutes on ice, samples were centrifuged for 15 min at 13000 rpm/ 4°C. Proteins contents were assessed using a BCA Protein Assay Kit. To this end an albumin dilution standard (BSA) and was prepared in a working range of 20-2.000 µg/ml protein. For BCA-analysis, 25 µl of standard or muscle sample solution was replenished with 200 µl of BCA working Reagent and transferred to a 96-well plate. Absorbance was then measured after 30 minutes of 37°C incubation at λ=562 nm. 40 µg of EDL, SOL or QUAD protein was blotted onto nitrocellulose-membranes using a semi dry buffer system. 10% sodium dodecyl sulfate (SDS)-polyacrylamide gels were used for western blot analysis. Nitrocellulose membranes were blocked 1 hour at 4°C with 5% (w/v) milk powder in TBS. The first antibody was diluted in 6 ml 4% milk in TBS-T and incubated over night at 4°C followed by three washing steps with TBS-T. The second antibody was used in a dilution of 1:5000 and incubated for a further 30 minutes at room temperature followed by three final washing steps with TBS-T. Anti-dysferlin and anti-tubulin primary antibodies were detected by Odyssey infrared imaging system and software. Protein bands were quantified using ImageJ 1.46e.

3.6 Statistical methods

All data obtained for the mice metabolic profiling were normalized to cinnamic acid as internal standard. Cell metabolite data were normalized to the intensity output of all metabolites measured in the samples. Mean ± s.e.m. was calculated for metabolic profiling data and fold changes comparing WT and DYSF cells/mice used for the illustration of diagrams. Samples were measured in technical triplicates and differences between groups were calculated using Student´s t-test on all data points obtained. Significance was accepted for $p = <0.05$ (shown as *) and $p=0.001$ (shown as **), respectively. Microsoft Excel version 2010 was used for sorting and normalization of raw data, further calculations and formations of diagrams were conducted with Graph Pad Prism 4.

4. Results

Table 4.: Experimental design study

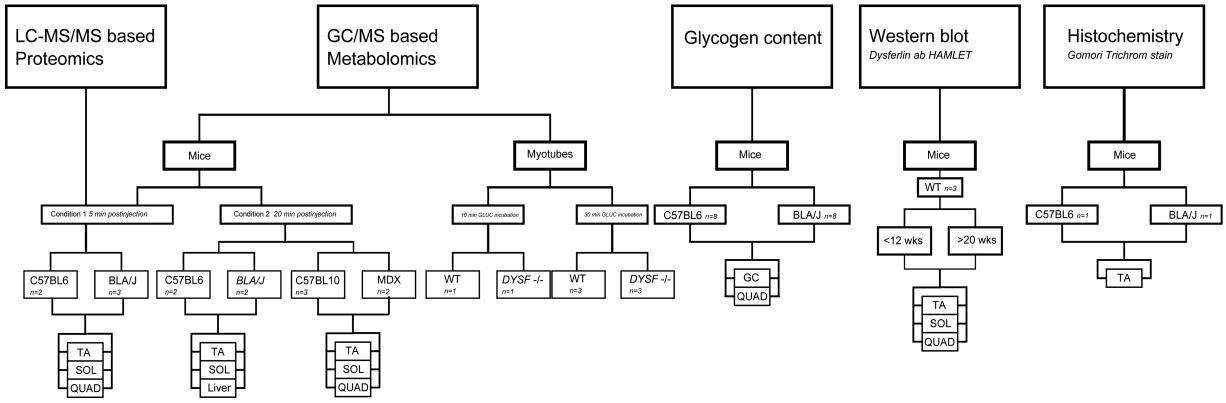

4.1 Metabolic profiling of dysferlin-deficient myotubes

4.1.1 Glycolysis and TCA-cycle

Metabolite profiles regarding the central carbon metabolism of human myotubes were assessed under two sets of conditions depending on the glucose incubation time after twelve hours of cultivation in glucose and insulin free medium. For data visualization, all technical and biological replicates obtained during GC/MS analysis are depicted in the diagrams. Mean and *p* values were calculated from replicate data and fold changes were assessed using this formula:

$$Fold\ change\ DYSF/WT = Analyte_{DYSF} / Mean\ analytes_{WT}$$

As presumed, we found a significant reduction in metabolite levels of the glycolytic pathway in dysferlin-deficient myotubes compared to the healthy controls after 10 and 30 minutes of $^{13}C_6$ glucose incubation after 12 hours or serum-free starvation. Furthermore, metabolites especially associated with the upper glycolytic pathway like glucose-6-phosphate and fructose-6-phosphate showed a time dependent increase after 30 minutes thereby suggesting a stronger reduction during enhanced glucose uptake in the first minutes of glucose administration, whereas fold changes slightly approximated 30 minutes after glucose replenishment. (Figure 4.1a)

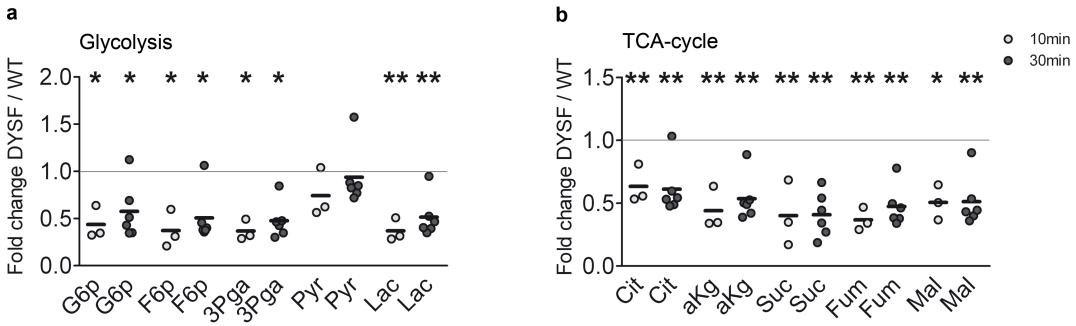

Figure 4.1 Metabolic profiles of primary human dysferlin-deficient (c.855+1delG; c.895G>A) **versus healthy control myotubes.** Data are illustrated as fold changes of metabolite intensities between DYSF versus control (Control =1.0). DYSF n=1, Control: n=1. Incubation for 10 and 30 minutes was performed on 1 and 3 myotube petri dishes, respectively. GC/MS analysis was done on technical triplicates. a) Glycolytic pathway metabolites b) TCA-cycle intermediates. We found a global reduction in glycolytic and TCA-cycle metabolites at both time points in dysferlin-deficient primary myotubes compared to control myotubes.

Interestingly, pyruvate levels were only slightly diminished compared to preceding metabolite intermediates, which might be due to additional pathways and uptake mechanisms yielding the synthesis of this metabolite. Despite the fact that pyruvate levels were less affected, lactate fold changes resembled the dramatical reduction of the upper glycolytic pathway, leading to the assumption that oxidative phosphorylation, starting with decarboxylation of pyruvate by the pyruvate dehydrogenase (PDH) for further downstream metabolization in the TCA-cycle, is not likely to be additionally affected in dysferlinopathy. Regarding the oxidative metabolism, also TCA-cycle intermediates like citrate, alpha-ketoglutaric acid, succinate, fumaric acid and malic acid, were strongly diminished compared to the healthy myotubes. Surprisingly, TCA-cycle intermediates like citrate and 2-ketoglutaric acids, as major targets for anaplerotic reactions like ketone body and free fatty acid (FFA) oxidation, were not increased, as it would be expected as a compensatory mechanism to secure fuel supply. (Figure 4.1 b)

4.1.2 Compensatory pathways

Bearing in mind the dramatic reduction of glycolytic and oxidative metabolites in *DYSF* myotubes, we were astonished to find markedly elevated levels of fructose, sorbitol, glutamine and glutamate, which might be a step towards balancing reduced glycolytic metabolites. Whereas fructose and sorbitol fold changes were significantly increased after 30 minutes of medium incubation, glutamine levels peaked in the first 10 minutes after twelve hours glucose depletion suggesting different conversion and/or uptake regulation. Glutamate, presumably synthesized by glutaminase or AAT, showed a corresponding increase compared to control myotubes. (Figure 4.1.2)

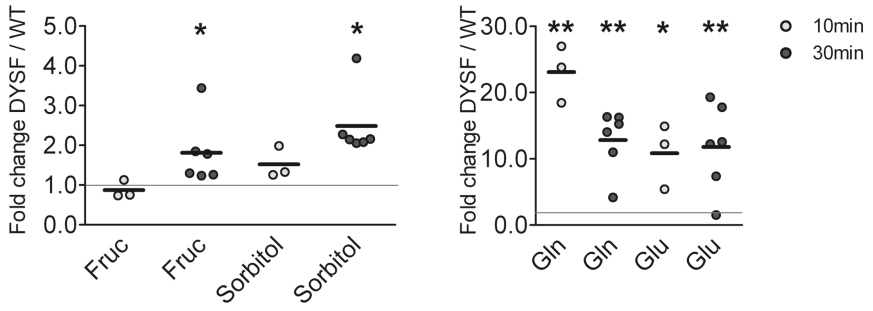

Figure 4.1.2 Compensatory elevated metabolite levels in primary human myotubes harbouring *DYSF* mutations. Illustrated is the fold change between dysferlin-deficient and control myotubes (=1.0). Single data points represent technical replicates at 10 and 30 minutes of glucose incubation. There is a significant increment of fructose and sorbitol levels after 30 minutes and of glutamine and glutamate after both incubation times.

4.2 Metabolic profiling of BLA/J and C57BL/6 mice

4.2.1 Muscle weight, macroscopic appearance and histology

Considering the different metabolic characteristics of oxidative type I and glycolytic type II muscle fibres, muscles used for the comparison between dysferlin-deficient BLA/J and wildtype mice reflected the basic characteristics of one or another fibre type. As Figure 4.2.1.1 illustrates, we could neither find any significant difference in muscle weight, nor was there any macroscopic evidence of muscle fibre atrophy or connective fibre hypertrophy detectable. There was also no difference in muscle weight and composition between young (<12 weeks) and older (>20 weeks) BLA/J mice.

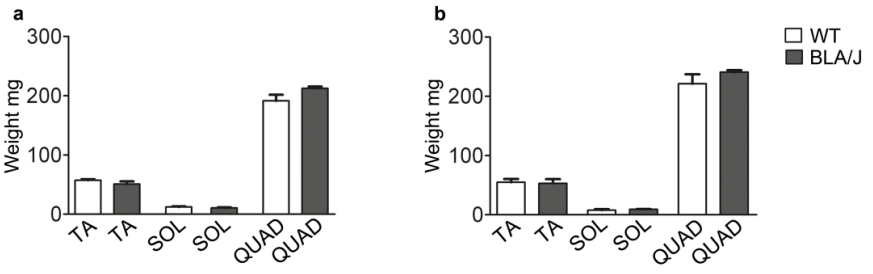

Figure 4.2.1.1Muscle weight of tibialis anterior (TA), soleus (SOL) and quadriceps (QUAD) muscle of BLA/J and C57BL6 wildtype mice. Data are illustrated as mean ±sem. a) Muscles used for metabolic analysis. BLA/J n=5, WT n=4. b) Muscles used for proteomic analysis. BLA/J n= 3, WT n=2. There is no difference in muscle weight between BLA/J and wildtype mice.

To assess the grade of histological muscle damage, a Gomori Trichrom stain of TA muscle transverse cryosections obtained from 12-week-old BLA/J and wildtype mice was performed. In agreement with others, we could not observe significant histopathological alterations before week 16 in BLA/J mice.

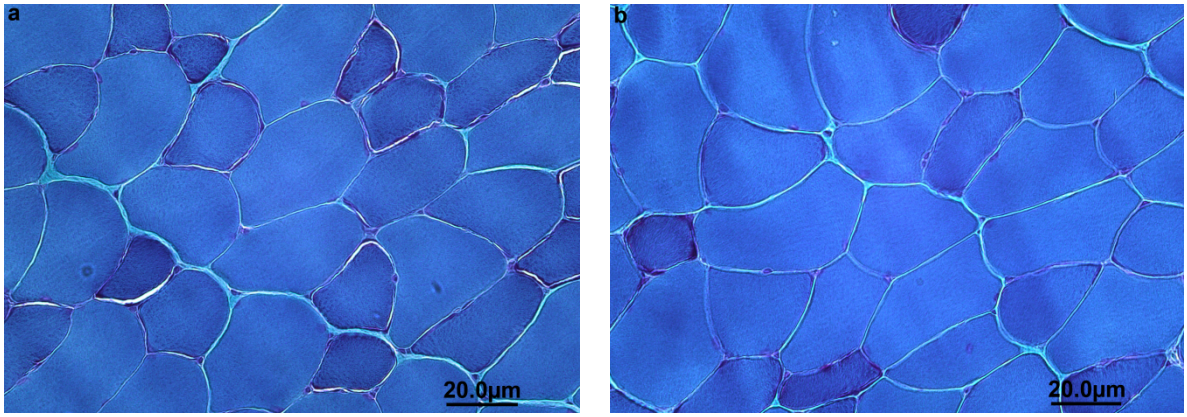

Figure 4.2.1.2 Gomori Trichrom stain of mouse transverse cryosections. a) C57BL/6 tibialis anterior muscle. b) BLA/J tibialis anterior muscle. Both cryosections exhibit a normal appearance, there is no marked atrophy or hypertrophy of connective tissue visible in the BLA/J mouse.

4.2.2 Alterations in central carbon metabolism

The metabolic profile of mice muscles was assessed after *in vivo* administration of 20 mg glucose intravenously to stimulate glucose uptake and metabolization. Two conditions regarding the time after glucose injection until killing of 5 and 20 minutes respectively were applied. In Figure 4.2.2 the fold change of each technical and biological replicate comparing BLA/J and wildtype mice is illustrated. Fold change ratios were calculated as described in chapter 4.1.1. Metabolite expression intensities strongly confirmed our hypothesis of disabled glucose uptake/metabolization in BLA/J mice, as there was a notable decrease, especially regarding the phosphorylated hexoses glucose-6-phosphate and fructose-6-phosphate. Considering the glycolytic fibre type composition of TA muscle, our hypothesis of predominant type II fibre affection was confirmed, as metabolite levels of the mainly oxidative SOL muscle were rather less influenced by the disease. Surprisingly, we detected the greatest decline of glucose-6-phosphate and fructose-6-phosphate in the QUAD muscle, constituting a mixed fibre type muscle with localization at the proximal lower limb. By and large, we were not able to find any greater difference between the metabolite expressions regarding the two post-injection time conditions applied. Only lactate showed a rather elevated fold change in the first 5 minutes and sequentially declined afterwards, suggesting a stronger utilization of substrates not entering the glycolysis to secure energy demand. There was no significant decrease in phosphoenolpyruvate levels detectable indicating that there are possible alternative pathways activated yielding this metabolite as their end product.

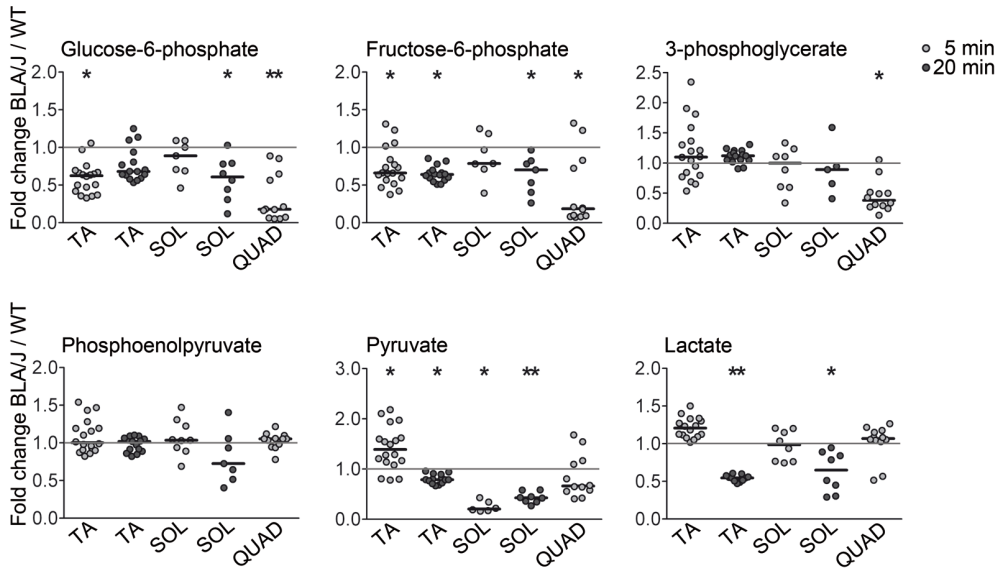

Figure 4.2.2 Glycolytic metabolites illustrated in fold changes between BLA/J and wildtype mice after iv glucose administration in two time conditions. Data are expressed as fold change of BLA/J to wildtype mice. Single data points represent biological and technical replicates, wildtype = 1.0. Metabolites of the upper glycolytic pathway were markedly reduced in BLA/J mice compared to their healthy littermates.

4.2.3 TCA-cycle intermediates in dysferlinopathy

Owing to the high sensitivity of GC/MS measurements, we were furthermore able to determine the metabolic profile regarding the TCA-cycle intermediates in mouse muscles. Compared to the expression levels of glycolytic intermediates, TCA-cycle metabolites were highly different in their abundance regarding the fibre type constitution of the three muscles assessed. Whereas citrate and alpha-ketoglutaric acid levels, as the main entries for anaplerotic reactions substituting the intermediate pool of the TCA-cycle, were reduced in the 5 minute resting condition, there was a significant peak up to a 1.5 elevation after 20 minutes of exercise detectable. Interestingly, we detected no increase in downstream intermediates like fumaric acid and malic acid, as we would have expected as a consequence of increased citrate and alpha-ketoglutaric acid levels. The mainly oxidative SOL muscle on the other hand, revealed a behaviour opposite to TA muscle, with significantly elevated citrate and succinate levels, followed by a slight increment of downstream metabolites like malic acid and fumaric acid. Unfortunately, we were not able to measure alpha-ketoglutaric acid levels in the 5 minute condition of SOL muscle. Consistent with our previous findings of extraordinarily affected metabolite levels in QUAD muscle, also TCA-cycle metabolites exhibited clear alterations. We found significant elevations of all TCA-cycle intermediates up to a 1.5 fold change in succinate and malic acid levels.

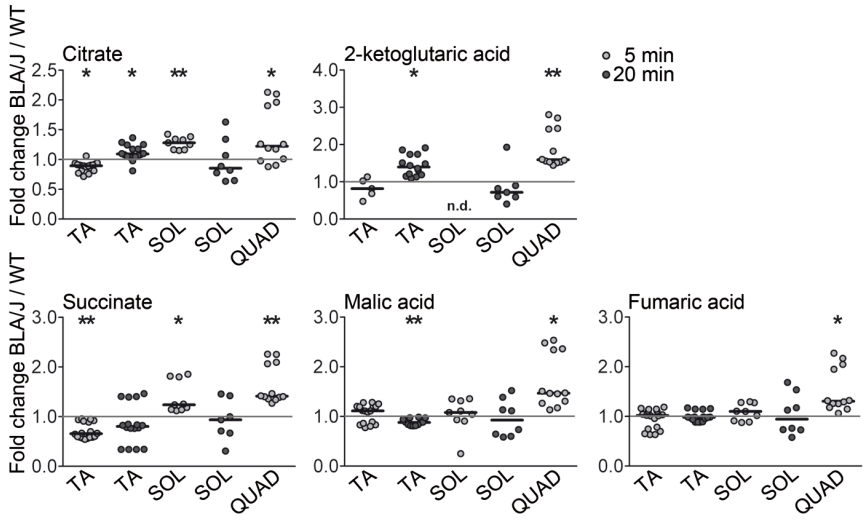

Figure 4.2.5 TCA-cycle intermediates in TA, SOL and QUAD muscle. Intermediates were assessed in the same GC/MS run as glycolytic metabolites. Data are expressed as fold change of BLA/J to wildtype mice. Single data points represent biological and technical replicates (wildtype = 1.0). TCA-cycle intermediates like citrate and alpha-ketoglutaric acid were upregulated, suggesting activated compensatory anaplerotic reactions.

4.2.4 Compensatory pathways securing fuel supply in dysferlinopathy

One important step towards elucidating alterations in the metabolic profile in dysferlinopathy is the assessment of metabolites reflecting compensatory pathways to alleviate the disabled glycolytic fuel supply. Contrary to our measurements under *in vitro* conditions in the primary human myotube model, the assessment of a dysferlin-deficient mouse model under different conditions ensured a more biological determination of on-going changes in the biological network, reflecting the whole organism interplay connected through blood flow and regulating hormones. Consistent with our myotube model, we found a significant increase in fructose levels in the TA muscle after 20 minutes of exercise as well as in QUAD muscle after 5 minutes of resting conditions, whereas no changes occurred in SOL muscle. Furthermore, 3-β-hydroxybutyrate, a ketone body, synthesized by liver cells upon starvation, was increased in QUAD and SOL muscle after 5 minutes of condition 1, and significantly decreased in TA muscle under the same condition. There were no changes in 3-β-hydroxybutyrate levels after 20 minutes of exercise either in TA muscle, or in SOL muscle detectable. Consistent with our hypothesis of enhanced ketone body synthesis and oxidation, we were able to determine increased intensity levels of this metabolite in the liver of BLA/J versus wildtype mice.

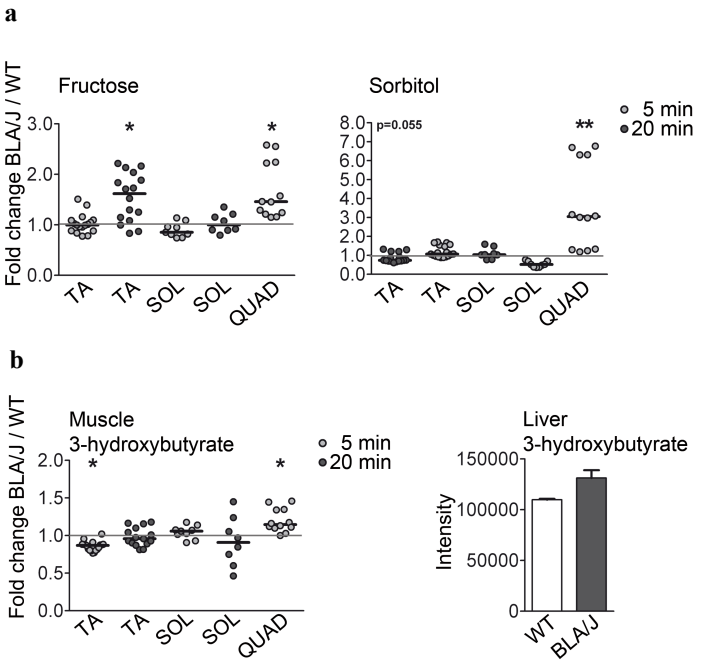

Figure 4.2.4 Altered metabolite levels reflecting *in vivo* compensatory mechanisms in the dysferlinopathy mouse model. Data are expressed as fold change of BLA/J to wildtype mice. Single data points represent biological and technical replicates, wildtype = 1.0. a-b) Muscle metabolites fructose, sorbitol and 3-β-hydroxybutyrate were found to be upregulated in BLA/J mice. c) Metabolic profiling of BLA/J and wildtype liver revealed an upregulated synthesis of 3-β-hydroxybutyrate. Intensity levels are illustrated.

4.2.5 Glycogen synthesis is significantly reduced in BLA/J mice

Although the GC/MS analysis of central carbon metabolites is a very sensitive method, there are certain limitations. Enzymes yielding muscle glycogen such as glucose-1-phosphate and activated uridine-diphosphate glucose (UDP-glucose) cannot be identified. To elucidate whether the decreased glycolytic flux is reduced due to abnormal glycogen synthesis or disabled glycogen breakdown, glycogen content in quadriceps and gastrocnemius muscle of eight male BLA/J and wildtype mice was assessed photometrically in cooperation with the group of Dr. Uwe Ahting, Institute for Clinical Chemistry, Hospital Munich-Schwabing, Munich. Glycogen content in QUAD and GC muscle was significantly reduced as compared to wildtype muscles, which is fully compatible with our hypothesis of disabled glucose uptake and consequently reduced glycogen synthesis in dysferlinopathy.

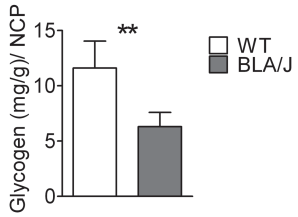

Figure 4.2.5 Glycogen content in gastrocnemius and quadriceps muscle of BLA/J and WT animals. Data are illustrated as mean ± s.e.m, (n=8). Experiments were conducted by Dr. Boris Rolinski, Institute for Clinical Chemistry, Hospital Munich-Schwabing, Munich, Germany.

4.2.6 Comparative metabolic profile of mdx mice

To assess the specificity of our findings in dysferlinopathy, we also determined the metabolic profile in a different muscular dystrophy mouse model, the dystrophin deficient mdx mouse. Two mdx mice and three C57BL/6 controls aged 36 and 38 weeks, respectively, were used for the application of condition 2 (20 min post-injection time).

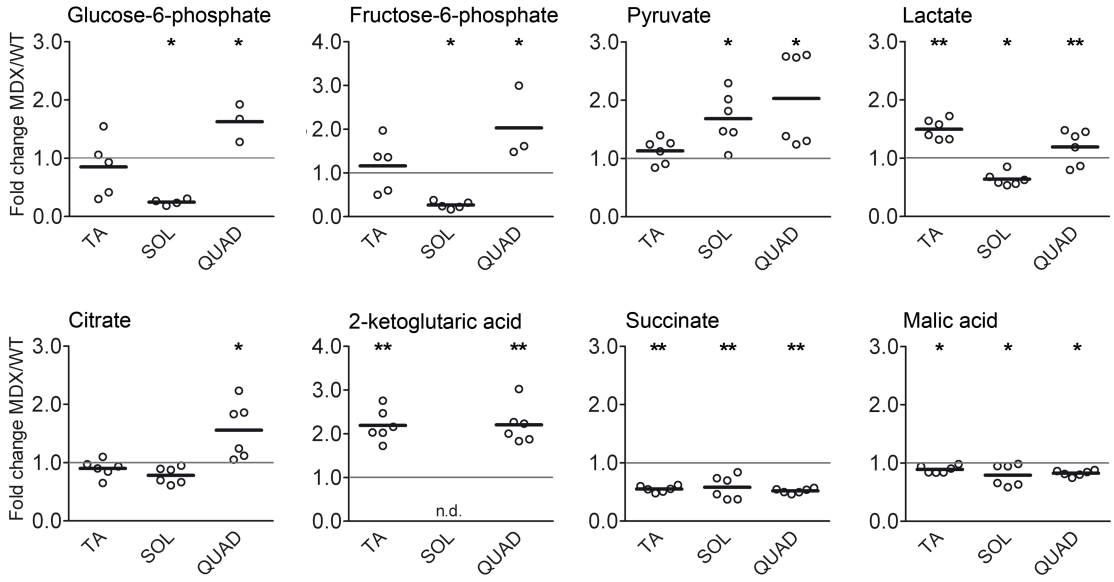

Figure 4.2.6 Metabolic profiling analysis of *mdx* and wildtype (C57BL/10) mice regarding intermediates of glycolysis and TCA-cycle (*mdx* n = 2; age 36 weeks, wildtype n=3, age 38 weeks). $^{13}C_6$ glucose injection followed the same protocol as that used for BLA/J and wildtype mice of condition 2. Glycolytic intermediates are significantly upregulated in TA and QUAD muscles, whereas the oxidative SOL muscle exhibits the contrary pattern. TCA-cycle intermediates citrate within normal ranges for citrate, 2-ketoglutaric acid is significantly increased; succinate and malic acid are decreased in *mdx* mice.

Mdx mice show a significant up to 2-fold increase in glucose-6-phosphate and fructose-6-phosphate in glycolytic and mixed muscles, whereas the oxidative SOL is depleted of upper glycolytic chain metabolites. Concordant with an enhanced anaerobic glycolysis, lactate levels are elevated in TA and QUAD and decreased in SOL muscle. Surprisingly, also 2-ketoglutaric acid is strongly increased in TA and QUAD, suggesting enhanced anaplerotic reactions refuelling the TCA-cycle, whereas succinate and malic acid levels are slightly reduced in all muscle types. Consistent with the GC/MS analysis of SOL muscle in BLA/J mice, we didn´t detect 2-ketoglutaric acid in *mdx* SOL muscle.

4.2.7 Detailed analysis of BLA/J quadriceps muscle

Because metabolic changes in dysferlin-deficient QUAD were more apparent than in “pure” type I or type II muscles, we analysed QUAD in further detail. In addition to the reduction in metabolite levels described above, we found that this mixed fibre type muscle exhibited signs of shifting its characteristic

metabolic pattern towards a more oxidative metabolism. In BLA/J quadriceps, key metabolites such as glucose-6-phosphate, fructose-6-phosphate, succinate and malic acid are expressed at levels similar to oxidative SOL, whereas wildtype QUAD shares type II glycolytic TA characteristics (Fig. 4.2.7.1).

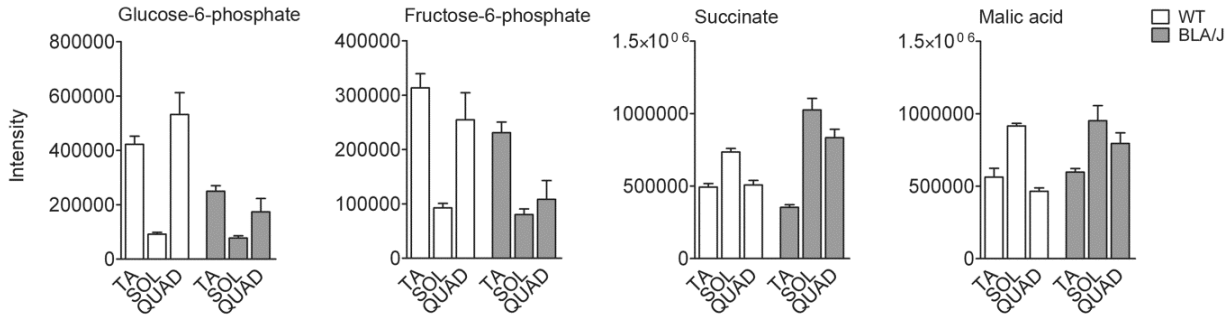

Figure 4.2.7.1 Metabolite intensity levels of 5 minute resting mice (Condition 1). Data are expressed as mean ± sem of wildtype (n=2) and BLA/J (n=3) mice, normalized to cinnamic acid. Metabolite levels of the mixed fibre type QUAD muscle are adapting to a more oxidative metabolism pattern as characteristic for SOL muscle.

The greater abundance of dysferlin in type II muscle fibers was visualized by immunohistochemistry in human muscle cryosections, illustrated in chapter 2.1. To confirm this finding on protein level in muscles of healthy mice, we performed a western blot analysis of homogenized muscle protein extracted from young (<12 weeks) and old (>20 weeks) wildtype mice. Western blot analysis confirmed a greater abundance of dysferlin in the type II muscle EDL compared to SOL muscle in young and old mice. Interestingly, highest protein expression levels were found in QUAD muscle. This finding was confirmed by the LC-MS/MS based proteomic analysis of mice conduced to condition 1 (Table 3.3.2 Experimental design of mice experiments).

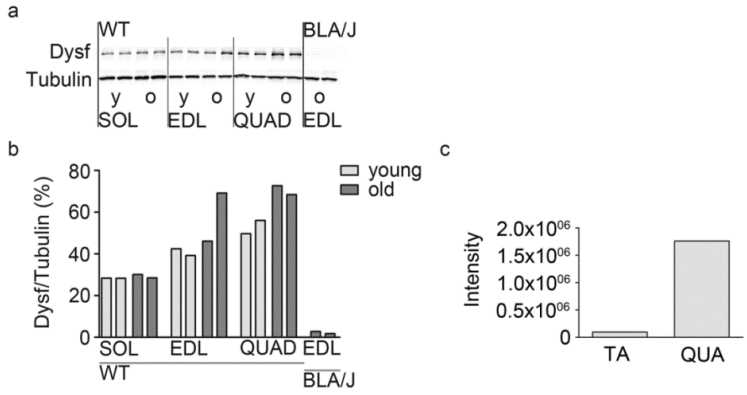

Figure 4.2.7.2 Western blot analysis confirmed by LC-MS/MS measurements of dysferlin in SOL, EDL/TA and QUAD muscles. a)/b) Western blot analysis of SOL (oxidative), EDL (glycolytic) and QUAD (mixed) muscles obtained from young (<12weeks) and old (>20weeks) wildtype (C57BL6) mice (n=1). b) Quantification by ImageJ visualizes differences in dysferlin expression normalized to tubulin. c) LC-MS/MS proteomic analysis further confirms the higher abundance of dysferlin in QUAD muscle compared to a type II fibre muscle.

4.3 Proteome of dysferlin-deficient muscle with focus on metabolic enzymes

4.3.1 Investigation of key metabolic enzymes driving central carbon metabolism

Metabolic alterations in muscular dystrophies are widely described for distinct subtypes as secondary affects due to multiple degradation and reconstruction events in the course of a muscular dystrophy. To elucidate the expression patterns of multiple enzymes involved in the energy metabolism of muscle cells, we applied a SILAC-based LC-MS/MS proteomic approach of the contralateral muscles extracted from mice according to the metabolic profiling protocol of condition 1. All LC-MS/MS based proteomic data depicted in the following chapters were measured from the same mouse muscles of the metabolic profiling analysis. A stable-isotope labelled reference (SILAC) muscle was obtained from mice, which fully incorporated a heavy labelled amino acid (lysine) by lifelong ingestion. It served as a standard to allow an exact quantification and normalization of protein intensities measured in our samples. The ratio of the heavy (labelled-^{13}C) to the light (unlabelled-^{12}C) reflects the abundance of a certain protein in the SILAC-reference compared to the sample. The calculation of the inverse ratio L/H is used to illustrate the protein abundance of our sample compared to the reference. For the detailed assessment of enzymes associated to the glycolytic pathway and TCA-cycle, we extracted nine enzyme ratios out of 1500 measured proteins.

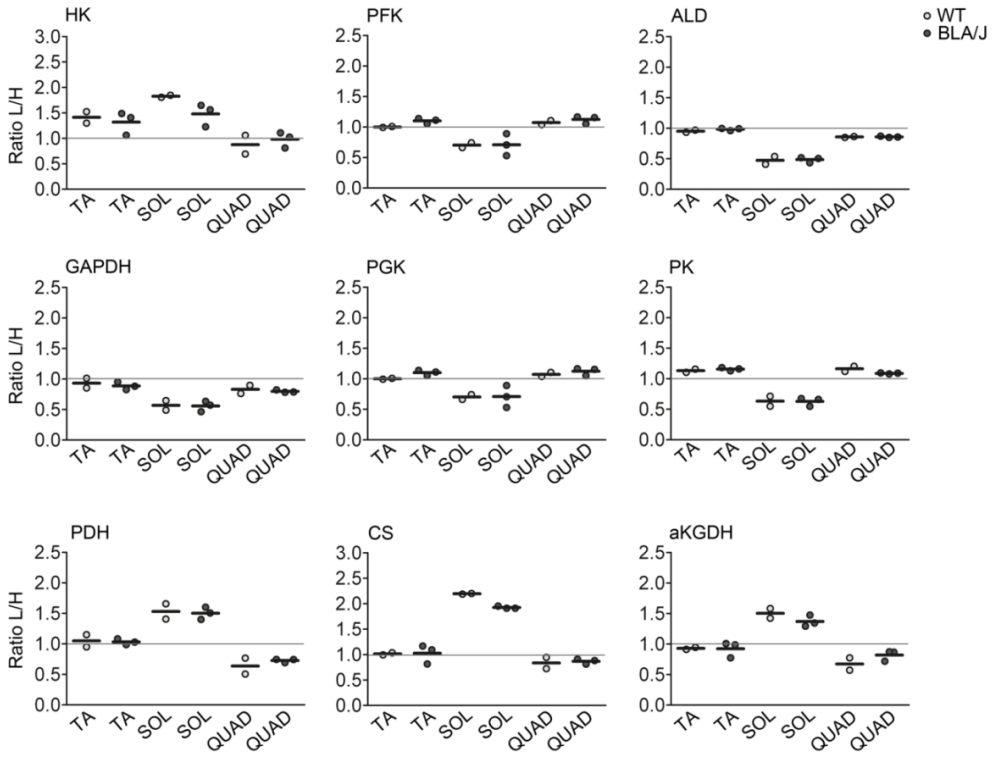

Figure 4.3.1 SILAC-based LC-MS/MS analysis of key metabolic enzymes in dysferlin-deficient BLA/J and wildtype mice TA, SOL and QUAD muscles. Contralateral muscles of mice undergoing condition 1 of metabolic profiling analysis protocol were used for the proteomic approach (wildtype n=2, BLA/J n=3). Data are illustrated as ratio L/H between sample enzymes and SILAC-reference (=1.0). There are no differences in glycolytic and TCA-cycle enzyme expression patterns detectable between BLA/J and wildtype mice.

All enzymes of the upper glycolytic pathway like hexokinase (HK), phosphofructokinase (PFK) and aldolase (ALD), as well as downstream glycolytic pathway enzymes like glyceraldehyde-3-phosphate dehydrogenase (GAPDH), phosphoglycerate kinase (PGK) and pyruvate kinase (PK) were similarly expressed in wildtype and BLA/J muscles. We further analysed enzymes involved in TCA-cycle metabolism, like pyruvate dehydrogenase (PDH), constituting the entry reaction by forming acetyl-CoA from pyruvate. There were no differences in enzyme expression between wildtype and BLA/J mice. Also citrate synthase (CS) and alpha-ketoglutarate dehydrogenase (KGDH) expressions, reflecting key metabolic enzymes for anaplerotic reactions by replenishing the TCA-cycle intermediate pool, were similar between wildtype and BLA/J mice. From another point of view on the enzyme pattern, regarding their expression pattern in oxidative and glycolytic muscles, the proteomic analysis clearly enabled the distinction of muscle fibre types due to their enzymatic profiles. Specifically, TA muscle, consisting mainly of type II fibres, as well as the mixed fibre type QUAD muscle, possessed higher levels of glycolysis-driving enzymes compared to the oxidative type I fibre muscle SOL, which in contrast revealed a much higher expression of TCA-cycle featuring enzymes, in both wildtype and BLA/J mice.

4.3.2 Respiratory chain enzymes

Another approach to elucidate the metabolic pathomechanism behind dysferlinopathy was the examination of enzymes involved in the oxidative phosphorylation (OXPHOS) of reduction equivalents like NAD/NADH to produce ATP. Due to the high sensitivity of LC-MS/MS proteomic analysis, we were able to detect various different subunits and isoforms belonging to one of the five respiratory chain complexes I – V. We could not find any differences in expression between distinct subtypes and isoforms building a certain complex. Figure 4.3.2 illustrates one representative subunit. We further conducted an analysis of the genetic background and proteomic designation of each subunit, using the Uniprot ID, as illustrated in the table of Figure 4.12. There were no differences in TA, SOL or QUAD between wildtype and BLA/J mice, but as described previously, there was a clear difference between expressions patterns of distinct fibre type muscles, with high abundance of respiratory chain complexes in the oxidative SOL muscle compared to TA and QUAD.

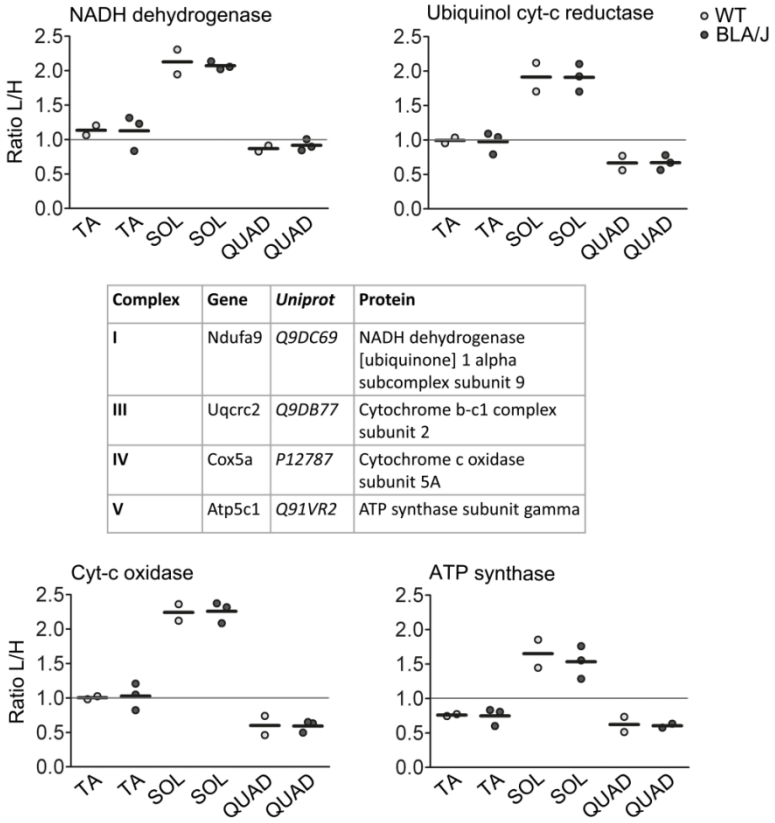

Complex	Gene	*Uniprot*	Protein
I	Ndufa9	*Q9DC69*	NADH dehydrogenase [ubiquinone] 1 alpha subcomplex subunit 9
III	Uqcrc2	*Q9DB77*	Cytochrome b-c1 complex subunit 2
IV	Cox5a	*P12787*	Cytochrome c oxidase subunit 5A
V	Atp5c1	*Q91VR2*	ATP synthase subunit gamma

Figure 4.3.2 Respiratory chain enzyme expression in BLA/J mice. All protein expressions are measured from the contralateral muscles of mice used for metabolic profiling analysis in condition 1. Data are illustrated as ratio L/H between muscle sample and SILAC-reference. Subtypes representing whole complexes are used for the visualization of potential differences between wildtype and BLA/J. The genetic background and Uniprot ID are presented in the associated table. There is no difference in respiratory chain enzymes visible between wildtype and BLA/J mice.

4.3.3 Elucidation of protein alterations associated with dysferlinopathy

Our proteomic approach enabled the detection of around 1500 proteins in muscle, contributing to various functions such as metabolism, cytoskeleton and membrane structure or prevention of oxidative damage. To sort out proteins with major alterations in dysferlinopathy, we calculated the fold change between H/L ratios of BLA/J and wildtype mice using this formula:

$$Ratio\ L/H\ fold\ change_{(BLA/J\ /WT)} = Ratio\ L/H_{BLA/J} / Ratio\ L/H_{WT}$$

Out of the vast range of proteins, we found only two to four, which were significantly altered in our mice model. Data illustrated in Figure 4.3.3 represent proteins altered at least in one of the three muscle types TA, QUAD and SOL. For each protein, the corresponding gene and Uniprot ID is presented in the table below. There were marked increments of adenosine monophosphate desaminase (Ampd1), an enzyme contributing to the purine nucleotide cycle by converting AMP to IMP by deamination, found in TA and QUAD muscle.

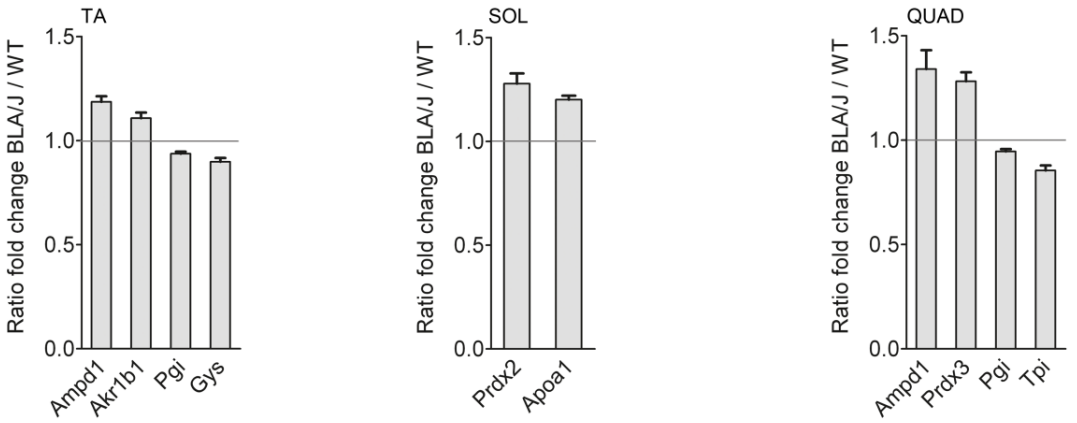

Gene	*Uniprot*	Protein
Ampd1	*Q3V1D3*	AMP desaminase 1
Akr1b1	*P45376*	Aldose reductase
Pgi	*P06745*	Phosphoglucose isomerase
Gys1	*Q9Z1E4*	Glycogen (starch) synthase

Gene	*Uniprot*	Protein
Prdx2	*Q61171*	Peroxiredoxin-2
Apoa1	*O08855*	Apolipoprotein A-I

Gene	*Uniprot*	Protein
Ampd1	*Q3V1D3*	AMP desaminase 1
Prdx3	*P20108*	Thioredoxin-dependent peroxid reductase, mitochondrial
Pgi	*P06745*	Phosphoglucose isomerase
Tpi1	*P17751*	Triosephosphate isomerase

Figure 4.3.3 Proteins differently expressed in BLA/J mice compared to healthy littermates. Proteins are expressed as fold change between L/H ratio of BLA/J and wildtype mice.

Aldose reductase, only increased in TA muscle, catalyses the reduction of glucose to sorbitol, thereby representing the major step of the pathway yielding the formation of fructose. It is worth to mention that this finding is fully consistent with our metabolic profiling data of increased fructose in dysferlin-deficient myotubes and the mice model. Phosphoglucoisomerase (Pgi), catalysing the conversion of glucose-6-phosphate to fructose-6-phosphate, was reduced in TA and QUAD muscle, furthermore we found reductions of glycogen synthase in TA and triosephosphate isomerase (Tpi), driving the reversible interconversion of dihydroxyacetone phosphate (DHAP) to glyceraldehyde-3-phosphate (GA3P) in QUAD muscle. Both QUAD and SOL muscle expressed higher levels of thioredoxin-peroxidase reductase (Pdx3) and peroxiredoxin 2 (Pdx2), respectively, two enzymes contributing to the protection of radical sensitive enzymes from oxidative damage. Interestingly, in the oxidative SOL muscle we found an upregulation of apolipoprotein A1 (Apoa1), a major component of high density lipoproteins (HDL), thus participating in lipid metabolism and transport.

4.3.4 IDH isoform expression coincides with alterations in NAD(P) transhydrogenase expression

Two proteins involved in the mitochondrial generation of oxidative stress due to reduction equivalents were of major interest for the elucidation of the metabolic pathomechanism underlying progressive muscle damage in dysferlinopathy. Isocitrate dehydrogenase (IDH), catalysing the oxidative decarboxylation of isocitrate to 2-ketoglutaric acid and CO_2, exhibited a clear isoform-dependent expression pattern be-

tween different muscle fibre types. Whereas IDH 3a and IDH 3g showed the same distribution in oxidative and glycolytic muscle fibres, IDH 2, using NADP+ as cofactor, was much more abundant in type I fibre muscle SOL. IDH isoforms were similarly expressed in BLA/J and wildtype mice. NAD(P) transhydrogenase catalysing the transfer of hydride ion equivalents between NAD(H) and NADP(H), was strikingly reduced in all three muscle types of dysferlin-deficient BLA/J mice.

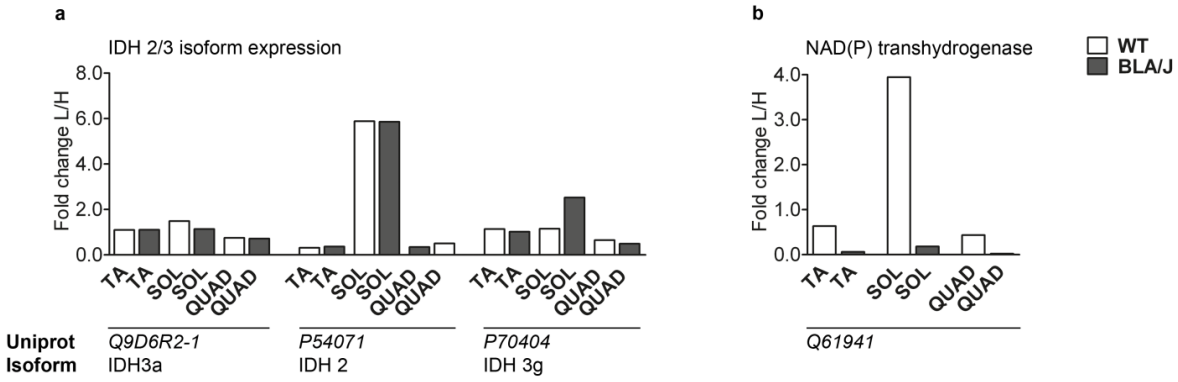

Figure 4.3.4 IDH isoform and NAD(P) transhydrogenase expression in oxidative and glycolytic muscles of BLA/J and WT mice. Data are illustrated as ratio L/H between muscle sample and SILAC-reference, proteomic analysis of TA, SOL and QUAD muscle of BLA/J and wildtype mice conducted to the metabolic profiling analysis of condition1. a) IDH 3a,2 and 3g isoform expression in wildtype and BLA/J mice. There is a great abundance of IDH 2 in oxidative type I muscle fibres (SOL) compared to IDH 3a,g. b) Mitochondrial NAD(P) transhydrogenase expression. No change of IDH 2 abundance is visible in BLA/J mice. NAD(P) transhydrogenase is strikingly decreased in all three muscles of BLA/J mice.

5. Discussion

5.1 Advantages and limitations of study

The skeletal muscle is a large metabolic organ. However, hereditary muscular dystrophies have mostly been interpreted in regard to their mechanical and structural consequences for the skeletal muscle. This is the first comprehensive investigation of metabolic consequences of a defined muscular dystrophy combining primary patient material and muscle cell cultures, suitable mice models and cell biology tools with the most advanced analytical methods such as GC/MS-based metabolomics and SILAC-based quantitative proteomics.

GC/MS-based metabolomics is a powerful tool to elucidate the impact of monogenic hereditary disorders on the metabolic network of various organs, thereby providing novel insights into the pathomechanism underlying a certain disease. However, the application of GC/MS settings, the cell incubation and the harvest for metabolite analysis carries certain pitfalls, especially regarding the analysis of slow-growing human primary myotubes compared to fast growing tumour cells, widely used for metabolic analysis. Bearing in mind the elaborative preparation and cultivation procedures of human primary myotubes obtained from patients muscle biopsies, the amount of cell material available for experiments is rather small and of great value. Although GC/MS based metabolic analysis is highly sensitive, the measurement in technical replicates and the metabolite extraction procedure require the utilization of high myotube counts. In contrast to the majority of cells available for research, human primary myotubes are adherent cells, only cleaved from the bottom of the petri dish for cell counting and splitting. For cell harvest and metabolite extraction, it was necessary to establish a new protocol compatible with the application of chloroform without damaging the plastic petri dish. Furthermore, GC/MS settings and software application had to be adapted, as the chromatography of our first analyses was shaded by noise contamination, prohibiting analysis of phosphorylated hexoses like glucose-6-phosphate and fructose-6-phosphate. As GC/MS based metabolic approaches cover a rather novel field in system biology compared to LC-MS/MS based proteomics, software tools and libraries for the identification and quantification of metabolites are still evolving. Unlike to proteomics, the application of metabolomic software tools like Pegasus ChromaTOF, still demands a large amount of manual evaluation like the validation and peak correction of identified metabolites. Hence, first and foremost the handling and understanding of those biotechnological tools is the underlying and most time-consuming step towards any metabolite data generation. Despite the fact that GC/MS based metabolomics enables the identification of various metabolites involved in the central carbon metabolism and connected pathways, there are still some metabolites that cannot be identified, thus resulting in holes in the metabolic network of the analysed organism. It is particularly important to mention that we were not able to identify metabolites connected to the glycogen synthesis and breakdown pathway like glucose-1-phosphate and uridine diphosphate glucose, which is why we had to con-

duct a different experiment to elucidate the impact of this major pathway, determining the fate of glucose in the muscle cell. As mice are widely used for metabolic analysis, the metabolite extraction and GC/MS identification followed an approved standard and proceeded without difficulties. Although *in vivo* experiments are usually not fully predictable, metabolite expressions levels within a certain mouse model were of lesser variance than expected. Nevertheless, one needs to bear in mind, that prior to our experiments, we did not apply any normalized protocol to the mice housing or feeding conditions such as limitation of mobility or feed. Furthermore, we were surprised that some wildtype and BLA/J mice reacted quite differently to intravenous glucose injection, exhibiting signs of fainting or weakness in the first minutes afterwards. The implementation of a 5 minute resting period after injection ensured that all mice, which underwent 20 minutes of treadmill exercise had time to recover from the injection procedure.

As GC/MS based metabolomic analysis not only enables the assessment of the steady state metabolic profile, but also the application of a metabolic flux analysis, which serves to determine the distribution and incorporation of a ^{13}C labelled substance like $^{13}C_6$ glucose after administration in the whole organism, we applied stable isotope labelled glucose to our myotube and mice models. Interestingly, despite multiple different incubation times and conditions, the determination of the metabolic flux was not satisfactory as these cells incorporated only 3-4% of the stable isotope, making a definitive flux analysis rather unreliable. There might be some reasons for the lack of stable isotope incorporation, first of all, which is that muscle cells usually prefer fatty acids as fuel substrate, unless they are contracting or stimulated with insulin. To determine the central carbon flux, the application of a stable isotope-labelled free fatty acids like $^{13}C_4$ palmitic acid might be a useful tool. As mentioned above, metabolites connected to the glycogen synthesis or breakdown pathway are not amenable to GC/MS metabolome approaches, which made it additionally difficult to assess if the $^{13}C_6$ glucose taken up was eventually directly conducted to this pathway, hence circumventing glycolytic metabolization.

Like the stable isotope labelling approach of human myotubes, the intravenous injection of $^{13}C_6$ glucose in mice models to measure substrate uptake of the skeletal muscle is a very novel procedure, which has not been attracted much attention in publications on stable isotope resolved metabolomics (SIRM) before. Our decision to use two injection conditions regarding post-injection time course was mainly based on one paper published 2011 by Fan et al., describing label incorporations of $^{13}C_6$ glucose and $^{13}C_6$ lactate over time after injection of these tracers into the tail vein of resting mice. Highest label incorporations into skeletal muscle lactate were found at 20 minutes post-injection time, however, the amount of label incorporation into lactate was the lowest compared to brain, heart, lung and kidney tissue (Fan, Lane et al. 2011). Concordantly with these findings, we found only slight label incorporations into lactate after 20 minutes post-injection time plus exercise, whereas mice of condition 1 (5 minutes post-injection time) barely exhibited any incorporated heavy tracer. Since skeletal muscle prefers free fatty acids as fuel substrates during rest and long term exercise, the intravenous injection of stable isotope labelled $^{13}C_4$ palmitate seems to be an interesting tool for efficient TCA-cycle flux analysis using the GC/MS approach. Another interesting tool is provided by the analysis of fatty acid flux by application of a liquid chromatog-

raphy/electrospray ionization ion-trap tandem MS (LC/ESI-itMS2) to circumvent the inefficient derivatization procedure of palmitoylcarnitine, which is necessary for GC/MS analyses (Guo, Yarasheski et al. 2006).

5.2 Revealing the dysferlinopathy metabotype

5.2.1 Decreased glycolysis in dysferlin-deficient myotubes

The GC/MS based metabolic profiling analysis revealed a striking reduction in glycolytic and TCA-cycle intermediates in human primary dysferlin-deficient myotubes, compared to the healthy control. Taking into account that the overall metabolism of primary cell myotubes undergoes marked changes within the time course of cultivation, one might argue that our observed metabolic profile is more likely due to age than disease related causes. However, applying the metabolic protocol, both myotube cell lines showed comparable passages and exhibited similar growth rates and fusion potentials. Furthermore, metabolic experiments measuring glucose uptake and oxidation, glycogen synthesis and β-oxidation of fatty acids in human myotube cultures undergoing senescence showed an overall metabolic reduction, without proof of compensatory pathways, which might be crucial for maintaining cell homeostasis (Nehlin, Just et al. 2011). Despite the fact that our dysferlin-deficient myotubes had markedly reduced glycolytic and oxidative capacities, some metabolites were exceedingly increased, thus indicating the activation of connected pathways as mean to circumvent reduced glycolytic supply.

5.2.2 Elucidating the impact of glutamate and glutamine in dysferlinopathy

Three amino acids - glutamate, glutamine and alanine - represent about 79 % of the total free amino acid pool, eligible to be incorporated into human proteins (Bergstrom, Furst et al. 1974). Of these, glutamate has the highest intracellular fraction, although its carrier transporting the dicarboxylic amino acids glutamate and aspartate is characterized by high specificity and low capacity with a maximum transport rate (V_{max}) of about 80 µmol/kg net weight/min (Rutten, Engelen et al. 2005). Glutamine uptake on the other hand is effected by a very high-activity transporter with a K_m above the *in vivo* plasma concentration, which leads to the assumption that glutamine uptake, its conversion into glutamate and sequential synthesis of alpha-ketoglutaric acid for TCA-cycle replenishment might serve as an additional energy source during exercise or disabled glycolytic supply. There are two main pathways predominant in different tissue, both involving glutamate as precursor for alpha-ketoglutaric acid. Whereas increased glutaminolysis is a key feature of cancer cells to meet the high energy demand, in skeletal muscle alanin-aminotransferase reaction (AAT), forming alpha-ketoglutaric acid out of alanine and glutamate, is predicted to be predominant (Sahlin, Katz et al. 1990; Chen and Russo 2012). Indeed, different studies confirmed an increase in glycogen storage due to intravenous or oral administration of glutamine after ex-

haustive exercise (Varnier, Leese et al. 1995; Bowtell, Gelly et al. 1999). Furthermore, one hour after glutamine ingestion, resting muscle glutamate content was elevated, whereas in the exercise induced protocol, this effect was blunted (Bowtell, Gelly et al. 1999). The postulation of an enhanced glutamine and glutamate uptake as a compensatory mechanism in our glucose-depleted dysferlin-deficient myotubes might be further reasonable, considering the fact that the labelling medium administered over 10 and 30 minutes of incubation was supplemented with glutamine and that intracellular glutamine levels peaked after 10 minutes of incubation, consistent with the different uptake velocities of both metabolites. On the other hand, unexpectedly TCA-cycle intermediates of dysferlin-deficient myotubes were not elevated, suggesting a disabled reaction chain either by limited enzymatic capacities or low transport activities of the mitochondrial carrier. Another rather simple explanation is given by the composition of the labelling medium used for the metabolic analysis. In contrast to the *in vivo* mouse model, dysferlin-deficient myotubes were not able to increase the uptake of ketone bodies or free fatty acids to secure their energy demand, as these substrates were not provided in the labelling medium. Considering the fact that transport kinetics for glutamine are highly active and downstream enzymatic capacities yielding the formation of alpha-ketoglutaric acid are rather limited and substrates like FFA and ketone bodies are not available, it is hardly surprising that we detected a 30-fold increment of glutamine without the expected increase in TCA-cycle intermediates. Another important function of glutamate is its involvement in intracellular glutathione synthesis, which represents the most abundant intracellular antioxidant. Several studies conducted under different catabolic conditions showed a correlation of decreased glutamate and glutathione levels in skeletal muscle (Luo, Hammarqvist et al. 1998; Flaring, Rooyackers et al. 2003). Moreover, Flaring et al. demonstrated that intravenous application of glutamine equated post-surgical glutathione depletion, suggesting that also in this case a conversion from glutamine to glutamate took place. Although reduced intracellular glutamate levels have been demonstrated for several acute and chronic diseases like emphysema and surgical trauma, this effect does not seem to be predominant in the progressive muscle wasting of dysferlinopathy. Taken together, increased levels of glutamine and glutamate seem to serve as a compensatory mechanism to circumvent the reduced energy supply of glycolysis in dysferlinopathy. Whether supplementation of these metabolites results in a slower disease progression due to a milder metabolic phenotype, requires further investigation.

5.2.3 Glutamate supplementation – a therapeutic strategy?

As described above, glutamate plays a broad functional and metabolic role in healthy and diseased skeletal muscle. Intravenous and oral supplementation of glutamate or glutamate-related substrates like glutamine, alpha-ketoglutaric acid and branched chain amino acids (BCAAs) has been evaluated in several studies focusing on the replenishment of glutamate in skeletal muscle of postoperative, coronary and healthy patients. Indeed, Thomassen et al. showed that intravenous administrated glutamate increased in myocardium and leg in a dose dependent manner whereas Graham et al. demonstrated that bolus oral

ingestion of high doses of monosodium glutamate (MSG) resulted in significant increases in plasma and muscle glutamate levels in healthy volunteers (Thomassen, Nielsen et al. 1991; Graham, Sgro et al. 2000). As the sodium salt of glutamate is also predicted to cause adverse effects, referred to as "Chinese restaurant syndrome" and deterioration of certain disease outcomes possibly through enhancement of oxidative stress has been described, no studies have been conducted so far to evaluate possible beneficial effects in muscular diseases (Murphy, Miyamoto et al. 1989; Rutten, Engelen et al. 2005). Furthermore, one needs to bear in mind that the AAT-reaction, which is predicted to be predominant in skeletal muscle, relies on pyruvate for the synthesis of alpha-ketoglutaric acid. A dietary supplementation with glutamate or MSG possibly requires the addition of pyruvate to achieve an effective therapeutic approach and to prevent a further reduction of glycolytic intermediates.

5.2.4 Pyruvate levels in dysferlin-deficient myotubes

Amongst all metabolites contributing to the metabolic profile of dysferlin-deficient myotubes, pyruvate showed a lesser reduction accompanied by a distinct increment after 30 minutes of incubation, indicating extra-glycolytic regulation or uptake mechanisms. Homeostasis of the pH in muscle cells is regulated by the pyruvate-lactate ratio, controlled by exchange transporters between extracellular, cytosolic and mitochondrial compartments. In skeletal muscle, the monocarboxylate transporters MCT1 in oxidative and MCT4 in glycolytic muscle fibres are the most abundant exchange carriers (Mengual, El Abida et al. 2003). Taking into account that, according to the skeletal muscle growth media composition, labelling medium used for myotube incubation contained sodium-pyruvate, it seems likely that dysferlin-deficient myotubes enhance pyruvate uptake to compensate the lack of metabolites derived from glycolysis. A decreased activity of pyruvate carboxylase or the pyruvate-dehydrogenase complex, leading to an accumulation of pyruvate is apparently not relevant, as one would expect a concomitant increase in lactate levels produced by lactate dehydrogenase, similar to exercise-induced lactate acidosis (Wells, Selvadurai et al. 2009). Furthermore, pyruvate and other ketoacids are predicted to act as efficient antioxidants by converting hydrogen peroxide to water in a non-enzymatic chemical reaction upon renal injury (Salahudeen, Clark et al. 1991). The role of oxidative stress and subsequent cell damage in dysferlinopathy will be addressed in chapter 5.2.6.

5.2.5 Fructose connected pathways

The increase in fructose and sorbitol levels both in our *in vitro* human myotube and *in vivo* mouse model for dysferlinopathy was a rather surprising finding, considering the role of possible pathways yielding that metabolite. In human skeletal muscle, fructose uptake is realized by the glucose transporter Glut5, which is exclusively localized at the sarcolemmal membrane. Unlike GLUT4, Glut5 is susceptible neither to inhibition by cytochalasin, nor to any activation through enhanced exercise or contraction, but insulin

was shown to increase Glut5 abundance and activity, mediated via activation of the Glut5 promoter (Hundal, Darakhshan et al. 1998; Hajduch, Litherland et al. 2003). Whether and to what extend fructose is conducted to the glycolytic pathway in skeletal muscle still requires further investigation. A major role of fructose uptake in our dysferlin-deficient myotubes seems unlikely, considering that no fructose was added to the labelling medium. It is more reasonable to assume that glucose is converted by aldose reductase (AR) and sorbitol dehydrogenase (SDH) in the so called polyol pathway. Indeed, our proteomic analysis detected an increased expression of aldose reductase in the TA muscle of BLA/J mice, further supporting this theory. Aldose reductase is a widely expressed NADPH-dependent enzyme, which has been linked to the development of secondary diabetic complications. In the presence of normal glucose levels (5.5 mM), AR activity accounts for only 3 % of total glucose consumption, whereas an increase up to 30 % is detected in a hyperglycaemic status (Gonzalez, Barnett et al. 1984). Furthermore, AR was recently shown to be implicated in the reduction of stress-generated lipid aldehydes, thereby mediating oxidative stress signals due to the regulating role of lipid peroxidation derived aldehydes (LDAs) in cell signals leading to cell death or growth (Dixit, Balendiran et al. 2000). Because NAPDH is essential for the detoxification of reactive oxygen species and hydroxyperoxides, like the glutathione peroxidase (GPx) and glutathione reductase (GR) system, high AR activity is also predicted to be involved in cell damage due to oxidative stress, thus additionally aggravating the sorbitol-induced hyperosmotic cell damage in diabetes (Srivastava, Ramana et al. 2005). Whether most of the diabetes-related secondary complications are due to high amounts of sorbitol or caused by increased levels of oxidative stress, is still a matter of debate. Nevertheless, experimental animal studies investigating the application of selective AR inhibitors like ranirestat (AS-3201), which is currently undergoing phase III clinical trial in Europe and the US, have been shown to attenuate diabetes-induced secondary complications (Giannoukakis 2008; Tang, Martin et al. 2012). Further research will be required to evaluate the potential negative or beneficial effects of enhanced fructose pathways in the pathogenesis of dysferlinopathy. Certainly, the use of AR-reductase inhibitors in dysferlinopathy to prevent ROS-induced muscular damage and deterioration could be a powerful option, at least in the long term.

5.2.6 Coplay of IDH isoforms and proton-translocating transhydrogenase

Reactive oxygen species are side products of a multitude of oxygen-metabolizing reactions with the majority generated by the mitochondrial electron transfer chain. Small molecule and protein-based redox-buffer systems like glutathione (GSH/GSSG) and oxidized/reduced thioredoxin are thiol-based reducing agents and antioxidants (Banerjee 2012). Furthermore, glutathione and thioredoxin (TRX) are predicted to be involved in various physiological reactions like cellular signalling pathways and metabolism (Kondo, Nakamura et al. 2006; Franco, Schoneveld et al. 2007). Signs of enhanced reactive oxygen species (ROS) have been shown by several groups for muscular dystrophies and dysferlinopathy (Rando, Disatnik et al. 1998; De la Torre, Illa et al. 2009). Furthermore, our proteomic analysis revealed an in-

creased expression of antioxidant enzymes belonging to the thioredoxin/peroxiredoxin family (TRX/PRXS). In addition the SILAC-based proteomic analysis revealed a strong reduction of NAD(P)-transhydrogenase levels in all muscle fiber types of dysferlin-deficient BLA/J mice. This enzyme, also known as H+-transhydrogenase (H+-Thase), is located in the inner mitochondrial membrane and catalyzes the transfer of hydride ion equivalents between NAD(H) and NADP(H) coupled to the translocation of protons (Sazanov and Jackson 1994). As NADPH is required for the combined action of glutathione reductase and glutathione peroxidase to reduce H_2O_2 produced by the respiratory chain, cells lacking NADPH-producing reactions rely on NAD(P)-transhydrogenase (Hatefi and Yamaguchi 1996). Hence, there hasn't been much research carried out on the evaluation of isocitrate dehydrogenase (IDH) isoforms in skeletal muscle. We were the first group to detect the predominance of IDH2 in oxidative type I fibres in SOL skeletal muscle. Taking into account that the oxidative phosphorylation cascade favoured in type I muscle fibres for energy consumption, produces higher amounts of ROS, it stands to reason that these muscle fibre types express an NADP-linked IDH isoform to form NADPH for ROS reduction. In dysferlin-deficient muscle cells, the central carbon metabolism in type II muscle fibres is shifted to rather oxidative characteristics, implicating higher amounts of oxidative phosphorylation and subsequent ROS production. Notably, IDH isoform expression is not changed in the course of dysferlinopathy, leading to the assumption that, despite the fact that ROS are increased due to enhancement of oxidative energy consumption, dysferlin-deficient type II fibres are not able to produce higher amounts of NADP reduction equivalents necessary to remove accruing ROS. Furthermore, NAD(P)-transhydrogenase, as the only enzyme capable of building NADPH, is strikingly reduced in dysferlinopathy, presumably because the proton translocating reaction of NAD(P)-transhydrogenase reduces the proton electrochemical gradient necessary for the generation of ATP in the respiratory chain. The combination of IDH isoform expression in different muscle fibre types associated with reduced levels of NAD(P)-transhydrogenase provides a reasonable explanation for the predominant involvement of type II muscle fibres due to metabolic alterations which concomitantly leads to enhanced levels of oxidative stress in affected muscle cells. Intensive research in this field to elucidate the exact involvement of these enzymes in progressive muscle damage in dysferlinopathy will open the field for possible therapeutic targets in future.

5.2.7 Metabolic alterations *in vivo* – analysing compensatory pathways

Bearing in mind that the application and evaluation of the newly found altered metabolic profile in dysferlin-deficient human primary myotubes was hampered by certain limitations, we decided to shift our attention to an *in vivo* model for dysferlinopathy, which enables a detailed assessment of compensatory pathways activated in the co-play of different organs either more or less affected by a certain disease. We used the BLA/J mouse model for our experiments because this strain is akin to the control strain as it is crossed onto a C57BL/6 background. Beyond that, since the widely used SJL/J mouse model harbouring a naturally occurring dysferlin mutation was recently shown to exhibit certain autoimmune and metabolic

alterations due to enhanced fatty acid oxidation in heart and skeletal muscle, we decided to study the BLA/J mouse model (Bittner, Anderson et al. 1999; Guan, Goldstein et al. 2009). As expected, we found an altered metabolic profile in both conditions applied to the BLA/J mouse model, highly similar to the metabotype of human dysferlin-deficient myotubes. The strongest metabolite reduction was visible in the upper glycolytic pathway (glucose-6-phosphate and fructose-6-phosphate), supporting our hypothesis of disabled glucose uptake in dysferlin-deficient muscle. Whereas upper glycolytic chain metabolites showed time- and condition-independent alterations and could not be regulated, metabolites like 3-phosphoglycerate, phosphoenolpyruvate and pyruvate were synthesized differently and were probably compensatory. Furthermore, pyruvate levels were much more affected in SOL muscle, which might be due to different regulations of the pyruvate-dehydrogenase complex (PDH) in oxidative fibre type muscles. The plainest time-dependent synthesis was detected for lactate, showing a slight rise under resting conditions followed by a marked decline after 20 minutes of exercise, thereby clearly underlining the activation of compensatory pathways and preference of oxidative metabolism in dysferlinopathy during light to moderate mobilization. While glycolytic energy metabolism showed highly similar disease related patterns *in vitro* and *in vivo*, the TCA-cycle metabolites in the mouse model were less affected. This finding strongly confirmed our hypothesis of activated compensatory pathways yielding TCA-cycle intermediates and shifting of the metabolism to more oxidative fuel utilization in dysferlinopathy. The strongest increment in citrate and alpha-ketoglutaric acid, especially in the more severely affected glycolytic and mixed muscles, TA and QUAD, respectively, indicated an enhanced FFA and ketone body oxidation, as these pathways yield both intermediates. Indeed, we also detected higher amounts of 3-β-hydroxybutyrate in the liver obtained from our BLA/J mice, underlining the theory of enhanced ketone body synthesis and oxidation in the disease course of dysferlinopathy. Beyond that, also enhanced glutaminolysis and alanin-amino-transferase (AAT) reactions could contribute to an increment of alpha-ketoglutaric acid, as discussed in chapter 5.1.2. In SOL and QUAD muscle, beta-oxidation of odd numbered FFA might further account for increased succinate levels.

5.2.8 Quadriceps muscle – shifting its metabolic origin?

Since preliminary studies conducted in our laboratory strongly suggested a correlation of dysferlinopathy-induced type II fibre loss with metabolic alterations, which also explained the correlation of disease onset with fibre type shifting during puberty, we were surprised to find an even more affected metabolic phenotype in the mixed fibre type muscle QUAD. The quadriceps muscle consists of unequal amounts of type I and II fibres and is located at the front site of the mouse's proximal hind limb. Due to a type II fibre preponderance in QUAD muscle, the metabolic characteristics in healthy mice are more similar to a type II fibre muscle. Interestingly, assessment of metabolite intensity levels in QUAD compared to SOL and TA muscle revealed rather distinct metabolic characteristics in the disease model as many metabolites con-

nected to switch points in the glycolytic and oxidative pathways changed their type II fibre characteristics in the wildtype to a type I fibre phenotype in dysferlinopathy. Figure 4.8 strikingly illustrates the adaptation of dysferlin-deficient QUAD muscle fibre type characteristics, thereby resembling the type I fibre muscle SOL. Recent publications describe the use of proteomic and immunohistochemical approaches to unveil important protein alterations in dysferlinopathy. Referring to these and other references, a loss of type II fibres in the course of dysferlinopathy is widely confirmed (Fanin and Angelini 2002; De la Torre, Illa et al. 2009). The answer as to whether these changes are caused by a progressive fibre type conversion or a selective loss of type II fibres in affected muscles remains elusive. Consistent with our proteomic data on dysferlin-deficient mice, 2D-gel electrophoresis and mass spectrometry of muscle biopsy specimens obtained from dysferlinopathy patients and healthy controls, we could not detect any conversion in fibre type specific myosin heavy chains (MyHC). However, the group of de Palma et al., who used 2D-electrophoresis for examining human dysferlin-deficient muscle biopsies, claimed anomalous behaviour of myosin regulatory light chains (MLC). In healthy controls, fast fibres are characterized by a predominance of regulatory MLC isoforms with different degrees of phosphorylation (2f1, 2f2) and a lower expression of regulatory non-phosphorylated isoforms 2f and 2s (Gonzalez, Negredo et al. 2002). Therefore, the authors concluded that the increment of MLC 2s, 2s1 and 2f, together with a decline in MLC2f1, upon their analysis, displays an increased portion of slow fibres (De Palma, Morandi et al. 2006).

It should be mentioned that the discrepancy between these proteomic analyses could be attributed to different species (human versus mouse) and muscle biopsies (needle biopsy versus whole mice muscle). Especially the investigation of needle biopsies harbours certain pitfalls, as only a small portion of a muscle is extracted and sampling errors may occur. Furthermore, BLA/J mice used for proteomic analysis were analysed in the early disease course whereas patient data published had a more advanced stage of disease. To summarize, it appears that the adaptation of dysferlin-deficient muscle to its metabolic shortcomings involves an increase in oxidative metabolism, although a switch in myosin heavy chain is not detectable at the time points investigated by us.

5.3 Shifting the view to metabolic enzyme expression in dysferlinopathy

As described in detail in chapter 5.1.3, two main studies were published between 2006 (De Palma, Morandi et al. 2006) and 2009 (De la Torre, Illa et al. 2009) with focus on protein alterations in human muscular biopsies of dysferlinopathy patients. Referring to these publications, only a few metabolic enzymes and metabolism-associated proteins were differently expressed in dysferlinopathy. De la Torre et al. used a 2D-gel electrophoresis followed by MALDI-MS and Western blot analysis of interesting spots. They found an increased expression of phosphopyruvate hydratase beta (Enolase 3), a glycolytic enzyme

that catalyzes the conversion of 2-phosphoglycerate (2PG) to phosphoenolpyruvate (PEP). Furthermore, an upregulation of fatty acid-binding protein (Fabp) and carbonic anhydrase III was detected, both predicted to participate in aerobic metabolism of type I fibres, thus leading the authors to the conclusion of enhanced oxidative metabolism in dysferlinopathy. De Palma et al., applied a 2D-gel electrophoresis analysis, followed by measurement of altered protein contents by electrospray MS/MS (Q-TOF MS). Several proteins were detected in altered expressions, where NADH-ubiquinone oxidoreductase (O75489) and ubiquinol cytochrome c reductase (P22695) were up-regulated, whereas alpha-enolase (P06733) and phosphoglycerate mutase (P15259), both enzymes of the glycolytic pathway, were down-regulated. Taking into account that both studies analysed human muscle protein, it is surprising that there is a wide variability referring to the results reported, which might be attributed to the different MS methods (matrix-assisted laser desorption/ionization, MALDI versus electrospray ionization, ESI) applied or to the lower sensitivity of 2D-electrophoresis. The SILAC-based LC-MS/MS analysis applied by our group provides a global insight into the muscle protein turnover under various conditions. The usage of a SILAC reference as internal standard additionally enables a highly accurate comparison of wildtype and knockout mice (Kruger, Moser et al. 2008). Focusing on glycolytic and TCA-cycle enzymes, we found most of the protein expression levels unchanged between dysferlin-deficient and wildtype mice. Furthermore, there were no alterations of enzymes connected to the mitochondrial respiratory chain, which clearly delineates the metabotype found in dysferlinopathy from other metabolic and hereditary muscular diseases, as outlined in chapter 5.4. Alterations between enzymes greatly varied between glycolytic and oxidative muscle fibre types, indicating different compensatory and secondary mechanisms activated to alleviate progressive muscle damage. The down-regulation of phosphoglucoisomerase (Pgi) in TA and QUAD muscle could be attributed to secondary effects due to decreased glucose uptake, since this enzyme catalyses one of the first steps in the glycolytic chain, converting glucose-6-phosphate to fructose-6-phosphate. The up-regulation of apolipoprotein A1 in SOL muscle is a rather unspecific sign, since apoA1 is a major protein of high density lipoproteins (HDL) in the blood plasma. There have been some studies published about a potential protective role of apoA1 by modulating the amyloid β (Aβ) induced neuronal damage in Alzheimer's disease (Flaring, Rooyackers et al. 2003; Rutten, Engelen et al. 2005). Whether these findings are applicable to the formation of non-β-amyloid plaques in muscle biopsy specimens of dysferlinopathy patients (Spuler, Carl et al. 2008) requires further investigation.

5.4 Metabolic alterations in other diseases – delineating dysferlinopathy metabotype

Deviations in the metabolism of distinct organs are common secondary findings in various systemic and muscular diseases. To which extent these metabolic changes are only secondary or confounding a certain disease sometimes remains subject to debate. The GC/MS metabolome approach provides a powerful tool

to ensure previous findings of metabolic research and provide a distinct insight into the biological network keeping an organism intact. To which extent dysferlinopathy causes a disease-specific metabotype, not only induced as secondary mechanism due to muscle fibre degradation and regeneration, will be illustrated on the basis of metabolic analyses performed of other muscular dystrophies like Duchenne muscular dystrophy (DMD) and Diabetes mellitus type 2 (T2DM).

5.4.1 Diabetes mellitus type 2 (T2DM)

Insulin resistance of the skeletal muscle is one of the key factors in the pathogenesis of type 2 diabetes. The underlying molecular mechanisms causing impaired insulin signalling are still elusive. Recent studies using transmission electron microscopy and nuclear magnetic resonance spectroscopy detected a reduced mitochondrial content and functional capacity in muscle cells (Cheng, Tseng et al. 2010). Within the past few years, proteomic approaches using the combination of 2D-gel electrophoresis followed by nano-HPLC/ESI-MS/MS to elucidate the role of metabolic enzyme abundance in diabetes mellitus have been published (Giebelstein, Poschmann et al. 2012). According to these data, muscle protein expression of glycolytic enzymes like GAPDH, PGAM2 and ENO3 was increased in vastus lateralis muscle biopsies obtained from patients with insulin resistance, whereas proteins connected to the TCA-cycle, mitochondrial respiratory chain and function were markedly downregulated. Considering the metabotype of dysferlinopathy with reduced glycolytic metabolites and compensatory increased TCA-cycle metabolism, it appears reasonable that the dysferlin-associated metabolic changes are not due to an increased insulin resistance accompanying this muscular dystrophy. Metabolic profiling studies on dietary-induced T2DM or insulin resistance mouse models have been conducted by several groups and produced further insights into diabetes research. However, most of these studies analysed extra-muscular material like liver, blood or urine and focused on perturbations in amino-acid and FFA metabolism, making a comparison to the central carbon metabolism of our mice model rather difficult (Lin, Yang et al. 2011; Friedrich 2012).

5.4.2 Duchenne muscular dystrophy (DMD)

Duchenne muscular dystrophy is an X-linked recessive muscular disorder, affecting one in 3500 male births and is characterized by progressive muscle wasting leading to an early death due to respiratory and cardiac failure.

One of the most widely used mouse models for DMD is the *mdx* mouse, harbouring a missense mutation in the dystrophin gene (Sicinski, Geng et al. 1989). Various approaches using combinations of ^{1}H NMR spectroscopy and principal component analysis were used in the recent years to elucidate the metabolic and proteomic alteration in the disease models of DMD. Most striking were findings of increased taurine and lactate, and decreased creatine levels in dystrophic heart, diaphragm and soleus muscle obtained from *mdx* mice, clearly pointing towards metabolic disturbances in this disorder (Griffin, Williams et al. 2001).

Unexpected insights into the metabotype of *mdx* mice were provided by Kairallah et al., using ^{13}C labelled substrates to assess the metabolic flux of *mdx* hearts versus control in an *ex vivo* perfusion working mode (Khairallah, Khairallah et al. 2007). Compared to wildtype (C57BL/10) mice, *mdx* hearts revealed an altered mitochondrial energy substrate metabolism, reflected by the preference of carbohydrates ($^{13}C_6$ glucose, $^{13}C_3$ pyruvate) for long chain fatty acids ($^{13}C_{18}$ oleate) for energy production. Whether these novel findings are secondary changes due to progressive cell damage preceding overt cardiomyopathy in the disease course still remains a matter of debate. Another interesting study was published by Onopiuk et al. dealing with metabolic alterations in immortalized *mdx* mouse (SC-5) myoblasts (Onopiuk, Brutkowski et al. 2009). The most striking findings of this study were substantially lower levels of oxygen consumption, expression of respiratory complexes III and V, but similar rates of total cellular ATP content in *mdx* myoblasts, compared to dystrophin-positive control (IMO) myoblasts, thus indicating a shift from oxidative to glycolytic metabolism, a finding which is quite contradictory to the metabolic profile of dysferlin-deficient myotubes and mice models. These experiments were further underpinned by studies conducted by Even et al. here investigating the glucose uptake and heat production rate, as a marker for mitochondrial respiration in EDL and SOL muscles derived from *mdx* and wildtype (C57BL/10) mice (Even, Decrouy et al. 1994). Whereas basal and insulin stimulated 2-deoxy-glucose (2DG) glucose uptake values were similar between *mdx* and wildtype mice, there was a marked decrease in basal heat production upon incubation with glucose, indicating that despite normal glucose uptake kinetics, an impairment in the downstream glycolytic pathway or TCA-cycle leads to an altered metabolic profile in *mdx* mice. These studies focussing on metabolic alterations in the *mdx* mouse model for muscular dystrophy are comparable to our data obtained with this mouse model upon the GC/MS based *metabolic* profiling analysis. Consistent with data published by Kairallah et al., we detected an increased levels of glycolytic intermediates in glycolytic and mixed fibre type muscles (TA and QUAD), pointing towards an enhanced glycolytic flux presumably due to an upregulation of glucose uptake. Furthermore, lactate levels were also found to be elevated as TA and partly QUAD muscle support a rather anaerobic glucose metabolism. Interestingly, 2-ketoglutaric acid levels were markedly increased in TA and QUAD muscle, possibly due to anaplerotic reactions activated in these muscles. SOL muscle, consisting of type I muscle fibres on the other hand exhibited a glycolytic metabolite pattern contrary to TA and QUAD muscle with significantly decreased levels of phosphorylated hexoses and lactate, whereas TCA-cycle metabolite expression patterns resembled the fibre type counterpart.

To summarize, our data obtained from *mdx* mice and controls, as well as previous published metabolic studies on dystrophin-deficient muscle cells and mice models revealed the presence of distinct perturbations in the biochemical network of the central carbon metabolism in Duchenne muscular dystrophy and dysferlinopathy. Furthermore, metabolite expression patterns in both diseases strongly point towards different pathomechanisms underlying the respective disorder, but whereas metabolic alterations seem to be specific in dysferlinopathy, the *mdx* metabolic profile resembles general alterations also described for systemic disorders.

5.5 Conclusion and impact of study

In this study we applied the novel and still evolving techniques of GC/MS based metabolomics and SILAC-based LC-MS/MS proteomics to elucidate the metabolic pathomechanism underlying the very rare hereditary limb girdle muscular dystrophy type 2B. It is worth to mention that the hypothesis of disabled glucose uptake leading to metabolic alterations proposed by our group was not based on published findings, as a possible connection between dysferlin and muscle metabolism has never been published before. Beyond that, GC/MS based metabolic profiling not only allowed the assessment of glucose uptake, but we were also able to detect connected pathways and evaluate their impact on the compensation cascade of muscle fuel supply. Furthermore, this study was the first one combining the application of proteomics and metabolomics techniques to assess the metabotype of a muscular disorder *in vitro* and *in vivo*, as both procedures are elaborative and only conducted at specialized biotechnological platforms. The study of metabolic alterations in dysferlinopathy can therefore be estimated as the ground work for further experiments on different models of muscular diseases. Beyond that our analyses revealed an unique insight into the complex metabolic network of muscle energy metabolism, metabolic and proteomic differences regarding the distinct muscle fibre type characteristics, as it has not been evaluated to this extend before. One major advantage of our study was the elucidation of compensatory mechanisms activated in dysferlinopathy to circumvent or to alleviate the energy misbalance due to decreased glucose uptake. The knowledge of compensatory pathways and switch points could prove a powerful tool for therapeutic approaches to decelerate disease progression in the near future. As discussed in detail above, AR inhibitors, already undergoing phase III clinical studies as therapeutic agents to diminish diabetes-induced secondary complications could possibly serve to reduce oxidative damage in dysferlinopathy. Much more research will be required in that field to elucidate the role of these mechanisms. Although not a therapeutic option to heal dysferlinopathy, dietary approaches to compensate the lack of glucose metabolism in dysferlin-deficient muscle cells could prove an efficient and well tolerated option, such as the emphasis of diets rich in unsaturated fatty acids or the supplementation of branched chain amino acids and glutamine. As the focus on metabolic alterations was just set by our group and the knowledge about the definitive pathomechanisms leading to the dysferlin metabotype is still developing, future research will determine the direction of therapeutic approaches.

6. Zusammenfassung/Summary (German)

Die seltene autosomal-rezessiv vererbbare Gliedergürtelmuskeldystrophie Typ 2B (Dysferlinopathie) entsteht durch Mutationen im Dysferlin Gen auf Chromosom 2p13, welches das 230 kDa große Transmembranprotein Dysferlin kodiert. Klinisch wird zwischen der LGMD 2B mit primärem Befall der proximalen stammbetonten Muskulatur und der Miyoshi Myopathie der distalen Extremität differenziert. Beiden Unterformen ist die progrediente Muskeldystrophie mit einem durchschnittlichen Verlust der Gehfähigkeit circa zehn Jahre nach Erkrankungsbeginn gemeinsam. Trotz intensiver Forschung in den letzten Jahren ist der exakte Pathomechanismus der Dysferlinotpathie bisher unbekannt. Eine wichtige Funktion scheint Dysferlin bei der Kalzium-abhängigen Fusion von zytoplasmatischen Vesikeln nach Muskelzelltrauma zu spielen. Darüber hinaus wurde in Dysferlin-defizienten Muskelzellen eine erhöhte Suszeptibilität für membran-vermittelte Komplementaktivierung und damit assoziierter Muskelzellschädigung gezeigt. Ein spezifisches Charakteristikum der Dysferlinopathie ist die Koinzidenz von postpubertärem Krankheitsbeginn und dem pubertätsbedingtem Adaptation des Muskelmetabolismus von einem vormals dominierenden oxidativen (Typ I) zu einem mehr glykolytischen (Typ II) Stoffwechsel. Vorstudien aus unserer Arbeitsgruppe konnten eine abnorme Verteilung und Akkumulation des muskelspezifischen Glukosetransporters GLUT4 in Kryosektionen von Patientenmuskelbiopsien, sowie einen bevorzugten Substratmetabolismus der Ketonkörper Acetoacetat und 3-β-Hydroxybutyrat in Dysferlin-defizienten humanen primären Myotuben nachweisen. Das Ziel dieser Studie war demnach, den zentralen Kohlenstoffmetabolismus von Glykolyse und Citratzyklus mittels der neuen Technologien der Gaschromatographie gekoppelten Massenspektrometrie (GC/MS) anhand von ^{13}C-markierten Isotopen ($^{13}C_6$-Glukose) in zwei Dysferlinopathie Modellen, *in vitro* in humanen primären Myotuben und *in vivo* im Mausmodell (BLA/J), jeweils im Vergleich zum Wildtypen, zu messen. Als Vergleichsmodell erfolgte eine zusätzliche Analyse des metabolischen Profils von *mdx* (C57BL/10ScSn-Dmdmdx/J) Mäusen und deren Kontrollgruppe (C57BL/10). Unter Berücksichtigung unterschiedlicher metabolischer Eigenschaften der Muskelfasertypen (I-IIa,b,x) wurden drei, in ihrem Substratmetabolismus differierende Skelettmuskeln evaluiert. Eine SILAC-basierte Proteomanalyse mittels Flüssigkeitschromatographie gekoppelter Tandem-Massenspektrometrie (LC-MS/MS) ermöglichte die Untersuchung von Proteinexpressionsmustern in Dysferlin-defizienten Mäusen und Wildtypen. Zur Quantifizierung der Proteomdaten wurde ein Referenzmuskel einer vollständig mit einem stabilen Isotopen ($^{13}C_6$ Lysin) markierten Maus gemessen und die Ratio aus der gelabelten und ungelabelten ($Ratio_{heavy/light}$) berechnet.

Unsere Messungen konnten ein klares metabolisches Profil der Dysferlinopathie im humanen Zellmodell und dem Mausmodell nachweisen. Konform mit unserer Hypothese einer beeinträchtigten Glukoseaufnahme zeigte sich eine deutliche Verminderung des glykolytischen Flusses, sichtbar an den phosphorylierten Hexosen Glucose-6-Phosphat und Fructose-6-Phosphat, die Intermediate des oberen Glykolyse darstellen. Dem entgegengesetzt waren die potentiell kompensatorischen Metaboliten (3-β-

Hydroxybutyrat, Glutamat, Glutamin) und Zielintermediate anaplerotischer Reaktionen im Citratzyklus (Citrat, alpha-Ketoglutarat), vermutlich als Ausdruck eines gesteigerten oxidativen Metabolismus von freien Fettsäuren (FFA) und Ketonkörpern hochreguliert. Die GC/MS basierte Metabolomanalyse der Leber von BLA/J Mäusen erbrachte zusätzlich den Nachweis einer erhöhten Syntheserate des Ketonkörpers 3-β-Hydroxybutyrat, entsprechend einer systemischen Anpassungsreaktion an den veränderten Muskelstoffwechsel. Wie primär, unter Berücksichtigung des klinischen Verlaufes der Dysferlinopathie, angenommen, zeigten die glykolytischen Typ II Faser Muskeln (M. tibialis anterior) die höchste Beeinträchtigung. Darüber hinaus fanden sich Anzeichen für einen frühen metabolischen Shift des gemischten (oxidativ-glykolytischen) M. Quadriceps, mit Adaptation einer Typ I Faser spezifischen Metabolitenverteilung im Vergleich. Der von uns gefundene Dysferlin-spezifische Metabotyp war über verschiedene Konditionen von intravenöser Glukosezufuhr und Postinjektionszeiten über verschiedene Messungen stabil und repetierbar. Unsere Metabolomanalyse von dystrophin-defizienten *mdx* Mäusen als Dystrophiekontrolle konnte unsere Hypothese eines Dysferlin-spezifischen Phänotyps bestätigen, denn hier zeigte sich ein komplett distinkter Phänotyp mit gleicher bis leicht hochregulierter Glykolyse und beeinträchtigtem Citratzyklus. Unsere weiterführende quantitative LC-MS/MS basierte Proteomanalyse Dysferlin-defizienter BLA/J Mausmuskeln stütze unsere Hypothese einer Dysferlin-assoziierten Beeinträchtigung der Glukose Aufnahme bei gleichbleibenden Expressionen von Glykolyse und Citratzyklus-assoziierten Enzymen und normaler Ausprägung respiratorischer Enzymkomplexe. Veränderte Expressionslevel waren von Proteinen der Peroxiredoxinfamilie (PRXs) und der mitochondrialen NAD(P)-Transhydrogenase nachweisbar, dies möglicherweise als ein Indiz für erhöhten oxidativen Stress. Darüber hinaus fanden wir eine muskelfaserspezifische Isoformexpression der Isocitratdehydrogenase (IDH) sowohl in der BLA/J Maus als auch dem Wildtyp, mit dominierender Expression von IDH 2 in oxidativen (Typ I) Muskeln. Es ist anzunehmen, dass die stärker in ihrem glykolytischen Substratmetabolismus eingeschränkten Dysferlin-defizienten Typ II Muskeln durch die vermehrte ROS Produktion in der Atmungskette im Rahmen eines gesteigerten oxidativen Substratmetabolismus, sowie fehlendem NADP(H) als Reduktionsäquivalent durch geminderte Expression der NAD(P)-Transhydrogenase und der Typ I Faser-spezifischen Isoform der NAD(P)-abhängigen IDH 2, besonders beeinträchtigt sind.
Diese im Rahmen unserer Analysen gewonnenen Erkenntnisse, sowie die Dechiffrierung eines komplexen metabolischen Netzwerkes, stellen neue Hypothesen über die essentielle Funktion von Dysferlin her und setzen einen wichtigen Grundstein für mögliche therapeutische Angriffspunkte zur Prävention der progressiven Muskeldystrophie im Verlauf der Erkrankung.

7. Bibliography

Achanzar, W. E. and S. Ward (1997). "A nematode gene required for sperm vesicle fusion." Journal of cell science **110 (Pt 9)**: 1073-1081.

Al-Hasani, H., R. K. Kunamneni, et al. (2002). "Roles of the N- and C-termini of GLUT4 in endocytosis." Journal of cell science **115**(Pt 1): 131-140.

Ampong, B. N., M. Imamura, et al. (2005). "Intracellular localization of dysferlin and its association with the dihydropyridine receptor." Acta myologica : myopathies and cardiomyopathies : official journal of the Mediterranean Society of Myology / edited by the Gaetano Conte Academy for the study of striated muscle diseases **24**(2): 134-144.

Anderson, L. V., K. Davison, et al. (1999). "Dysferlin is a plasma membrane protein and is expressed early in human development." Hum Mol Genet **8**(5): 855-861.

Aoki, M., J. Liu, et al. (2001). "Genomic organization of the dysferlin gene and novel mutations in Miyoshi myopathy." Neurology **57**(2): 271-278.

Armstrong, N. and A. R. Barker (2009). "Oxygen uptake kinetics in children and adolescents: a review." Pediatric exercise science **21**(2): 130-147.

Babiychuk, E. B. and A. Draeger (2000). "Annexins in cell membrane dynamics. Ca(2+)-regulated association of lipid microdomains." The Journal of cell biology **150**(5): 1113-1124.

Balasse, E. O. and F. Fery (1989). "Ketone body production and disposal: effects of fasting, diabetes, and exercise." Diabetes Metab Rev **5**(3): 247-270.

Banerjee, R. (2012). "Redox outside the box: linking extracellular redox remodeling with intracellular redox metabolism." The Journal of biological chemistry **287**(7): 4397-4402.

Bansal, D., K. Miyake, et al. (2003). "Defective membrane repair in dysferlin-deficient muscular dystrophy." Nature **423**(6936): 168-172.

Barnes, J. A. and A. V. Gomes (2002). "Proteolytic signals in the primary structure of annexins." Molecular and cellular biochemistry **231**(1-2): 1-7.

Bashir, R., S. Britton, et al. (1998). "A gene related to Caenorhabditis elegans spermatogenesis factor fer-1 is mutated in limb-girdle muscular dystrophy type 2B." Nature genetics **20**(1): 37-42.

Bashir, R., S. Keers, et al. (1996). "Genetic and physical mapping at the limb-girdle muscular dystrophy locus (LGMD2B) on chromosome 2p." Genomics **33**(1): 46-52.

Bergstrom, J., P. Furst, et al. (1974). "Intracellular free amino acid concentration in human muscle tissue." Journal of applied physiology **36**(6): 693-697.

Bernard, C. C. and P. R. Carnegie (1975). "Experimental autoimmune encephalomyelitis in mice: immunologic response to mouse spinal cord and myelin basic proteins." Journal of immunology **114**(5): 1537-1540.

Betz, R. C., B. G. Schoser, et al. (2001). "Mutations in CAV3 cause mechanical hyperirritability of skeletal muscle in rippling muscle disease." Nature genetics **28**(3): 218-219.

Bittner, R. E., L. V. Anderson, et al. (1999). "Dysferlin deletion in SJL mice (SJL-Dysf) defines a natural model for limb girdle muscular dystrophy 2B." Nature genetics **23**(2): 141-142.

Blandin, G., C. Beroud, et al. (2012). "UMD-DYSF, a novel locus specific database for the compilation and interactive analysis of mutations in the dysferlin gene." Hum Mutat **33**(3): E2317-2331.

Bochner, B. R., M. Siri, et al. (2011). "Assay of the multiple energy-producing pathways of mammalian cells." PloS one **6**(3): e18147.

Boiteux, A. and B. Hess (1981). "Design of glycolysis." Philosophical transactions of the Royal Society of London. Series B, Biological sciences **293**(1063): 5-22.

Bowtell, J. L., K. Gelly, et al. (1999). "Effect of oral glutamine on whole body carbohydrate storage during recovery from exhaustive exercise." Journal of applied physiology **86**(6): 1770-1777.

Bowtell, J. L., S. Marwood, et al. (2007). "Tricarboxylic acid cycle intermediate pool size: functional importance for oxidative metabolism in exercising human skeletal muscle." Sports medicine **37**(12): 1071-1088.

Bulfield, G., W. G. Siller, et al. (1984). "X chromosome-linked muscular dystrophy (mdx) in the mouse." Proceedings of the National Academy of Sciences of the United States of America **81**(4): 1189-1192.

Bushby, K. (1996). "Towards the classification of the autosomal recessive limb-girdle muscular dystrophies." Neuromuscular disorders : NMD **6**(6): 439-441.

Bushby, K. (2009). "Diagnosis and Treatment of MD." Practical Neurology.

Bushby, K. M. (1999). "Making sense of the limb-girdle muscular dystrophies." Brain **122 (Pt 8)**: 1403-1420.

Campbell, K. P. and S. D. Kahl (1989). "Association of dystrophin and an integral membrane glycoprotein." Nature **338**(6212): 259-262.

Chen, J. Q. and J. Russo (2012). "Dysregulation of Glucose Transport, Glycolysis, TCA Cycle and Glutaminolysis by Oncogenes and Tumor Suppressors in Cancer Cells." Biochimica et biophysica acta.

Cheng, Z., Y. Tseng, et al. (2010). "Insulin signaling meets mitochondria in metabolism." Trends Endocrinol Metab **21**(10): 589-598.

Chiu, Y. H., M. A. Hornsey, et al. (2009). "Attenuated muscle regeneration is a key factor in dysferlin-deficient muscular dystrophy." Human molecular genetics **18**(11): 1976-1989.

Cohn, R. D. and K. P. Campbell (2000). "Molecular basis of muscular dystrophies." Muscle Nerve **23**(10): 1456-1471.

Confalonieri, P., L. Oliva, et al. (2003). "Muscle inflammation and MHC class I up-regulation in muscular dystrophy with lack of dysferlin: an immunopathological study." Journal of neuroimmunology **142**(1-2): 130-136.

Constantin-Teodosiu, D., N. S. Peirce, et al. (2004). "Muscle pyruvate availability can limit the flux, but not activation, of the pyruvate dehydrogenase complex during submaximal exercise in humans." The Journal of physiology **561**(Pt 2): 647-655.

Cooper, B. J. (1989). "Animal models of Duchenne and Becker muscular dystrophy." Br Med Bull **45**(3): 703-718.

Cox, J. and M. Mann (2008). "MaxQuant enables high peptide identification rates, individualized p.p.b.-range mass accuracies and proteome-wide protein quantification." Nat Biotechnol **26**(12): 1367-1372.

Cox, J., I. Matic, et al. (2009). "A practical guide to the MaxQuant computational platform for SILAC-based quantitative proteomics." Nature protocols **4**(5): 698-705.

Davies, K. E. and K. J. Nowak (2006). "Molecular mechanisms of muscular dystrophies: old and new players." Nat Rev Mol Cell Biol **7**(10): 762-773.

Davis, E. J., O. Spydevold, et al. (1980). "Pyruvate carboxylase and propionyl-CoA carboxylase as anaplerotic enzymes in skeletal muscle mitochondria." European journal of biochemistry / FEBS **110**(1): 255-262.

De la Torre, C., I. Illa, et al. (2009). "Proteomics identification of differentially expressed proteins in the muscle of dysferlin myopathy patients." Proteomics. Clinical applications **3**(4): 486-497.

De Luna, N., A. Freixas, et al. (2007). "Dysferlin expression in monocytes: a source of mRNA for mutation analysis." Neuromuscular disorders : NMD **17**(1): 69-76.

De Palma, S., L. Morandi, et al. (2006). "Proteomic investigation of the molecular pathophysiology of dysferlinopathy." Proteomics **6**(1): 379-385.

DeFronzo, R. A., R. C. Bonadonna, et al. (1992). "Pathogenesis of NIDDM. A balanced overview." Diabetes care **15**(3): 318-368.

Dhoot, G. K. and S. V. Perry (1979). "Distribution of polymorphic forms of troponin components and tropomyosin in skeletal muscle." Nature **278**(5706): 714-718.

Dixit, B. L., G. K. Balendiran, et al. (2000). "Kinetic and structural characterization of the glutathione-binding site of aldose reductase." The Journal of biological chemistry **275**(28): 21587-21595.

Doherty, K. R., A. Cave, et al. (2005). "Normal myoblast fusion requires myoferlin." Development **132**(24): 5565-5575.

Drexler, H. C., A. Ruhs, et al. (2011). "On marathons and sprints: an integrated quantitative proteomics and transcriptomics analysis of differences between slow and fast muscle fibers." Molecular & cellular proteomics : MCP.

Dunaway, G. A. (1983). "A review of animal phosphofructokinase isozymes with an emphasis on their physiological role." Molecular and cellular biochemistry **52**(1): 75-91.

Durbeej, M. and K. P. Campbell (2002). "Muscular dystrophies involving the dystrophin-glycoprotein complex: an overview of current mouse models." Current opinion in genetics & development **12**(3): 349-361.

Emery, A. E. (1998). "The muscular dystrophies." BMJ **317**(7164): 991-995.

Even, P. C., A. Decrouy, et al. (1994). "Defective regulation of energy metabolism in mdx-mouse skeletal muscles." The Biochemical journal **304 (Pt 2)**: 649-654.

Fan, T. W., A. N. Lane, et al. (2011). "Stable isotope resolved metabolomics of lung cancer in a SCID mouse model." Metabolomics : Official journal of the Metabolomic Society **7**(2): 257-269.

Fanin, M. and C. Angelini (2002). "Muscle pathology in dysferlin deficiency." Neuropathol Appl Neurobiol **28**(6): 461-470.

Fernie, A. R., R. N. Trethewey, et al. (2004). "Metabolite profiling: from diagnostics to systems biology." Nat Rev Mol Cell Biol **5**(9): 763-769.

Finn, P. F. and J. F. Dice (2006). "Proteolytic and lipolytic responses to starvation." Nutrition **22**(7-8): 830-844.

Flaring, U. B., O. E. Rooyackers, et al. (2003). "Glutamine attenuates post-traumatic glutathione depletion in human muscle." Clinical science **104**(3): 275-282.

Flaring, U. B., O. E. Rooyackers, et al. (2003). "Temporal changes in muscle glutathione in ICU patients." Intensive care medicine **29**(12): 2193-2198.

Forster, J., I. Famili, et al. (2003). "Genome-scale reconstruction of the Saccharomyces cerevisiae metabolic network." Genome research **13**(2): 244-253.

Franco, R., O. J. Schoneveld, et al. (2007). "The central role of glutathione in the pathophysiology of human diseases." Archives of physiology and biochemistry **113**(4-5): 234-258.

Frayn, K. N. (2010). "Fat as a fuel: emerging understanding of the adipose tissue-skeletal muscle axis." Acta Physiol (Oxf) **199**(4): 509-518.

Friedrich, N. (2012). "Metabolomics in Diabetes Research." J Endocrinol.

Gallardo, E., R. Rojas-Garcia, et al. (2001). "Inflammation in dysferlin myopathy: immunohistochemical characterization of 13 patients." Neurology **57**(11): 2136-2138.

Gaster, M., J. O. Nehlin, et al. (2012). "Impaired TCA cycle flux in mitochondria in skeletal muscle from type 2 diabetic subjects: Marker or maker of the diabetic phenotype?" Archives of physiology and biochemistry.

Gentil, B. J., C. Delphin, et al. (2003). "Expression of the giant protein AHNAK (desmoyokin) in muscle and lining epithelial cells." The journal of histochemistry and cytochemistry : official journal of the Histochemistry Society **51**(3): 339-348.

Giannoukakis, N. (2008). "Ranirestat as a therapeutic aldose reductase inhibitor for diabetic complications." Expert Opin Investig Drugs **17**(4): 575-581.

Gibala, M. J., M. A. Tarnopolsky, et al. (1997). "Tricarboxylic acid cycle intermediates in human muscle at rest and during prolonged cycling." The American journal of physiology **272**(2 Pt 1): E239-244.

Giebelstein, J., G. Poschmann, et al. (2012). "The proteomic signature of insulin-resistant human skeletal muscle reveals increased glycolytic and decreased mitochondrial enzymes." Diabetologia.

Gleeson, T. T. (1983). "A histochemical and enzymatic study of the muscle fiber types in the water monitor, Varanus salvator." J Exp Zool **227**(2): 191-201.

Glover, L. and R. H. Brown, Jr. (2007). "Dysferlin in membrane trafficking and patch repair." Traffic **8**(7): 785-794.

Goll, D. E., V. F. Thompson, et al. (2003). "The calpain system." Physiological reviews **83**(3): 731-801.

Gonzalez, B., P. Negredo, et al. (2002). "Protein variants of skeletal muscle regulatory myosin light chain isoforms: prevalence in mammals, generation and transitions during muscle remodelling." Pflugers Archiv : European journal of physiology **443**(3): 377-386.

Gonzalez, R. G., P. Barnett, et al. (1984). "Direct measurement of polyol pathway activity in the ocular lens." Diabetes **33**(2): 196-199.

Gotoh, N., K. Moroda, et al. (2008). "Metabolism of odd-numbered fatty acids and even-numbered fatty acids in mouse." J Oleo Sci **57**(5): 293-299.

Graham, T. E., V. Sgro, et al. (2000). "Glutamate ingestion: the plasma and muscle free amino acid pools of resting humans." Am J Physiol Endocrinol Metab **278**(1): E83-89.

Griffin, J. L., H. J. Williams, et al. (2001). "Metabolic profiling of genetic disorders: a multitissue (1)H nuclear magnetic resonance spectroscopic and pattern recognition study into dystrophic tissue." Analytical biochemistry **293**(1): 16-21.

Guan, H. P., J. L. Goldstein, et al. (2009). "Accelerated fatty acid oxidation in muscle averts fasting-induced hepatic steatosis in SJL/J mice." The Journal of biological chemistry **284**(36): 24644-24652.

Guglieri, M., V. Straub, et al. (2008). "Limb-girdle muscular dystrophies." Curr Opin Neurol **21**(5): 576-584.

Guo, Z., K. Yarasheski, et al. (2006). "High-precision isotopic analysis of palmitoylcarnitine by liquid chromatography/electrospray ionization ion-trap tandem mass spectrometry." Rapid Commun Mass Spectrom **20**(22): 3361-3366.

Gygi, S. P., G. L. Corthals, et al. (2000). "Evaluation of two-dimensional gel electrophoresis-based proteome analysis technology." Proceedings of the National Academy of Sciences of the United States of America **97**(17): 9390-9395.

Hajduch, E., G. J. Litherland, et al. (2003). "Insulin regulates the expression of the GLUT5 transporter in L6 skeletal muscle cells." FEBS letters **549**(1-3): 77-82.

Han, R., D. Bansal, et al. (2007). "Dysferlin-mediated membrane repair protects the heart from stress-induced left ventricular injury." The Journal of clinical investigation **117**(7): 1805-1813.

Han, R., E. M. Frett, et al. (2010). "Genetic ablation of complement C3 attenuates muscle pathology in dysferlin-deficient mice." The Journal of clinical investigation **120**(12): 4366-4374.

Hatefi, Y. and M. Yamaguchi (1996). "Nicotinamide nucleotide transhydrogenase: a model for utilization of substrate binding energy for proton translocation." FASEB journal : official publication of the Federation of American Societies for Experimental Biology **10**(4): 444-452.

Hayashi, T., M. F. Hirshman, et al. (1998). "Evidence for 5' AMP-activated protein kinase mediation of the effect of muscle contraction on glucose transport." Diabetes **47**(8): 1369-1373.

Hernandez-Deviez, D. J., S. Martin, et al. (2006). "Aberrant dysferlin trafficking in cells lacking caveolin or expressing dystrophy mutants of caveolin-3." Human molecular genetics **15**(1): 129-142.

Ho, M., E. Gallardo, et al. (2002). "A novel, blood-based diagnostic assay for limb girdle muscular dystrophy 2B and Miyoshi myopathy." Annals of neurology **51**(1): 129-133.

Ho, M., C. M. Post, et al. (2004). "Disruption of muscle membrane and phenotype divergence in two novel mouse models of dysferlin deficiency." Hum Mol Genet **13**(18): 1999-2010.

Huang, Y., A. de Morree, et al. (2008). "Calpain 3 is a modulator of the dysferlin protein complex in skeletal muscle." Human molecular genetics **17**(12): 1855-1866.

Huang, Y., S. H. Laval, et al. (2007). "AHNAK, a novel component of the dysferlin protein complex, redistributes to the cytoplasm with dysferlin during skeletal muscle regeneration." FASEB journal : official publication of the Federation of American Societies for Experimental Biology **21**(3): 732-742.

Hundal, H. S., F. Darakhshan, et al. (1998). "GLUT5 expression and fructose transport in human skeletal muscle." Advances in experimental medicine and biology **441**: 35-45.

Illa, I., C. Serrano-Munuera, et al. (2001). "Distal anterior compartment myopathy: a dysferlin mutation causing a new muscular dystrophy phenotype." Annals of neurology **49**(1): 130-134.

Kaplan, J. C. (2011). "The 2012 version of the gene table of monogenic neuromuscular disorders." Neuromuscular disorders : NMD **21**(12): 833-861.

Keller, A., J. Demeurie, et al. (2000). "Fibre-type distribution and subcellular localisation of alpha and beta enolase in mouse striated muscle." Biology of the cell / under the auspices of the European Cell Biology Organization **92**(7): 527-535.

Kemp, R. G. and L. G. Foe (1983). "Allosteric regulatory properties of muscle phosphofructokinase." Molecular and cellular biochemistry **57**(2): 147-154.

Kempa, S., J. Hummel, et al. (2009). "An automated GCxGC-TOF-MS protocol for batch-wise extraction and alignment of mass isotopomer matrixes from differential 13C-labelling experiments: a case study for photoautotrophic-mixotrophic grown Chlamydomonas reinhardtii cells." J Basic Microbiol **49**(1): 82-91.

Kersey, P. J., J. Duarte, et al. (2004). "The International Protein Index: an integrated database for proteomics experiments." Proteomics **4**(7): 1985-1988.

Keseler, I. M., J. Collado-Vides, et al. (2005). "EcoCyc: a comprehensive database resource for Escherichia coli." Nucleic Acids Res **33**(Database issue): D334-337.

Khairallah, M., R. Khairallah, et al. (2007). "Metabolic and signaling alterations in dystrophin-deficient hearts precede overt cardiomyopathy." J Mol Cell Cardiol **43**(2): 119-129.

Kiens, B., T. J. Alsted, et al. (2011). "Factors regulating fat oxidation in human skeletal muscle." Obes Rev **12**(10): 852-858.

Kirschner, J. and C. G. Bonnemann (2004). "The congenital and limb-girdle muscular dystrophies: sharpening the focus, blurring the boundaries." Archives of neurology **61**(2): 189-199.

Klinge, L., A. Aboumousa, et al. (2010). "New aspects on patients affected by dysferlin deficient muscular dystrophy." Journal of neurology, neurosurgery, and psychiatry **81**(9): 946-953.

Klinge, L., A. F. Dean, et al. (2008). "Late onset in dysferlinopathy widens the clinical spectrum." Neuromuscular disorders : NMD **18**(4): 288-290.

Klinge, L., S. Laval, et al. (2007). "From T-tubule to sarcolemma: damage-induced dysferlin translocation in early myogenesis." FASEB journal : official publication of the Federation of American Societies for Experimental Biology **21**(8): 1768-1776.

Kobayashi, K., T. Izawa, et al. (2010). "The distribution and characterization of skeletal muscle lesions in dysferlin-deficient SJL and A/J mice." Exp Toxicol Pathol **62**(5): 509-517.

Kolwicz, S. C., Jr. and R. Tian (2011). "Glucose metabolism and cardiac hypertrophy." Cardiovasc Res **90**(2): 194-201.

Kondo, N., H. Nakamura, et al. (2006). "Redox regulation of human thioredoxin network." Antioxidants & redox signaling **8**(9-10): 1881-1890.

Kopka, J., N. Schauer, et al. (2005). "GMD@CSB.DB: the Golm Metabolome Database." Bioinformatics **21**(8): 1635-1638.

Krahn, M., C. Beroud, et al. (2009). "Analysis of the DYSF mutational spectrum in a large cohort of patients." Hum Mutat **30**(2): E345-375.

Krook, A., H. Wallberg-Henriksson, et al. (2004). "Sending the Signal: Molecular Mechanisms Regulating Glucose Uptake." Medicine & Science in Sports & Exercise **36**(7): 1212-1217.

Kruger, M., M. Moser, et al. (2008). "SILAC mouse for quantitative proteomics uncovers kindlin-3 as an essential factor for red blood cell function." Cell **134**(2): 353-364.

Laffel, L. (1999). "Ketone bodies: a review of physiology, pathophysiology and application of monitoring to diabetes." Diabetes Metab Res Rev **15**(6): 412-426.

Lambert, O., V. Gerke, et al. (1997). "Structural analysis of junctions formed between lipid membranes and several annexins by cryo-electron microscopy." Journal of molecular biology **272**(1): 42-55.

Laval, S. H. and K. M. Bushby (2004). "Limb-girdle muscular dystrophies--from genetics to molecular pathology." Neuropathol Appl Neurobiol **30**(2): 91-105.

Lek, A., M. Lek, et al. (2010). "Phylogenetic analysis of ferlin genes reveals ancient eukaryotic origins." BMC Evol Biol **10**: 231.

Lennon, N. J., A. Kho, et al. (2003). "Dysferlin interacts with annexins A1 and A2 and mediates sarcolemmal wound-healing." The Journal of biological chemistry **278**(50): 50466-50473.

Lin, S., Z. Yang, et al. (2011). "Beyond glucose: metabolic shifts in responses to the effects of the oral glucose tolerance test and the high-fructose diet in rats." Mol Biosyst **7**(5): 1537-1548.

Liu, J., M. Aoki, et al. (1998). "Dysferlin, a novel skeletal muscle gene, is mutated in Miyoshi myopathy and limb girdle muscular dystrophy." Nature genetics **20**(1): 31-36.

Lopaschuk, G. D., D. D. Belke, et al. (1994). "Regulation of fatty acid oxidation in the mammalian heart in health and disease." Biochim Biophys Acta **1213**(3): 263-276.

Lostal, W., M. Bartoli, et al. (2010). "Efficient recovery of dysferlin deficiency by dual adeno-associated vector-mediated gene transfer." Hum Mol Genet **19**(10): 1897-1907.

Luo, J. L., F. Hammarqvist, et al. (1998). "Surgical trauma decreases glutathione synthetic capacity in human skeletal muscle tissue." The American journal of physiology **275**(2 Pt 1): E359-365.

MacLennan, D. H. and T. Toyofuku (1992). "Structure-function relationships in the Ca2+ pump of the sarcoplasmic reticulum." Biochemical Society transactions **20**(3): 559-562.

Mahjneh, I., M. R. Passos-Bueno, et al. (1996). "The phenotype of chromosome 2p-linked limb-girdle muscular dystrophy." Neuromuscular disorders : NMD **6**(6): 483-490.

Matsuda, C., M. Aoki, et al. (1999). "Dysferlin is a surface membrane-associated protein that is absent in Miyoshi myopathy." Neurology **53**(5): 1119-1122.

Matsuda, C., Y. K. Hayashi, et al. (2001). "The sarcolemmal proteins dysferlin and caveolin-3 interact in skeletal muscle." Hum Mol Genet **10**(17): 1761-1766.

Mattevi, A., M. Bolognesi, et al. (1996). "The allosteric regulation of pyruvate kinase." FEBS letters **389**(1): 15-19.

McNally, E. M., C. T. Ly, et al. (2000). "Splicing mutation in dysferlin produces limb-girdle muscular dystrophy with inflammation." American journal of medical genetics **91**(4): 305-312.

Mengual, R., K. El Abida, et al. (2003). "Pyruvate shuttle in muscle cells: high-affinity pyruvate transport sites insensitive to trans-lactate efflux." Am J Physiol Endocrinol Metab **285**(6): E1196-1204.

Minetti, C., F. Sotgia, et al. (1998). "Mutations in the caveolin-3 gene cause autosomal dominant limb-girdle muscular dystrophy." Nature genetics **18**(4): 365-368.

Moore, S. A., C. J. Shilling, et al. (2006). "Limb-girdle muscular dystrophy in the United States." Journal of neuropathology and experimental neurology **65**(10): 995-1003.

Munoz, M. E. and E. Ponce (2003). "Pyruvate kinase: current status of regulatory and functional properties." Comparative biochemistry and physiology. Part B, Biochemistry & molecular biology **135**(2): 197-218.

Murphy, T. H., M. Miyamoto, et al. (1989). "Glutamate toxicity in a neuronal cell line involves inhibition of cystine transport leading to oxidative stress." Neuron **2**(6): 1547-1558.

Nalini, A. and N. Gayathri (2008). "Dysferlinopathy: a clinical and histopathological study of 28 patients from India." Neurology India **56**(3): 379-385; discussion 386-377.

Nehlin, J. O., M. Just, et al. (2011). "Human myotubes from myoblast cultures undergoing senescence exhibit defects in glucose and lipid metabolism." Biogerontology **12**(4): 349-365.

Nguyen, K., G. Bassez, et al. (2005). "Dysferlin mutations in LGMD2B, Miyoshi myopathy, and atypical dysferlinopathies." Human mutation **26**(2): 165.

Nigro, V., S. Aurino, et al. (2011). "Limb girdle muscular dystrophies: update on genetic diagnosis and therapeutic approaches." Curr Opin Neurol **24**(5): 429-436.

Oh-Ishi, M., M. Satoh, et al. (2000). "Preparative two-dimensional gel electrophoresis with agarose gels in the first dimension for high molecular mass proteins." Electrophoresis **21**(9): 1653-1669.

Okumura, N., A. Hashida-Okumura, et al. (2005). "Proteomic analysis of slow- and fast-twitch skeletal muscles." Proteomics **5**(11): 2896-2906.

Ong, S. E. and M. Mann (2006). "A practical recipe for stable isotope labeling by amino acids in cell culture (SILAC)." Nature protocols **1**(6): 2650-2660.

Onopiuk, M., W. Brutkowski, et al. (2009). "Mutation in dystrophin-encoding gene affects energy metabolism in mouse myoblasts." Biochemical and biophysical research communications **386**(3): 463-466.

Owen, O. E., S. C. Kalhan, et al. (2002). "The key role of anaplerosis and cataplerosis for citric acid cycle function." The Journal of biological chemistry **277**(34): 30409-30412.

Paradas, C., L. Gonzalez-Quereda, et al. (2009). "A new phenotype of dysferlinopathy with congenital onset." Neuromuscular disorders : NMD **19**(1): 21-25.

Paradas, C., J. Llauger, et al. (2010). "Redefining dysferlinopathy phenotypes based on clinical findings and muscle imaging studies." Neurology **75**(4): 316-323.

Pardridge, W. M. (1991). "Blood-brain barrier transport of glucose, free fatty acids, and ketone bodies." Advances in experimental medicine and biology **291**: 43-53.

Parton, R. G. (1996). "Caveolae and caveolins." Current opinion in cell biology **8**(4): 542-548.

Petrof, B. J., J. B. Shrager, et al. (1993). "Dystrophin protects the sarcolemma from stresses developed during muscle contraction." Proceedings of the National Academy of Sciences of the United States of America **90**(8): 3710-3714.

Pette, D. and R. S. Staron (2000). "Myosin isoforms, muscle fiber types, and transitions." Microsc Res Tech **50**(6): 500-509.

Piccolo, F., S. A. Moore, et al. (2000). "Intracellular accumulation and reduced sarcolemmal expression of dysferlin in limb--girdle muscular dystrophies." Annals of neurology **48**(6): 902-912.

Posey, A. D., Jr., A. Demonbreun, et al. (2011). "Ferlin proteins in myoblast fusion and muscle growth." Current topics in developmental biology **96**: 203-230.

Pramono, Z. A., C. L. Tan, et al. (2009). "Identification and characterisation of human dysferlin transcript variants: implications for dysferlin mutational screening and isoforms." Hum Genet **125**(4): 413-420.

Rando, T. A., M. H. Disatnik, et al. (1998). "Muscle cells from mdx mice have an increased susceptibility to oxidative stress." Neuromuscular disorders : NMD **8**(1): 14-21.

Rappsilber, J., M. Mann, et al. (2007). "Protocol for micro-purification, enrichment, pre-fractionation and storage of peptides for proteomics using StageTips." Nature protocols **2**(8): 1896-1906.

Ritov, V. B. and D. E. Kelley (2001). "Hexokinase isozyme distribution in human skeletal muscle." Diabetes **50**(6): 1253-1262.

Rosales, X. Q., J. M. Gastier-Foster, et al. (2010). "Novel diagnostic features of dysferlinopathies." Muscle Nerve **42**(1): 14-21.

Rowin, J., M. N. Meriggioli, et al. (1999). "Prominent inflammatory changes on muscle biopsy in patients with Miyoshi myopathy." Neuromuscular disorders : NMD **9**(6-7): 417-420.

Rutten, E. P., M. P. Engelen, et al. (2005). "Skeletal muscle glutamate metabolism in health and disease: state of the art." Current opinion in clinical nutrition and metabolic care **8**(1): 41-51.

Sahlin, K., A. Katz, et al. (1990). "Tricarboxylic acid cycle intermediates in human muscle during prolonged exercise." The American journal of physiology **259**(5 Pt 1): C834-841.

Salahudeen, A. K., E. C. Clark, et al. (1991). "Hydrogen peroxide-induced renal injury. A protective role for pyruvate in vitro and in vivo." The Journal of clinical investigation **88**(6): 1886-1893.

Santoni, V., M. Molloy, et al. (2000). "Membrane proteins and proteomics: un amour impossible?" Electrophoresis **21**(6): 1054-1070.

Sazanov, L. A. and J. B. Jackson (1994). "Proton-translocating transhydrogenase and NAD- and NADP-linked isocitrate dehydrogenases operate in a substrate cycle which contributes to fine regulation of the tricarboxylic acid cycle activity in mitochondria." FEBS letters **344**(2-3): 109-116.

Schiaffino, S. (2010). "Fibre types in skeletal muscle: a personal account." Acta Physiol (Oxf) **199**(4): 451-463.

Schiaffino, S. and C. Reggiani (1994). "Myosin isoforms in mammalian skeletal muscle." Journal of applied physiology **77**(2): 493-501.

Schwanhausser, B., M. Gossen, et al. (2009). "Global analysis of cellular protein translation by pulsed SILAC." Proteomics **9**(1): 205-209.

Selcen, D., G. Stilling, et al. (2001). "The earliest pathologic alterations in dysferlinopathy." Neurology **56**(11): 1472-1481.

Sicinski, P., Y. Geng, et al. (1989). "The molecular basis of muscular dystrophy in the mdx mouse: a point mutation." Science **244**(4912): 1578-1580.

Sola-Penna, M., D. Da Silva, et al. (2010). "Regulation of mammalian muscle type 6-phosphofructo-1-kinase and its implication for the control of the metabolism." IUBMB life **62**(11): 791-796.

Spuler, S., M. Carl, et al. (2008). "Dysferlin-deficient muscular dystrophy features amyloidosis." Annals of neurology **63**(3): 323-328.

Spuler, S., v. Moers, A. (2004). Muskelkrankheiten. Stuttgart, Schattauer Verlag.

Srivastava, S. K., K. V. Ramana, et al. (2005). "Role of aldose reductase and oxidative damage in diabetes and the consequent potential for therapeutic options." Endocr Rev **26**(3): 380-392.

Stephens, B. R., A. S. Cole, et al. (2006). "The influence of biological maturation on fat and carbohydrate metabolism during exercise in males." International journal of sport nutrition and exercise metabolism **16**(2): 166-179.

Suarez, R. K. (2003). "Shaken and stirred: muscle structure and metabolism." The Journal of experimental biology **206**(Pt 12): 2021-2029.

Taggart, A. K., J. Kero, et al. (2005). "(D)-beta-Hydroxybutyrate inhibits adipocyte lipolysis via the nicotinic acid receptor PUMA-G." The Journal of biological chemistry **280**(29): 26649-26652.

Takekura, H. and T. Yoshioka (1987). "Determination of metabolic profiles on single muscle fibres of different types." J Muscle Res Cell Motil **8**(4): 342-348.

Tang, W. H., K. A. Martin, et al. (2012). "Aldose reductase, oxidative stress, and diabetic mellitus." Front Pharmacol **3**: 87.

Taylor, D. J., G. J. Kemp, et al. (1997). "Ageing: effects on oxidative function of skeletal muscle in vivo." Molecular and cellular biochemistry **174**(1-2): 321-324.

Thomassen, A., T. T. Nielsen, et al. (1991). "Effects of intravenous glutamate on substrate availability and utilization across the human heart and leg." Metabolism **40**(4): 378-384.

Timmons, B. W., O. Bar-Or, et al. (2003). "Oxidation rate of exogenous carbohydrate during exercise is higher in boys than in men." Journal of applied physiology **94**(1): 278-284.

Timmons, B. W., O. Bar-Or, et al. (2007). "Influence of age and pubertal status on substrate utilization during exercise with and without carbohydrate intake in healthy boys." Applied physiology, nutrition, and metabolism = Physiologie appliquee, nutrition et metabolisme **32**(3): 416-425.

Urtizberea, J. A., G. Bassez, et al. (2008). "Dysferlinopathies." Neurology India **56**(3): 289-297.

Vafiadaki, E., A. Reis, et al. (2001). "Cloning of the mouse dysferlin gene and genomic characterization of the SJL-Dysf mutation." Neuroreport **12**(3): 625-629.

Varnier, M., G. P. Leese, et al. (1995). "Stimulatory effect of glutamine on glycogen accumulation in human skeletal muscle." The American journal of physiology **269**(2 Pt 1): E309-315.

Vavvas, D., A. Apazidis, et al. (1997). "Contraction-induced changes in acetyl-CoA carboxylase and 5'-AMP-activated kinase in skeletal muscle." The Journal of biological chemistry **272**(20): 13255-13261.

Wagenmakers, A. J. (1998). "Muscle amino acid metabolism at rest and during exercise: role in human physiology and metabolism." Exercise and sport sciences reviews **26**: 287-314.

Walton, J. N. (1956). "The inheritance of muscular dystrophy: further observations." Annals of human genetics **21**(1): 40-58.

Walton, J. N. and F. J. Nattrass (1954). "On the classification, natural history and treatment of the myopathies." Brain : a journal of neurology **77**(2): 169-231.

Ward, S., Y. Argon, et al. (1981). "Sperm morphogenesis in wild-type and fertilization-defective mutants of Caenorhabditis elegans." The Journal of cell biology **91**(1): 26-44.

Wasserman, D. H., L. Kang, et al. (2011). "The physiological regulation of glucose flux into muscle in vivo." The Journal of experimental biology **214**(Pt 2): 254-262.

Wattjes, M. P., R. A. Kley, et al. (2010). "Neuromuscular imaging in inherited muscle diseases." European radiology **20**(10): 2447-2460.

Weller, A. H., S. A. Magliato, et al. (1997). "Spontaneous myopathy in the SJL/J mouse: pathology and strength loss." Muscle Nerve **20**(1): 72-82.

Wells, G. D., H. Selvadurai, et al. (2009). "Bioenergetic provision of energy for muscular activity." Paediatric respiratory reviews **10**(3): 83-90.

Wenzel, K., M. Carl, et al. (2006). "Novel sequence variants in dysferlin-deficient muscular dystrophy leading to mRNA decay and possible C2-domain misfolding." Hum Mutat **27**(6): 599-600.

Wenzel, K., C. Geier, et al. (2007). "Dysfunction of dysferlin-deficient hearts." J Mol Med (Berl) **85**(11): 1203-1214.

Wenzel, K., J. Zabojszcza, et al. (2005). "Increased susceptibility to complement attack due to down-regulation of decay-accelerating factor/CD55 in dysferlin-deficient muscular dystrophy." Journal of immunology **175**(9): 6219-6225.

Wilson, J. E. (2003). "Isozymes of mammalian hexokinase: structure, subcellular localization and metabolic function." The Journal of experimental biology **206**(Pt 12): 2049-2057.

Wu, G. and J. R. Thompson (1990). "The effect of ketone bodies on protein turnover in isolated skeletal muscle from the fed and fasted chick." Int J Biochem **22**(3): 263-268.

Yasunaga, S., M. Grati, et al. (1999). "A mutation in OTOF, encoding otoferlin, a FER-1-like protein, causes DFNB9, a nonsyndromic form of deafness." Nature genetics **21**(4): 363-369.

Zacharias, U., B. Purfurst, et al. (2011). "Ahnak1 abnormally localizes in muscular dystrophies and contributes to muscle vesicle release." J Muscle Res Cell Motil **32**(4-5): 271-280.

Zancan, P., M. M. Marinho-Carvalho, et al. (2008). "ATP and fructose-2,6-bisphosphate regulate skeletal muscle 6-phosphofructo-1-kinase by altering its quaternary structure." IUBMB life **60**(8): 526-533.

Eidesstattliche Versicherung/Declaration of originality

„Ich, Sarah Keller, versichere an Eides statt durch meine eigenhändige Unterschrift, dass ich die vorgelegte Dissertation mit dem Thema: „GC/MS- and LC/MS-based metabolic and proteomic analysis of dysferlin-deficient muscle from patients and animal models“ selbstständig und ohne nicht offengelegte Hilfe Dritter verfasst und keine anderen als die angegebenen Quellen und Hilfsmittel genutzt habe.
Alle Stellen, die wörtlich oder dem Sinne nach auf Publikationen oder Vorträgen anderer Autoren beruhen, sind als solche in korrekter Zitierung (siehe „Uniform Requirements for Manuscripts (URM)“ des ICMJE -www.icmje.org) kenntlich gemacht. Die Abschnitte zu Methodik (insbesondere praktische Arbeiten, Laborbestimmungen, statistische Aufarbeitung) und Resultaten (insbesondere Abbildungen, Graphiken und Tabellen) entsprechen den URM (s.o) und werden von mir verantwortet.
Meine Anteile an etwaigen Publikationen zu dieser Dissertation entsprechen denen, die in der untenstehenden gemeinsamen Erklärung mit dem/der Betreuer/in, angegeben sind. Sämtliche Publikationen, die aus dieser Dissertation hervoregangen sind und bei denen ich Autor bin, entsprechen den URM (s.o) und werden von mir verantwortet.

Die Bedeutung dieser eidesstattlichen Versicherung und die strafrechtlichen Folgen einer unwahren eidesstattlichen Versicherung (§§ 156, 161 des Strafgesetzbuches) sind mir bekannt und bewusst.

Datum Unterschrift

Curriculum vitae

Mein Lebenslauf wird aus datenschutzrechtlichen Gründen in der elektronischen Version meiner Arbeit nicht veröffentlicht.

Danksagung/Acknowledgment

An erster Stelle danke ich herzlichst Professor Dr. Simone Spuler nicht nur für die intensive fachliche Betreuung meiner Promotionsarbeit, sondern auch für die persönlich sehr bereichernde Unterstützung und Ermutigung.

Dr. Stefan Kempa möchte ich für die Aufnahme in seine Arbeitsgruppe am Max Delbrück Zentrum, die zeitaufwändige Einarbeitung und die vielen fachlichen Diskussionen danken. Mein ausdrücklicher Dank gilt weiterhin Christin Zasada für die unermüdliche Unterstützung bei meiner Datenauswertung und unserer freundschaftlichen Beziehung, die auch bei Rückschlägen meine Motivation aufrecht erhalten hat. Dr. Guido Mastrobouni, Matthias Pietzke und Julia Diesbach danke ich sehr für die Einarbeitung in die laborchemischen Messverfahren. Für die geduldige und flexible Einarbeitung in die Zellkultur und die Bereitstellung von Myoblastenkulturen danke ich sehr herzlich Stephanie Meyer. Ein sehr großer Dank gebührt auch Dr. Stephanie Adams für die intensive und selbstlose Unterstützung meiner Mäuseexperimente aber auch für die sehr bereichernden persönlichen Gespräche und Diskussionen. Professor Dr. Friedrich Luft danke ich ausdrücklich für die sprachliche Korrektur meiner Dissertation.

Zuletzt danke ich von Herzen meinen Eltern, Marianne und Jürgen Keller für die vielen Ratschläge und die immer fortwährende Unterstützung bei jeder neuen Herausforderung im beruflichen und privaten Bereich. Ein großer Dank gebührt Dustin Scheuer, Judy Han und David Keller für die tiefe Freundschaft, Motivation, Geduld und auch Kritik.